1983

Numerical Solution Of Three Instability Problems

Jacob Greydanus

CANADIAN THESES ON MICROFICHE

I.S.B.N.

THESES CANADIENNES SUR MICROFICHE

National Library of Canada
Collections Development Branch

Canadian Theses on
Microfiche Service

Ottawa, Canada
K1A 0N4

Bibliothèque nationale du Canada
Direction du développement des collections

Service des thèses canadiennes
sur microfiche

NOTICE

The quality of this microfiche is heavily dependent upon the quality of the original thesis submitted for microfilming. Every effort has been made to ensure the highest quality of reproduction possible.

If pages are missing, contact the university which granted the degree.

Some pages may have indistinct print especially if the original pages were typed with a poor typewriter ribbon or if the university sent us a poor photocopy.

Previously copyrighted materials (journal articles, published tests, etc.) are not filmed.

Reproduction in full or in part of this film is governed by the Canadian Copyright Act, R.S.C. 1970, c. C-30. Please read the authorization forms which accompany this thesis.

AVIS

La qualité de cette microfiche dépend grandement de la qualité de la thèse soumise au microfilmage. Nous avons tout fait pour assurer une qualité supérieure de reproduction.

S'il manque des pages, veuillez communiquer avec l'université qui a conféré le grade.

La qualité d'impression de certaines pages peut laisser à désirer, surtout si les pages originales ont été dactylographiées à l'aide d'un ruban usé ou si l'université nous a fait parvenir une photocopie de mauvaise qualité.

Les documents qui font déjà l'objet d'un droit d'auteur (articles de revue, examens publiés, etc.) ne sont pas microfilmés.

La reproduction, même partielle, de ce microfilm est soumise à la Loi canadienne sur le droit d'auteur, SRC 1970, c. C-30. Veuillez prendre connaissance des formules d'autorisation qui accompagnent cette thèse.

THIS DISSERTATION
HAS BEEN MICROFILMED
EXACTLY AS RECEIVED

LA THÈSE A ÉTÉ
MICROFILMÉE TELLE QUE
NOUS L'AVONS REÇUE

NL-339 (r. 82/08)

Canada

NUMERICAL SOLUTION OF THREE INSTABILITY PROBLEMS

by

Jacob Greydanus

Department of Applied Mathematics

Submitted in partial fulfillment
of the requirements for the degree of
Doctor of Philosophy

Faculty of Graduate Studies
The University of Western Ontario
London, Ontario
July, 1983

ABSTRACT

This thesis obtains numerical solutions for three instability problems.

The first is a Rayleigh-Taylor interfacial instability problem. Numerical solutions are obtained using a co-ordinate transformation technique and two approaches are tested for use in solving the field equation: (a) transformation and extremization of the variational integral, and (b) transformation of the differential equation itself. The latter is also tested with the use of higher order finite difference formulae. Solutions are generated with the most suitable method and compared with the predictions of Nayfeh's non-linear perturbation theory. While there is good qualitative agreement it is found that the quantitative agreement degrades with increases in the magnitude of the interfacial distortion.

The second problem is a generalized Stefan problem that models the behaviour of the interface between two components of a system that is undergoing melting or solidification. A co-ordinate transformation is employed and the numerical results are compared with the qualitative predictions of the linear perturbation theory of Chadam and Ortoleva. Agreement is excellent.

The third problem examines the onset of convective instability in a porous medium that is saturated with a fluid that has a temperature-dependent viscosity similar to that of heavy oil. A linear stability analysis is performed to determine the onset conditions and numerical solutions are generated for convective flow near these conditions. It is found that problems with convergence arise when the numerical method is used with small grid sizes.

ACKNOWLEDGEMENTS

I thank Dr. H. Rasmussen for suggesting these problems and for his help, guidance and encouragement. I would also like to express my appreciation to the many other members of the Department of Applied Mathematics (both faculty and student) with whom I have had many fruitful discussions concerning this and other work; especially D.S. Salhani, Y. Beaudoin and D.G. Meredith. Last, but not least, I thank the Faculty of Graduate Studies and NSERC for the funding that I have received.

TABLE OF CONTENTS

LIST OF TABLES

LIST OF FIGURES

GENERAL INTRODUCTION

In this thesis we obtain numerical solutions for three different problems which are all based on physical systems that may exhibit behaviour that can be defined as "unstable". In Chapters I and II, the instability is defined with regard to the behaviour of the interface between two components of the system while in Chapter III the instability is defined with regard to the transition within the system from a purely conductive state of heat transfer to a state of combined conduction and convection. For each case stable or unstable situations are identified with the values of a critical parameter of the system.

The solutions that are obtained in Chapters I and II involve the use of a particular co-ordinate transformation method. Forsyth and Rasmussen [1979] and Rasmussen and Salhani [1981] have successfully used this method in obtaining solutions for free surface problems in electrochemical machining and porous flow. In these cases however, the boundary conditions have been relatively simple. To determine the effectiveness of the method when more complicated boundary conditions are involved we have, in Chapter I, applied it to a Rayleigh-Taylor instability

problem which is a well-known problem in hydrodynamics. Then, in Chapter II, we have applied the method to a generalized Stefan problem that models the development of a melting or solidification front in a simple system. In both cases, the numerical results are compared with perturbative results that have been obtained by other authors.

A general review of numerical methods for free surface flows can be found in Yeung [1982] and a review of co-ordinate transformation methods in particular is given in Thompson, Warsi, and Mastin [1982].

In Chapter III we examine the effects of a temperature-dependent viscosity that is similar to that of heavy oil on the onset of convective flow, and on the convective flow near these conditions for a paradigm system with fixed boundaries. A linear stability analysis is performed and straightforward numerical solutions are obtained.

Due to the fact that these problems are largely physically and mathematically dissimilar to each other, each chapter has been written to "stand alone" so to speak. Each has its own introduction, formulation, review and so on and reference to previous chapters is minimal.

CHAPTER I

SOLUTION OF A RAYLEIGH-TAYLOR INSTABILITY PROBLEM

1.1 INTRODUCTION

Consider the situation involving two immiscible fluids in which a more dense fluid overlies one that is less dense and is also bounded on the lower side by a static wall. We shall also assume the presence of a gravitational field directed so as to cause acceleration from the heavier toward the lighter fluid along the normal to the interface between them. Due to the inherent instability of this initial configuration we would expect the interface to deform as the two fluids seek the eventual achievement of a dynamically stable state in which their original positions would be reversed.

The presence of the static wall has, initially, the effect of causing the lighter fluid to de-accelerate the heavier fluid from free fall. Bearing this in mind, as well as the fact that we have ignored possibly stabilizing influences in the preceding, we may define the Rayleigh-Taylor instability (R.T.I.) as the dynamic instability (if any) of the interface between two fluids when a more dense fluid is accelerated by a less dense fluid pushing against it.

In the sense that R.T.I. is primarily an inertial phenomenon, and could occur even in an inviscid system, it is closely related to Kelvin-Helmholtz instability (K.H.I.) which is a phenomenon associated with the case of changing tangential flow velocities across an interface separating two different fluids or two regions of the same fluid (see Birkhoff [1962]).

In any real system both phenomena may be influenced by many physical factors including such as molecular diffusion, evaporation and condensation. However, for purposes of mathematical analysis or numerical simulation, only the effects of all or some of the group including viscosity, density, compressibility, surface tension and fluid layer depth are usually considered. Naturally, a different mathematical problem is posed for each choice of physical parameters (and boundary conditions) used in studying these phenomena. In general, while some valuable insights have been gained through perturbative techniques of mathematical analysis, these problems are too complex to obtain complete analytic solutions and numerical methods must be applied.

To give an indication of the type of motion that may be involved we shall quote Lewis [1950] who conducted experiments on R.T.I. using density ratios and accelerations

chosen to ensure that an initial interfacial disturbance would become unstable. Lewis identifies the following three stages of growth for a small initial sinusoidal disturbance in the particular case of air accelerating a liquid (towards the earth but with an acceleration greater than gravitational):

"(1) an exponential increase in amplitude as given by the first-order theory until the amplitude is about 0.4λ;

(2) a transition stage during which the amplitude increases from 0.4 to $3/4\lambda$ and the surface disturbance changes to the form of round-ended columns of air penetrating into the liquid which forms narrow upstanding columns in the interstices;

(3) a final stage of penetration through the liquid of the air columns at a uniform velocity proportional to $\sqrt{g_1 - g}$."

In the above, the first order theory mentioned is that of G.I. Taylor [1950] and it will be referred to later, λ refers to the wavelength of the initial disturbance and g_1, g, refer respectively, to the applied and gravitational accelerations. Birkhoff [1962] notes that Lewis' stage (3) would normally also be unstable under Kelvin-Helmholtz instability and that this leads to the development of two further stages for an initially sinusoidal disturbance.

He describes these as

"(4) an irregular transition stage during which the periodic interface becomes irregular and blurred, due to continued Helmholtz instability;

(5) a statistical asymptotic stage, in which the interface is only statistically predictable; it is not clear whether or not statistical equilibrium will ultimately be attained."

From the above it seems probable that numerical solutions could be obtained for the first three stages but not likely beyond. Indeed, some numerical methods appear to have successfully simulated the growth of an instability into the third stage. "Successfully", at least, in the sense that the results seem physically plausible when compared with experimental data. Because a rigorous and meaningful error analysis is not generally possible, the overall accuracy of the numerical results cannot be ascertained. Instead, comparisons are usually made with the results of perturbation analyses (for early stage growth), experiment, and alternate numerical methods. Comparison with experimental results are often of little more than qualitative value however, since the mathematical formulation of the problem may not take into account all of the real effects (this may be intentional so as to determine the effects of a particular physical parameter) and because

of uncertainties concerning the initial conditions of the experiment (for example, it would never be possible to deform the initial interface into a perfect sine wave). With regard to the numerical methods used so far, it can be said that in addition to other possible drawbacks they exhibit either of the following features:

1) they cannot be used to large distortions of the interface, or
2) they can be used to large distortions but only with the use of *ad hoc* techniques such as variable smoothing or only for certain physically restrictive cases.

Because of these unsatisfactory elements, research continues on the numerical solution of R.T.I.

In this chapter we shall present numerical solutions for a R.T.I. problem using a co-ordinate transformation technique. Our purpose is to numerically verify, if possible, some predictions of the non-linear perturbation theory of Nayfeh [1969].

In the next section, we shall present the formulation of the R.T.I. problem to be solved. Sections 1.3 and 1.4 respectively, will review some of the more important analytic and numerical results relevant to this work. Section 1.5 will give details of three sub-methods tested for use with the co-ordinate transformation technique as

well as details of the overall mode of solution. In section 1.6 a test determining which sub-method is ultimately used and the results of other numerical tests are presented. Section 1.7 will present numerical and perturbation solutions and give a concomitant discussion. Finally, section 1.8 will present conclusions.

1.2 MATHEMATICAL FORMULATION

We consider the interface between two inviscid and incompressible fluids and assume the flow to be two dimensional. The x and y co-ordinates are in and normal to the undisturbed interface. We assume the top fluid to be a gas bounded at infinity and to have negligible density compared to the bottom fluid which we assume to be a liquid of thickness h, and to have one surface always adjacent to a solid face. The liquid/gas interface is assumed to be initially corrugated in the shape of a standing sinusoidal wave of amplitude a, wave number k, and the effects of surface tension are considered. The whole system is started from rest and accelerated in a direction normal to the undisturbed interface with uniform acceleration g. For instability, the acceleration is directed from the liquid to the gas.

The equations of momentum for the liquid are

$$\rho\left(\frac{\partial u}{\partial t} + u\frac{\partial u}{\partial x} + v\frac{\partial u}{\partial y}\right) = -\frac{\partial p}{\partial x}$$

$$\rho\left(\frac{\partial v}{\partial t} + u\frac{\partial v}{\partial x} + v\frac{\partial v}{\partial y}\right) = -\frac{\partial p}{\partial y} + \rho g \qquad (1.2.1)$$

where ρ, p, t represent density, pressure, and time and $u\hat{i} + v\hat{j} = \vec{q}$ is the velocity.

Equations (1.2.1) can be written in vector form as:

$$\rho\left[\frac{\partial \vec{q}}{\partial t} + \vec{\nabla}\left(\frac{q}{2}\right)^2 - \vec{q} \times \vec{\nabla} \times \vec{q}\right] = -\vec{\nabla}p + \rho g\hat{j} \qquad (1.2.2)$$

where $q = |\vec{q}|$.

Since the motion starts from rest under the action of a conservative field, the vorticity $\vec{\nabla} \times \vec{q}$, vanishes and we can introduce a potential function ϕ such that $\vec{q} = -\vec{\nabla}\phi$ (Milne-Thompson [1949]§ 2.52, 3.51). Thus (1.2.2) can be written as

$$-\vec{\nabla}\left[\frac{p}{\rho} - gy - \phi_t + \frac{1}{2}(\phi_x^2 + \phi_y^2)\right] = 0 \qquad (1.2.3)$$

and therefore

$$\frac{p}{\rho} - gy - \phi_t + \frac{1}{2}(\phi_x^2 + \phi_y^2) = c(t) \qquad (1.2.4)$$

where $c(t)$ denotes an instantaneous constant i.e. a function of t only. At the interface let $y = \eta(x,t)$, then the pressure jump due to a surface tension force of magnitude T is (Milne-Thompson [1949]§ 14.50)

$$p - 0 = -T\frac{\eta_{xx}}{(1+\eta_x^2)^{3/2}} + c(t) - 0 \qquad (1.2.5)$$

where $\eta_{xx}/(1+\eta_x^2)^{3/2}$ represents the curvature. Using (1.2.4) and (1.2.5) we obtain the pressure condition at the interface

$$-g\eta - \phi_t + \frac{1}{2}(\phi_x^2 + \phi_y^2) = \frac{T}{\rho}\frac{\eta_{xx}}{(1+\eta_x^2)^{3/2}} . \qquad (1.2.6)$$

On the interface, $y-\eta(x,t) = 0$, and since the surface moves with the fluid, $d[y-\eta(x,t)] = 0$, so that in terms of the velocity potential ϕ we have the kinematic condition

$$\eta_t - \eta_x\phi_x + \phi_y = 0 \qquad (1.2.7)$$

The initial conditions on the interface are $\eta(x,o) = a \cos kx + h$ and $\eta_t(x,o) = 0$.

Conservation of mass requires $u_x + v_y = 0$ (Milne-Thompson [1949]§ 3.20), which in terms of ϕ becomes:

$$\phi_{xx} + \phi_{yy} = 0 . \qquad (1.2.8)$$

Since we assume no flow across the liquid/solid interface we have the boundary condition $\phi_y = 0$ at $y = 0$.

If we now non-dimensionalize distances, velocities, and time by $1/k$, $(g/k)^{1/2}$ and $(gk)^{-1/2}$ respectively, the associated non-dimensionalized quantities are then given by

$h^* = kh$, $\eta^* = k\eta$, $x^* = kx$, $y^* = ky$, $t^* = (gk)^{1/2}t$ and

$$\phi^* = k^{3/2}g^{-1/2}\phi.$$

In terms of these non-dimensionalized quantities, the formulation becomes (dropping the star superscripts for convenience):

$$-\eta-\phi_t + \frac{1}{2}(\phi_x^2+\phi_y^2) = K^2\eta_{xx}(1+\eta_x^2)^{-3/2} \qquad (1.2.9)$$

on $y=\eta(x,t)$

$$\eta_t - \eta_x\phi_x + \phi_y = 0 \qquad (1.2.10)$$

where $K = k/k_c$

$$k_c = (\rho g/T)^{1/2}$$

$$\eta(x,o) = \varepsilon \cos x + h \qquad (1.2.11)$$

where $\varepsilon = ak$

$$\eta_t(x,o) = 0 \qquad (1.2.12)$$

$$\phi_{xx} + \phi_{yy} = 0 \qquad (1.2.13)$$

$$-\infty < x < \infty,\ \eta \geq y \geq 0,\ t \geq 0$$

$$\phi_y(x,y,t) = 0 \quad \text{at } y = 0. \qquad (1.2.14)$$

It is noted that the parameter K can be interpreted as the ratio of the surface tension force to the gravity force.

1.3 REVIEW OF PERTURBATION ANALYSES

Lord Rayleigh ([1945]§ 365) examined the case of two inviscid, incompressible fluids in which one of density ρ', velocity $\vec{u}'$, and thickness ℓ' overlies a fluid of density ρ, velocity $\vec{u}$ and thickness ℓ under the action of surface tension and gravity. From his analysis, the following correct qualitative insights are obtained:

(1) the condition $\rho' > \rho$ is destabilizing, (R.T.I.)

(2) the velocity difference $|u'-u|$ is destabilizing, (K.H.I.)

(3) surface tension is a stabilizing influence, in particular, it prevents the growth of infinitesimal wavelengths.

Lamb ([1945]§ 231) analysed the case where the interface between two inviscid, incompressible, semi-infinite fluids is accelerated from the denser to the less dense fluid. Designating g as the magnitude of the acceleration, k as the wave number of an initial standing wave disturbance, and ρ, ρ' as the densities of the denser and less dense fluid, he found the rate of growth to be given by

$$[gk(\rho-\rho')/(\rho+\rho')]^{1/2} \qquad (1.3.1)$$

Then taking into account surface tension he found ([1945]§ 267) that disturbances with wave numbers greater than

$k = k_c$ where

$$k_c = [g(\rho-\rho')/T]^{1/2} \qquad (1.3.2)$$

are stabilized (i.e. do not grow) where T is the magnitude of the surface tension force.

Taylor [1950] extended Lamb's first result to the case where the denser fluid has a finite thickness and is bounded on either side by a semi-infinite less dense fluid. The top surface was assumed to have an initial sinusoidal disturbance and the bottom surface was assumed to be initially flat. The acceleration on the system was assumed to be made up of a gravitational acceleration directed downward plus an arbitrary acceleration acting along the same lines of force as the first but possibly oppositely directed (anti-parallel). In the case that this second acceleration acts parallel to the first but with greater magnitude, the situation is analogous to the experiments of Lewis [1950] who used accelerations great enough to ensure that surface tension effects would be unimportant. As already indicated in section 1.1, the experimental and analytical results appear to agree (within experimental scatter) for early growth.

Bellman and Pennington [1954] considered two semi-infinite incompressible fluids under an appropriate

acceleration made up of two components as above. They found, as did Lamb, that the effect of surface tension is to produce a critical (or "cut-off") wave number below which an initial standing wave disturbance will grow in amplitude and above which it will merely oscillate without such growth. They also found that the addition of viscosity will act to reduce the rate of growth of unstable disturbances and to dampen stable ones, but, by itself viscosity will only reduce the rate of growth to zero asymptotically as the wave number becomes infinite. Their results also determine values of the wave numbers which have maximum growth rate for the cases where surface tension only, viscosity only, and both are considered.

The preceding analyses are all first order theories and can only be considered applicable during first stage growth i.e., only until times when the disturbance amplitude has grown to approximately $.4\lambda$. Also, in the absence of surface tension or viscosity, the linearized theories may be ill-posed since they predict that the growth rate of a disturbance would increase without limit with decreasing wavelength.

Chandrasekhar ([1961] Chapter X) extended many of the preceding results to three dimensions by considering the fluids to be confined between two rigid planes and allowing amplitude perturbations in two space directions. He also

examined the effects of rotation and magnetic fields.

Emmons et al. [1960] did a combined experimental and analytic study. They obtained a third order theory by considering two semi-infinite fluids and assuming the lighter fluid to have negligible mass. Both experimental and analytic results show that an initial sinusoidal disturbance will still grow at the cut-off wave number k_c, obtained by first order theory. They also predict that disturbances with wave numbers somewhat greater than k_c will oscillate with ever increasing amplitude. They refer to this phenomena as "overstability". Their experimental results however never showed more than a single oscillation before monotonic growth occurred. Nayfeh [1969] points out that their expansion is not valid near k_c and that while it is valid for wave numbers somewhat larger than k_c (as well as for those somewhat smaller) it is only valid for short times and cannot be used to explain this phenomenon. He shows analytically that the experimental setup may cause the overstability and also mentions that it may be due to small variations in the initial conditions.

Nayfeh [1969] also presents a second order analysis using the method of multiple time scales (Nayfeh [1973] Chapter 6). He also assumes the lighter fluid to have negligible mass but allows the denser fluid to have a

finite depth (although he does examine the limiting case of infinite depth as well). He considers both standing wave and travelling wave disturbances and determines an expansion for wave-numbers less than and greater than k_c and one for wave numbers near k_c. His expansion for values less than k_c is valid for short times and for longer times in the other two cases. He also determines a fourth-order amplitude dependent cut-off wave-number that is larger than the first order cut-off. Nayfeh's formulation is identical with that given in section 1.2 except that he places the liquid/solid interface at $y = -h$. Since his work will be used for later comparison we shall give his findings for initial standing wave disturbances in detail.

In terms of the non-dimensional variables used in 1.2 the quantitative results are as follows:

1) When $K-1 \neq O(\varepsilon^2)$

$$\eta(x,t) = \varepsilon\cos\sigma t\ \cos x + \varepsilon^2 P(t)\cos 2x + h + O(\varepsilon^3 t) \qquad (1.3.3)$$

where

$$P(t) = \frac{1}{4}\frac{\sigma_o^2 S}{\mu^2 - 4\sigma_o^2}(\cos 2\sigma t - \cos\mu t) + \frac{1}{4}\frac{\sigma_o^2}{\mu^2}\left(2 + \frac{1}{\sinh^2 h}\right)(1-\cos\mu t) \qquad (1.3.4)$$

$$S = -4 \coth h - \frac{\tanh 2h}{\sinh^2 h} + 2 \tanh 2h \qquad (1.3.5)$$

$$\mu = 2(4K^2-1)\tanh 2h \qquad (1.3.6)$$

$$\sigma = \sigma_o + \varepsilon^2 \tilde{\sigma}_2 + O(\varepsilon^3) \qquad (1.3.7)$$

$$\sigma_o = (K^2-1)\tanh h \qquad (1.3.8)$$

$$\tilde{\sigma}_2 = \frac{\sigma_o}{8} \{\frac{1}{2} \frac{\sigma_o^2 S}{\mu^2 - 4\sigma_o^2} [\frac{1}{2} \coth h + \coth 2h$$

$$+ \tanh h \, (\frac{\cosh 3h}{\sinh h \sinh 2h} - 2\frac{1}{2})]$$

$$- \frac{1}{2} \frac{\sigma_o^2}{\mu^2}(2 + \frac{1}{\sinh^2 h})(\coth h + \tanh h)\tanh 2h$$

$$- \frac{9}{8} K^2 \tanh h/\sigma_o^2 - \frac{1}{2} \coth h \coth 2h$$

$$- \frac{1}{2} \frac{\cosh 3h}{\sinh h \sinh 2h} + 1\} . \qquad (1.3.9)$$

If σ_o^2 is positive and not near zero, (1.3.3) is uniformly valid for times as large as $O(\varepsilon^{-2})$ and represents oscillatory standing waves. If σ_o^2 is negative, (1.3.3) represents growing waves and is valid for short times only, breaking down for times as large as $O(\varepsilon^{-1})$. One may note (although Nayfeh does not mention this specifically) that for the case K = .5 the expansion is singular i.e. the

expansion is not uniformly valid for $K < 1$.

2) When $K-1 = O(\varepsilon^2)$

$$\eta(x,t) = \varepsilon\, Z(\tau)\cos x + h + O(\varepsilon^2) \qquad (1.3.10)$$

where $\tau = \varepsilon t$ and $Z(\tau)$ satisfies the differential equation

$$\frac{d^2Z}{d\tau^2} + (\alpha Z - \frac{3}{8}Z^3)\tanh h = 0 \qquad (1.3.11)$$

with

$$Z(0) = 1 \text{ and } dZ(0)/d\tau = 0.$$

While α is initially assumed to be of $O(1)$ and may be positive or negative, Nayfeh shows that $\alpha = 3/8$ separates the stable and unstable regions.

3) The non-linear cut-off wave-number k_{cn}, is given by

$$k_{cn} = [1 + \frac{3}{8}\varepsilon^2 - \frac{21}{512}\varepsilon^4]^{1/2} + O(\varepsilon^6). \qquad (1.3.12)$$

Qualitatively, Nayfeh's conclusions are

1) contrary to the predictions of linear theory, the cut-off wave-number is amplitude dependent and disturbances with wave-numbers equal to the linear cut-off still grow,

2) while disturbances with wave-numbers less than the cut-off grow, those with greater values will oscillate with time independent amplitudes and amplitude

dependent frequencies,

3) decreasing the layer thickness decreases the growth rate of unstable disturbances and hence is stabilizing.

1.4 REVIEW OF NUMERICAL WORK

Harlow and Welch [1966] used the *marker and cell* method (MAC) developed by them [1965] to show the modifying effects of small and large viscosities on the speed and shape of interfacial development in R.T.I. They also did an inviscid study and compared the results with the third order theory of Emmons et al. [1960]. They claim that the results are in good agreement until the latest times that Emmons et al. show. At those times computer results show a slightly narrower spike and a broader bubble.

In its original form, MAC is a numerical method for solving the full non-linear, time-dependent Navier-Stokes equations for a viscous, incompressible fluid with a free surface. The region through which the fluid moves is divided into a fixed (Eulerian) co-ordinate mesh of rectangular cells and the fluid properties of pressure and velocity components are determined at the vertices. The fluid itself is represented by one or more marked particles within the appropriate cells. The motions of these are determined by the weighted average of the velocity components of the cells through which they move. In addition

to showing the changes of fluid configuration, the particles enable the surface position to be followed, so that the computer can automatically incorporate the free-surface boundary conditions.

In the inviscid study Harlow and Welch used a small non-zero value for the viscosity parameter. They claim that this is not necessary to ensure numerical stability but that the effect is to smooth the free surface which otherwise appears more turbulent.

Daly [1966] used an extended version of MAC to study viscous and inviscid R.T.I. for two fluids. The calculations for the former are compared to the analytic results of Chandrasekhar [1961] who predicts a certain variation of the linear growth rate with Reynolds number. The results are found to be in good agreement.

The purpose of the inviscid study was to examine the effect of varying the fluid density ratios on the rate of growth and the shape of both Rayleigh-Taylor and the late time Kelvin-Helmholtz instabilities and to compare these results with analytic predictions. They found that the growth rates were smaller than those predicted by the Rayleigh-Taylor theories and attribute the disagreement to form drag. They derive a first order modification to the first order theory in order to take this effect into

account and claim that their results correlate well with the modified theory during the early stages of unstable growth. Their results show that increasing the density ratio (of heavier fluid to lighter fluid) increases the growth rate of R.T.I. and decreases the growth rate of K.H.I. They also show that increasing the density ratio hastens the development of asymmetries in spike (denser fluid) and bubble (less dense fluid) shapes in that the spikes become "sharper" and narrower and the bubbles become rounder and broader.

Daly and Pracht [1968] developed a technique for including surface tension in MAC calculations. This involves the inclusion of another set of marked particles to represent the free surface more accurately and the use of a spline fit technique to determine surface curvature. The method is complicated and somewhat arbitrary when the interface is not monotone. Nevertheless, Daly [1969] uses this adaptation to show that surface tension tends to "squeeze-off" bulges at the fluid spike tip caused by K.H.I. thereby causing or hastening the formation of a separate fluid drop.

MAC methods seem to be most useful for problems involving large amplitude fluid motions. Their biggest drawback seems to be the lack of definition given

interfaces, small localized regions of the flow, and low amplitude motions. Also, interfaces between different fluid species can only be handled when density differences are small and the flow is of low viscosity (Hirt et al. [1970]).

Vortex methods have also been used in the study of inviscid R.T.I. Birkhoff [1962] showed that two-dimensional, inviscid, interfacial motion could be formulated in terms of variables describing the shape and circulation distribution of a vortex sheet representing the interface, thus reducing the effective space dimensionality of the problem by one (see Saffman and Baker [1979] for a description of vortex interactions). Baker et al. [1980] used a discrete vortex model to examine density ratio effects in the absence of surface tension. For the special case where the lighter fluid was assumed to have zero density, they were able to achieve spike amplitudes of nearly twice the initial wavelength. For non-zero values however, the K.H.I. induced "roll-up" of the interface produces computational instabilities for later times, in fact, they find that increasing the number of vortices per wavelength increases these instabilities.

Pullen [1982] used a continuous vortex sheet model to study the effects of surface tension on R.T.I. and K.H.I.

He found it necessary to apply a smoothing technique developed by Longuet-Higgins and Cokelet [1976] (in work on non-linear surface waves) in order to control saw-tooth irregularities in the solution. This generally allowed solution well into the non-linear regime before locally irregular behaviour again appeared. He found that surface tension counteracts the formation of curvature singularities at the fluid spike tip (which would lead to infinite jumps in the pressure across the interface) by causing the tip to bulge. In a simulation neglecting surface tension he finds the early development of a chaotic motion near the bubble tip. He mentions that this discrepancy with the results of Baker et al. [1980] may be due to an artificial surface tension induced by the smoothing.

Other numerical methods have also been used to treat R.T.I., for example, the Lagrangian technique for incompressible fluids (LINC) developed by Hirt et al. [1970] and the numerical conformal mapping technique of Baker et al. [1981]. However, in both of these papers, a R.T.I. calculation was included only as one of a group of test problems and in-depth studies or comparisons were not intended. In any event, the usefulness of these methods appears to be limited to small distortions.

1.5 NUMERICAL METHODS OF SOLUTION

Numerical solutions of the problem formulated in section 1.2 are obtained by three different methods: all involving the use of the same co-ordinate transformation. The differences lie purely in the way that solutions for the field equation (potential problem) are obtained. The first method is variational in character and is programmed for use with a variable grid. The second and third methods are more straight-forward and differ from each other only in the accuracy of the finite-difference approximations used. Comparisons are to be made (in section 1.6) from the perspective of accuracy and cost to determine which is the most suitable for use in the generation of the numerical solutions required for the comparison with Nayfeh's theory.

Referring back to equation (1.2.13) in the formulation it is evident that we must first remove the infinity in the x direction before we can treat the problem numerically. Since the initial displacement is a standing wave, we can do this by assuming that there is no lateral transfer of liquid (or gas) across the points on the x-axis that correspond to maximum and minimum displacements and that these points do not shift with time. Thus we can restrict the range in x to an interval of length π which corresponds to one-half the wavelength of the non-

dimensionalized disturbance and we can impose the conditions

$$\phi_x(o,y,t) = \phi_x(\pi,y,t) = 0 \qquad (1.5.1)$$

$$\eta_x(o,t) = \eta_x(\pi,t) = 0. \qquad (1.5.2)$$

Then the basic configuration at $t = 0$ is as shown in Figure 1.1.

To solve for the displacement of the interface, we utilize a predictor-corrector method along with an iteration procedure that often requires several solutions of the potential problem at any time step. We shall first solve the problem by applying a method suggested by Forsyth and Rasmussen [1979] (see also Forsyth [1979]). Using this method we apply a co-ordinate transformation to yield a rectangular domain but we deal with the potential problem by transforming the associated variational integral rather than Laplace's equation. The transformed variational integral is then approximated using the trapezoidal rule, discretized, and extremized directly. The advantages of this method are:

1) the cumbersome details of applying a square or rectangular finite difference grid near a curved boundary are eliminated,
2) only the first derivatives of the interface are

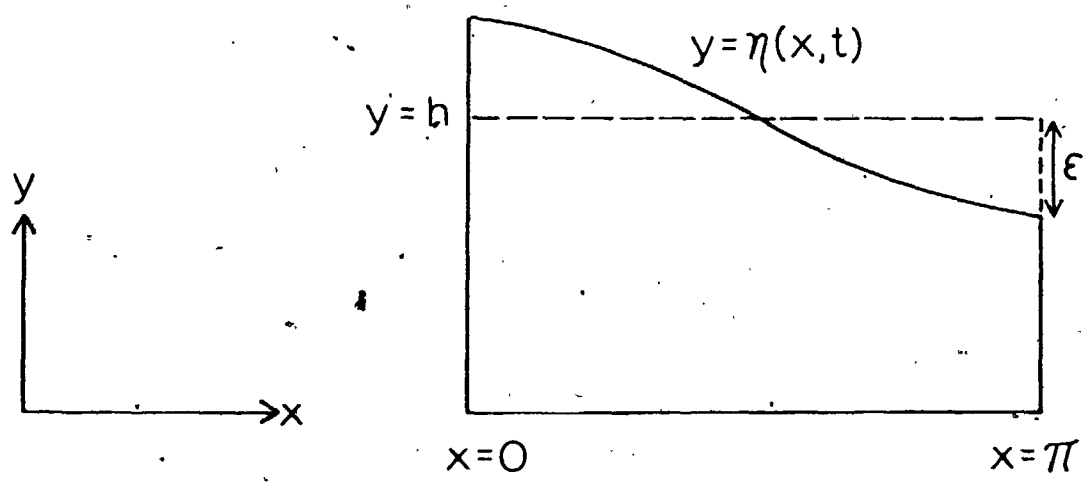

FIGURE 1.1 Basic configuration.

involved in calculations for the field potentials; thereby decreasing the likelihood of calculational instability,

3) the conditions imposed on the non-moving sections of the boundary are simply the natural boundary conditions of the variational problem i.e., normal derivatives are equal to zero,

4) a symmetric, positive definite system of equations for the potential can be obtained.

The variational integral, $J[\phi]$, is simply the Dirichlet integral in the x-y system i.e.,

$$J[\phi] = \int_0^{\pi} \int_0^{\eta(x,t)} [\phi_x^2 + \phi_y^2] dy dx . \qquad (1.5.3)$$

If we apply the co-ordinate transformation

$$x = x \qquad (1.5.4)$$

$$z = y/\eta(x,t) \quad (t \text{ fixed}),$$

which maps the domain of Figure 1.1 into a rectangle of length $x = \pi$ and height $z = 1$ as shown in Figure 1.2, then $J[\phi(x,y,t)]$ becomes:

$$J[\phi(x,z,t)] = \int_0^{\pi} \int_0^{1} \{\phi_z^2 A(x,z) + 2\phi_z \phi_x B(x,z) + \phi_x^2 C(x)\} dz dx \qquad (1.5.5)$$

where

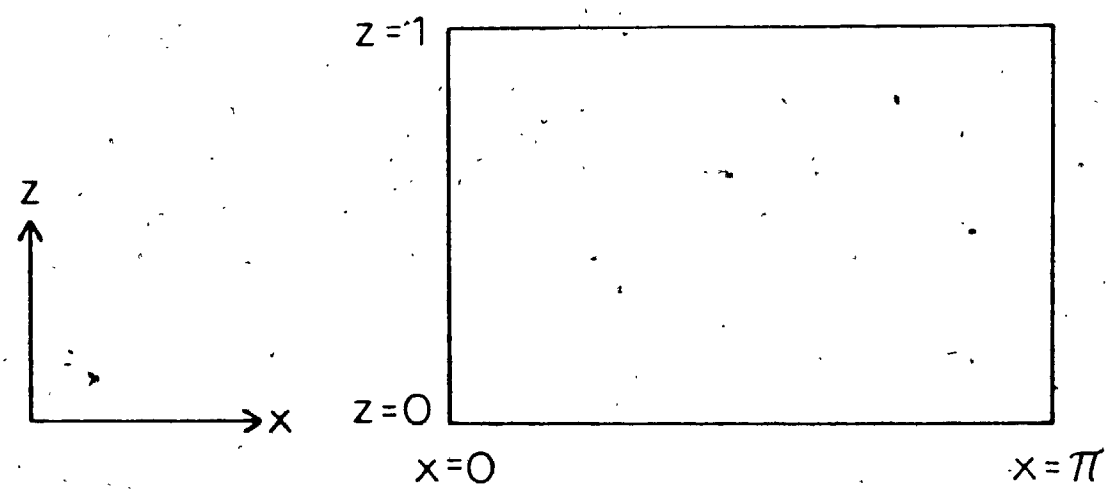

FIGURE 1.2 Configuration after co-ordinate transformation.

$$A(x,z) = (z_x^2 + z_y^2)\eta$$

$$B(x,z) = z_x\eta$$

$$C(x) = \eta$$

$$z_x = -z\,\eta_x/\eta$$

$$z_y = 1/\eta \text{ and } 0 \leq x \leq \pi,\ 0 \leq z \leq 1.$$

Let us form the finite difference grid as shown in Figure 1.3 where $\gamma_i = x_{i+1} - x_i$, $\Delta_j = z_{j+1} - z_j$ and $i = 1,2,\ldots,IMAX$, $j = 1,2,\ldots,JMAX$. If we discretize the integrand (see the Appendix for the appropriate formulae), and then approximate the integrand at the centre of each rectangle by the first order terms in a Taylor expansion, the trapezoidal rule approximation to $J[\phi]$ is:

$$J[\phi] = \sum_{i,j} \gamma_i \Delta_j \{ \frac{A_{i+1/2,j+1/2}}{2\Delta_j^2} [(T_z\phi_{i,j})^2 + (T_z\phi_{i+1,j})^2]$$

$$+ \frac{B_{i+1/2,j+1/2}}{2\gamma_i\Delta_j} [(T_z\phi_{i,j} + T_z\phi_{i+1,j})(T_x\phi_{i,j} + T_x\phi_{i,j+1})]$$

$$+ \frac{C_{i+1/2}}{2\gamma_i^2} [(T_x\phi_{i,j})^2 + (T_x\phi_{i,j+1})^2] \} \qquad (1.5.6)$$

where T_z and T_x are operators defined by

$$T_z\phi_{i,j} = \phi_{i,j+1} - \phi_{i,j}$$

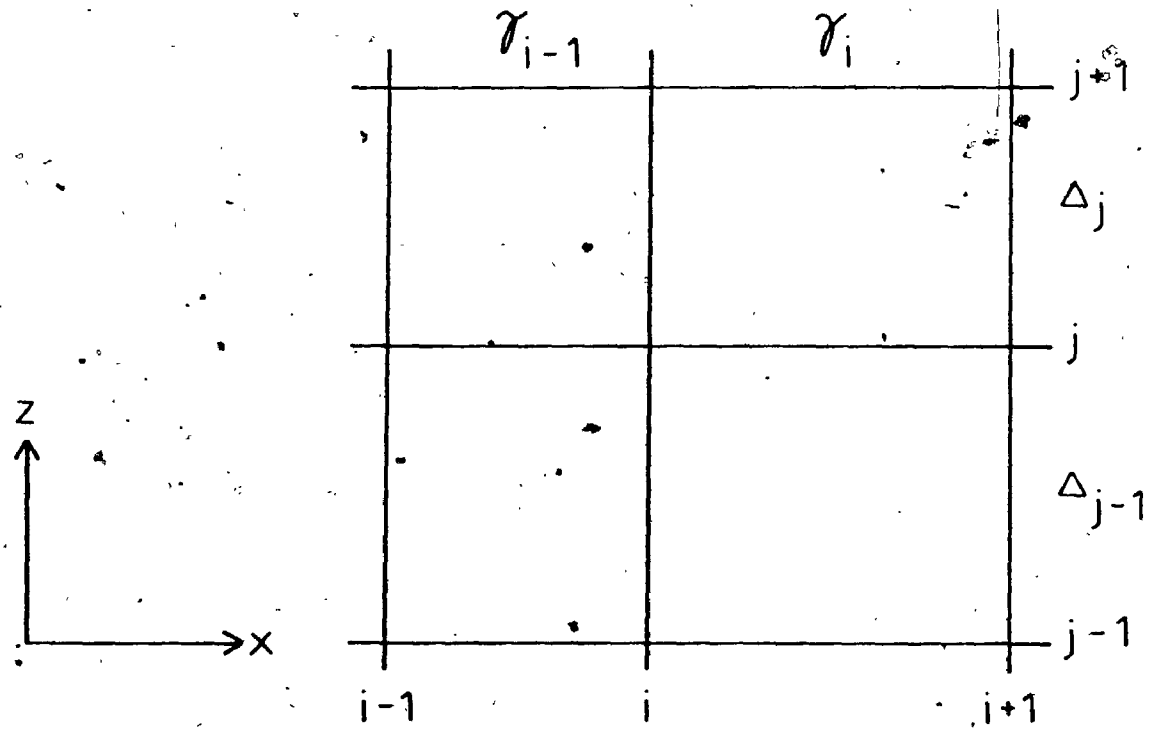

FIGURE 1.3 Finite difference grid.

$$T_x\phi_{i,j} = \phi_{i+1,j} - \phi_{i,j}.$$

If $J[\phi]$ is stationary with respect to ϕ, then

$$\frac{\partial J}{\partial \phi_{\ell,k}} = 0 \qquad (1.5.7)$$

and we get from (1.5.5):

$$Q_{\ell,k}\phi_{\ell,k} + R_{\ell,k}\phi_{\ell,k+1} + R_{\ell,k-1}\phi_{\ell,k-1}$$

$$+ S_{\ell,k}\phi_{\ell+1,k} + S_{\ell-1,k}\phi_{\ell-1,k}$$

$$- B_{\ell+1/2,k+1/2}\phi_{\ell+1,k+1} - B_{\ell-1/2,k-1/2}\phi_{\ell-1,k-1}$$

$$+ B_{\ell-1/2,k+1/2}\phi_{\ell-1,k+1} + B_{\ell+1/2,k-1/2}\phi_{\ell+1,k-1}$$

$$+ O\{\max(\gamma_\ell - \gamma_{\ell-1},\ \Delta_k - \Delta_{k-1},\ \Delta_k^2, \Delta_{k-1}^2, \gamma_\ell^2, \gamma_{\ell-1}^2)\} = 0 \qquad (1.5.8)$$

where

$$Q_{\ell,k} = \frac{\gamma_\ell A_{\ell+1/2,k-1/2}}{\Delta_{k-1}} + \frac{\gamma_\ell A_{\ell+1/2,k+1/2}}{\Delta_k} + \frac{\gamma_{\ell-1} A_{\ell-1/2,k-1/2}}{\Delta_{k-1}}$$

$$+ \frac{\gamma_{\ell-1} A_{\ell-1/2,k+1/2}}{\Delta_k} + \frac{C_{\ell-1/2}\Delta_k}{\gamma_{\ell-1}} + \frac{C_{\ell+1/2}\Delta_k}{\gamma_\ell} + \frac{C_{\ell-1/2}\Delta_{k-1}}{\gamma_{\ell-1}}$$

$$+ \frac{C_{\ell+1/2}\Delta_{k-1}}{\gamma_\ell} - B_{\ell-1/2,k+1/2} + B_{\ell+1/2,k+1/2}$$

$$+ B_{\ell-1/2,k-1/2} - B_{\ell+1/2,k-1/2}$$

---

† We shall use i,j interchangeably with the dummy variables ℓ,k where $\begin{cases} \ell = 1,2,\ldots,\text{LMAX}(=\text{IMAX}) \\ k = 1,2,\ldots,\text{KMAX}(=\text{JMAX}) \end{cases}$

$$R_{\ell,k} = - \frac{\gamma_\ell A_{\ell+1/2,k+1/2}}{\Delta_k} - \frac{\gamma_{\ell-1} A_{\ell-1/2,k+1/2}}{\Delta_k}$$

$$S_{\ell,k} = - \frac{C_{\ell+1/2}\Delta_k}{\gamma_\ell} - \frac{C_{\ell+1/2}\Delta_{k-1}}{\gamma_\ell} .$$

In determining the truncation error in (1.5.6) it was assumed that $\Delta_k/\gamma_\ell \sim O(1)$ and thus the use of long thin rectangles are prohibited. If the grid is variable such that at some points $\gamma_\ell \neq \gamma_{\ell-1}$ or $\Delta_k \neq \Delta_{k-1}$, then (1.5.6) is accurate only to first order. It should be noted that as a consequence of the fact that we have natural boundary conditions on the non-interface sides of the domain (1.5.8) still holds at points on these sides if we assign a value of zero to those quantities in the equation that fall outside the domain. On the interface, a predicted or corrected value of the potential is always specified prior to the solution for the potential at other points.

Let $\phi^N_{\ell,k}$ be the Nth iterate of $\phi_{\ell,k}$, then (1.5.8) is solved by the following algorithm:

$$S_{\ell-1,k}\lambda_{\ell-1} + Q_{\ell,k}\lambda_\ell + S_{\ell,k}\lambda_{\ell+1} = W_{\ell,k} \qquad (1.5.9a)$$

$$\phi^{N+1}_{\ell,k} = (1-\omega)\phi^N_{\ell,k} + \omega\lambda_\ell \quad (k \text{ fixed}) \qquad (1.5.9b)$$

where ω is a relaxation parameter and

$$W_{\ell,k} = -[R_{\ell,k}\phi^{N+1}_{\ell,k+1} - B_{\ell+1/2,k+1/2}\phi^{N+1}_{\ell+1,k+1}$$

$$+ B_{\ell-1/2,k+1/2}\phi^{N+1}_{\ell-1,k+1} + R_{\ell,k-1}\phi^{N}_{\ell,k-1}$$

$$- B_{\ell-1/2,k-1/2}\phi^{N}_{\ell-1,k-1} + B_{\ell+1/2,k-1/2}\phi^{N}_{\ell+1,k-1}] .$$

At any row (fixed k) we regard the right-hand side of (1.5.9a) as a function of ℓ only and then the left-hand side is solved directly by the Thomas algorithm (Ames [1977] 2.3). Thus the algorithm (1.5.9) is simply SOR by rows with scanning from the top to the bottom and it is terminated when a specified convergence criterion is met. It is noted that we reverse the direction of the Thomas algorithm after each time step (i.e., if we back-substitute from left to right during one time step we then back-substitute from right to left during the next and vice versa) in order to spread any round-off error as evenly as possible over the whole grid.

The disadvantage (apart from programming considerations) of using the variational method to solve the potential problem lies in the fact that the trapezoidal approximation of the integral introduces another possible source of error and higher order approximations such as Simpson's rule are not easily implemented.

A more straight-forward method may be used if we transform Laplace's equation. Under the transformation (1.5.4) this becomes:

$$\phi_{xx} + P(x,z)\phi_{zz} + Q^*(x,z)\phi_{xz} + U(x,z)\phi_z = 0 \quad (1.5.10)$$

where

$$\begin{aligned} P(x,z) &= (1 + z^2\eta_x^2)/\eta^2 \\ Q^*(x,z) &= -2z\eta_x/\eta \\ U(x,z) &= z(2\eta_x^2/\eta^2 - \eta_{xx}/\eta). \end{aligned} \quad (1.5.11)$$

We first discretize the derivatives of the potential in (1.5.10) using central difference formulae of second order accuracy that can be found in the Appendix. These formulae can be used even at the non-interface boundaries due to the "no-flow" conditions there which require symmetry in the potential about these boundaries. Then, given the discretizations $P_{\ell,k}$, $Q^*_{\ell,k}$, $U_{\ell,k}$, of the terms $P(x,z)$, $Q^*(x,z)$, $U(x,z)$, (the discretization of the interfacial terms involved will be discussed later) and the interfacial values of the potential, we can solve for the field potentials by the algorithm (1.5.9) if we take

$$S_{\ell-1,k} = -1$$

$$Q_{\ell,k} = 2 + 2P_{\ell,k}\,\gamma_\ell^2/\Delta_k^2 \qquad (1.5.12)$$

$$S_{\ell,k} = -1$$

$$W_{\ell,k} = \gamma_\ell^2[P_{\ell,k}\phi^N_{zz_{\ell,k}} + Q^*_{\ell,k}\phi^N_{xz_{\ell,k}} + U_{\ell,k}\phi^N_{z_{\ell,k}}]$$

$$+ 2P_{\ell,k}\phi^N_{\ell,k}\,\gamma_\ell^2/\Delta_k^2$$

for $k = 1,\ldots,KMAX-1$.

In this case, the algorithm is modified at the beginning and end point of each row using the symmetry property. For example, for the leftmost point on each row (1.5.9a) becomes:

$$Q_{1,k}\lambda_1 + 2S_{1,k}\lambda_2 = W_{1,k}.$$

Also, a LINPACK band matrix solver (that uses L-U decomposition and consists of the subroutines SGBFA, SGBSL) is used rather than the Thomas algorithm.

We next discretize the potential derivatives using difference formulae of fourth order accuracy (see the Appendix). Again, due to the no-flow boundaries central differences can still be used due to the symmetry of the potential about these boundaries. In particular, even derivatives (including zeroth order) are symmetric while odd derivatives are skew-symmetric. However, at field

points nearest to the interface (first row down), combination forward-backward difference formulae are used for derivatives involving z. The SOR algorithm now involves the solution along each row of a banded system of equations of width five rather than three. The new algorithm is

$$M_{\ell-2,k}\lambda_{\ell-2} + M_{\ell-1,k}\lambda_{\ell-1} + M_{\ell,k}\lambda_{\ell} + M_{\ell+1,k}\lambda_{\ell+1} + M_{\ell+2,k}\lambda_{\ell+2} = W_{\ell,k} \qquad (1.5.13a)$$

$$\phi^{N+1}_{\ell,k} = (1-\omega)\phi^{N}_{\ell,k} + \omega\lambda_{\ell} \quad (k \text{ fixed}). \qquad (1.5.13b)$$

For the row beneath the interface we have

$$\begin{aligned}
M_{\ell-2,k} &= 1 - 10Q^{*}_{\ell,k}\,\gamma_{\ell}/12\Delta_{k} \\
M_{\ell-1,k} &= -16 + 80Q^{*}_{\ell,k}\,\gamma_{\ell}/12\Delta_{k} \\
M_{\ell,k} &= 30 + 15P_{\ell,k}\,\gamma^{2}_{\ell}/\Delta^{2}_{k} - 10U_{\ell,k}\,\gamma^{2}_{\ell}/\Delta_{k} \\
M_{\ell+1,k} &= -16 - 80Q^{*}_{\ell,k}\,\gamma_{\ell}/12\Delta_{k} \\
M_{\ell+2,k} &= 1 + 10Q^{*}_{\ell,k}\,\gamma_{\ell}/12\Delta_{k} \qquad (1.5.14) \\
W_{\ell,k} &= 12\gamma^{2}_{\ell}[P_{\ell,k}\phi^{N}_{zz_{\ell,k}} + Q^{*}_{\ell,k}\phi^{N}_{xz_{\ell,k}} \\
&\quad + U_{\ell,k}\phi^{N}_{z_{\ell,k}}] + 15P_{\ell,k}\phi^{N}_{\ell,k}\,\gamma^{2}_{\ell}/\Delta^{2}_{k} \\
&\quad - 10U_{\ell,k}\phi^{N}_{\ell,k}\,\gamma^{2}_{\ell}/\Delta_{k}.
\end{aligned}$$

For the second row from the bottom we have

$$M_{\ell-2,k} = 1 - Q^*_{\ell,k}\,\gamma_\ell/12\Delta_k$$

$$M_{\ell-1,k} = -16 + 8Q^*_{\ell,k}\,\gamma_\ell/12\Delta_k$$

$$M_{\ell,k} = 30 + 31P_{\ell,k}\,\gamma_\ell^2/\Delta_k^2 - U_{\ell,k}\,\gamma_\ell^2/\Delta_k$$

$$M_{\ell+1,k} = -16 - 8Q^*_{\ell,k}\,\gamma_\ell/12\Delta_k$$

$$M_{\ell+2,k} = 1 + Q^*_{\ell,k}\,\gamma_\ell/12\Delta_k \qquad (1.5.15)$$

$$W_{\ell,k} = 12\gamma_\ell^2[P_{\ell,k}\phi^N_{zz_{\ell,k}} + Q^*_{\ell,k}\phi^N_{xz_{\ell,k}} + U_{\ell k}\phi^N_{z_{\ell,k}}]$$

$$+ 31P_{\ell,k}\phi^N_{\ell,k}\,\gamma_\ell^2/\Delta_k^2 - U_{\ell,k}\phi^N_{\ell,k}\,\gamma_\ell^2/\Delta_k$$

$$+ Q^*_{\ell,k}[-\phi^N_{\ell-2,k} + 8\phi^N_{\ell-1,k} - 8\phi^N_{\ell+1,k}$$

$$+ \phi^N_{\ell+2,k}]\gamma_\ell/12\Delta_k.$$

For all the other rows we have

$$M_{\ell-2,k} = 1$$

$$M_{\ell-1,k} = -16$$

$$M_{\ell,k} = 30 + 30P_{\ell,k}\,\gamma_\ell^2/\Delta_k^2 \qquad (1.5.16)$$

$$M_{\ell+1,k} = -16$$

$$M_{\ell+2,k} = 1$$

$$W_{\ell,k} = 12\gamma_\ell^2 [P_{\ell,k}\phi^N_{zz_{\ell,k}} + Q^*_{\ell,k}\phi^N_{xz_{\ell,k}} + U_{\ell,k}\phi^N_{z_{\ell,k}}]$$

$$+ 30P_{\ell,k}\phi^N_{\ell,k}\ \gamma_\ell^2/\Delta_k^2 .$$

Again, the algorithm is easily modified for the first two and last two points of each row by considering the symmetry in the potential. It should be noted that neither of the two non-variational methods have been adapted for use with a variable grid.

After transformation, the boundary conditions at the interface (z=1) can be written as:

$$\eta_t = \eta_x\phi_x - \phi_z(1+\eta_x^2)/\eta \qquad (1.5.17)$$

$$\phi_t = \tfrac{1}{2}[\phi_x^2 - 2\eta_x\phi_x\phi_z/\eta + \phi_z^2(1+\eta_x^2)/\eta^2]$$

$$- [\eta+K^2\eta_{xx}/(1+\eta_x^2)^{3/2}] . \qquad (1.5.18)$$

At $x = 0,\pi$ we have $\eta_x = \phi_x = 0$ as well as $\phi_z = 0$ on $z=0$. We discretize the spatial derivatives on the interface using finite difference formulae of at least fourth order accuracy rather than second order formulae because it is found that the increased accuracy is necessary to stabilize the calculations† i.e., the programs run longer. Since

† Increasing the accuracy to sixth order was found not to yield further improvement.

this eliminates the possibility of using a variable grid in the x direction we shall henceforth replace the use of γ_ℓ by γ. Central differences are used throughout the interval for the quantities $\eta_x, \eta_{xx}, \phi_x$ and a backward difference formula is used for ϕ_z. We approximate η_{xx} by using η_x values rather than η values since this is found to give better results. In particular, it is found that the direct use of η values tends to yield oscillatory behaviour of the second derivative near the end points after a short time while the use of first derivative values (which are fixed to zero at the end points) is found to reduce this problem. In this case the use of (A.3) which has a truncation error of $O(\gamma^4)$ when used for calculation of the first derivative is only $O[(2\gamma)^4]$ when used for the second derivative. Therefore we use (A.4) which is then $O[(2\gamma)^6]$ for the second derivative. While the effect of this change is found to be truly negligible it allows us to assert that when the fourth order field method is used the truncation error in all spatial derivatives is at least as good as $O(\gamma^4)$.

Discretizing the time as $t = p\Delta t$ where $p=0,1,2,\ldots$ we shall define $\eta(x_\ell, t+\Delta t) = \eta_{\ell,p+1}$ and $\phi(x_\ell, z_{KMAX}, t+\Delta t) = \phi_{\ell,p+1}$. Then we may solve for the displacement of the interface at time $t+\Delta t$ by an algorithm consisting of the following steps:

1) we predict

$$\eta_{\ell,p+1} = \eta^{o}_{\ell,p+1} = \eta_{\ell,p} + \Delta t \eta_{t_{\ell,p}} \tag{1.5.19a}$$

$$\phi_{\ell,p+1} = \phi^{o}_{\ell,p+1} = \phi_{\ell,p} + \Delta t \phi_{t_{\ell,p}} \tag{1.5.19b}$$

where $\eta^{o}_{\ell,p+1}$ and $\phi^{o}_{\ell,p+1}$ are forward difference approximations determined by using the right-hand side of (1.5.17) and (1.5.18):

2) using these new values we solve the potential problem and then re-calculate the quantities involved on the right-hand side of (1.5.17) and (1.5.18) in order to calculate $\eta^{o}_{t_{\ell,p+1}}$ and $\phi^{o}_{t_{\ell,p+1}}$;

3) we take the first corrected values as

$$\eta_{\ell,p+1} = \eta^{1}_{\ell,p+1} = (1-\omega^*)\eta^{o}_{\ell,p+1} + \omega^* \{\eta_{\ell,p} + \frac{\Delta t}{2} [\eta_{t\ell,p} + \eta^{o}_{t\ell,p+1}]\} \tag{1.5.20a}$$

$$\phi_{\ell,p+1} = \phi^{1}_{\ell,p+1} = (1-\omega')\phi^{o}_{\ell,p+1} + \omega' \{\phi_{\ell,p} + \frac{\Delta t}{2} [\phi_{t\ell,p} + \phi^{o}_{t\ell,p+1}]\} \tag{1.5.20b}$$

where ω^*, ω' are relaxation parameters;

4) we continue correction by repeating steps 2) and 3),

increasing the superscripts in (1.5.20) by one unit each cycle until a convergence criterion is met at which time the iteration is stopped;

5) lastly, we solve the potential problem again in readiness for the next time step.

This algorithm is repeated for each successive time step. It represents a Crank-Nicholson method and has a truncation error of $O(\Delta t^2+\gamma^4)$. This implicit method is to be preferred over an explicit method because of its inherent stability and lower truncation error in time (Ames [1977]§ 2.5). The iteration in the algorithm is stopped when both of the conditions

$$\max \left| \frac{n^{N+1}_{\ell,p+1} - n^{N}_{\ell,p+1}}{n^{N}_{\ell,p+1}} \right| < 10^{-5} \qquad (1.5.21a)$$

and

$$\max \left| \frac{\phi^{N+1}_{\ell,p+1} - \phi^{N}_{\ell,p+1}}{\phi^{N}_{\ell,p+1}} \right| < 10^{-4} \qquad (1.5.21b)$$

are met. The convergence criterion used to stop iteration in the solution of the potential problem is

$$\max \left| \phi^{N+1}_{\ell,k} - \phi^{N}_{\ell,k} \right| < 10^{-4} . \qquad (1.5.22)$$

We were fortunate in discovering that the number of

iterations in the potential problem could be reduced dramatically by predicting

$$\phi_{\ell,k,p+1} = \phi_{\ell,k,p} + [\phi_{\ell,k,p} - \phi_{\ell,k,p-1}] \qquad (1.5.23)$$

at the beginning of each time step. In a trial calculation this scheme was found to reduce execution times on the CDC 170-835 by approximately two-thirds for the second order methods and by about nine-tenths for the fourth order method. Hence, this scheme has been incorporated into all of the following calculations.

1.6 TESTING OF NUMERICAL METHODS

Recalling that $\gamma_\ell = x_{\ell+1} - x_\ell$, $\Delta_k = z_{k+1} - z_k$ and that $x_1 = 0$, $x_{LMAX} = \pi$, $z_1 = 0$, $z_{KMAX} = 1$, then the grid we shall use is given by

$$\begin{aligned} &LMAX = 33 \\ &KMAX = 11. \\ &\gamma_\ell = \pi/32 = \gamma \qquad \ell = 1,\ldots,32 \\ &\Delta_k = .1 \qquad\qquad k = 1,\ldots,10 \end{aligned} \qquad (1.6.1)$$

with a time step of

$$\Delta t = .02.$$

The physical parameters are

$$\begin{aligned} &K = .5 \quad (\text{recall } K = k/k_c) \\ &\varepsilon = .4 \\ &h = 4.0. \end{aligned}$$

These conditions will prevail for all of the following tests unless otherwise specified.

Table 1.1 details the results of calculations performed using the three different methods under the conditions listed above. For each calculation the values of the whole interface are printed out every .5 seconds of the non-dimensionalized time and the values of $\eta(0,t)$ (spike tip displacement) and $\eta(\pi,t)$ (bubble tip displacement) are indicated in the table. The constancy of the area (conservation of mass) is also monitored and is taken as an indicator of numerical stability. Since for this value of K we expect monotonic growth of the disturbance we test the interface for continuing monoticity after each time step. For both second order methods failure of this test results in termination of the program and the time of failure and the cumulated central processor execution time are recorded. In the case of the fourth order method, the program is allowed to run past the point of monoticity test failure until the program stops due to the failure of meeting the convergence criteria (1.5.21) or (1.5.22) in a specified number of iterations. The time of this latter occurrence and the total execution time are recorded.

From the results it is seen that SOV is clearly inferior to the other two methods in conserving mass when

TABLE 1.1 TEST OF NUMERICAL METHODS

(a) Second Order Variational Method (SOV)

t	$\eta(0,t)$	$\eta(\pi,t)$	area
0.0	4.400	3.600	12.566
0.5	4.432	3.568	12.564
1.0	4.534	3.470	12.556
1.5	4.718	3.297	12.537
2.0	4.991	2.042	12.492
2.5	5.353	2.705	12.392

Monoticity test failure at $t \doteq 2.96$

Execution time = 79 sec.

TABLE 1.1 (cont'd)

(b) Second Order Non-Variational Method (SONV)

t	$\eta(0,t)$	$\eta(\pi,t)$	area
0.0	4.400	3.600	12.566
0.5	4.435	3.565	12.566
1.0	4.547	3.457	12.566
1.5	4.750	3.263	12.565
2.0	5.053	2.969	12.564
2.5	5.456	2.567	12.559

Monoticity test failure at t = 2.80

Execution time = 182 sec.

TABLE 1.1 (cont'd)

(c) Fourth Order Non-Variational Method (FONV)

t	$\eta(0,t)$	$\eta(\pi,t)$	area
0.0	4.400	3.600	12.566
0.5	4.435	3.565	12.566
1.0	4.548	3.456	12.566
1.5	4.751	3.257	12.566
2.0	5.055	2.957	12.567
2.5	5.460	2.542	12.568

Monoticity test failure at t = 2.68

Convergence failure at t = 2.76

Execution time = 470 sec.

used with a similar grid but that it has the most favourable execution time. To determine if the variable grid option (now restricted to the z direction) would increase the numerical stability enough for the method to be competitive with SONV and FONV we did a calculation with the following grid change from (1.6.1):

$$KMAX = 14$$

$$\Delta_k = \begin{cases} .1 & k = 1,\ldots,7 \\ .5 & k = 8,\ldots,13 \end{cases}$$

The results are given in Table 1.2.

It is seen that the use of the variable grid has decreased the change in area at t = 2.5 from .174 to .123 but has increased the execution time from 79 to 236 seconds for .06 seconds less program time. The corresponding values for SONV are .007 and 182 seconds respectively and since SONV is superior on both counts we reject the use of SOV.†

Examination of Tables 1.1 and 1.2 reveals a clear and seemingly contradictory pattern; methods that conserve the area the best fail the monoticity test first. Since both conservation of the area and maintenance of monoticity

---

† Earlier and related calculations using SOV can be found in Greydanus and Rasmussen [in press].

TABLE 1.2 TEST OF SOV WITH VARIABLE GRID

t	$\eta(0,t)$	$\eta(\pi,t)$	area
0.0	4.400	3.600	12.566
0.5	4.433	3.567	12.565
1.0	4.539	3.465	12.558
1.5	4.730	3.283	12.542
2.0	5.016	3.013	12.508
2.5	5.399	2.650	12.443

Monoticity test failure at t = 2.90

Execution time = 236 sec.

would appear to indicate numerical stability this pattern seems paradoxical. It may partially be explained by the observation that better conservation of mass is also directly related to increased spike and bubble amplitudes at any particular time so that these earlier failures of monoticity test may be directly related to these larger amplitudes i.e., especially the concomitant increase in η_x and η_{xx} (recall 1.5). As would be expected FONV conserves the area better than SONV giving a change of magnitude .002 at t = 2.5 compared to .007 for SONV. However, we consider the improvement to be slight given the fact that the execution times indicate that the cost of using FONV would appear to be approximately two and a half times that of using SONV. Hence, all remaining tests and calculations are done with the use of SONV.

In Table 1.3 we present results obtained by halving the time step size from .02 to .01. Comparison of Table 1.3 with Table 1.1(b) shows that they are virtually identical and so we conclude that a time step of .02 is small enough to give convergence in time. The possibly surprising increase in execution time of only 2 seconds for the use of $\Delta t = .01$ is attributable to the fact that the number of iterations in the program at each time step is approximately halved.

TABLE 1.3 TEST WITH $\Delta t = .1$

t	$\eta(0,t)$	$\eta(\pi,t)$	area
0.0	4.400	3.600	12.566
0.5	4.435	3.566	12.566
1.0	4.547	3.457	12.566
1.5	4.750	3.263	12.565
2.0	5.053	2.970	12.564
2.5	5.456	2.568	12.559

Monoticity test failure at t = 2.79

Execution time = 183 sec.

In an earlier test using SOV a calculation similar to that of Table 1.2 was made to a time of t = 2.0. The results were found to agree to three decimals with those obtained by halving the grid size in the x direction to $\gamma = \pi/64$ (details can be found in Greydanus and Rasmussen [in press]). Hence, since we do not consider it necessary to repeat a similar calculation using SONV, we shall continue to use the spatial grid given by (1.6.1).

If the program is allowed to simply run until convergence is not obtained within the required number of iterations the solutions eventually develop a "saw-tooth" pattern. This phenomenon has been previously reported by Longuet-Higgins and Cokelet [1976] and Ohring [1979] in studies of non-linear water waves and by Pullen [1982] in work on R.T.I. Although no rigorous explanation of this instability has been developed, the cause is generally assumed to be numerical and these authors use a "smoothing" or "filtering" technique developed by Longuet-Higgins and Cokelet to control the problem. Their second-order smoothing algorithm is given by

$$\bar{f}_\ell = (-f_{\ell-2} + 4f_{\ell-1} + 10f_\ell + 4_{\ell+1} - f_{\ell+2}). \quad (1.6.2)$$

Pullen found that by applying this algorithm to interfacial terms in his vortex method that he was able to obtain solutions well into the third stage of growth but that

eventually the instability reappeared and was resistant to any subsequent attempts at suppression. He also found that calculations for zero surface tension soon developed an instability near the bubble tip that precluded extended solution times. This is contrary to the results of Baker et al. [1980] who were able to produce solutions for longer times for this case using their vortex method which does not include smoothing. In consequence, Pullen conjectures that the use of (1.6.2) may generate an artificial surface tension in the calculations.

In an effort to extend the solution times we first applied (1.6.2) to the interface displacement $\eta(x,t)$ and then to both $\eta(x,t)$ and $\phi(x,1,t)$ every five time steps. The results are given below in Table 1.4.

Comparison of Table 1.4 with Table 1.1(b) reveals that except for extensions in program run time that the applications of the smoothing have had no other discernible effect. This does appear to give some heuristic validation for its use. However, as may be implied from the experience of Pullen, we cannot be sure that this will always be the case. Also the best extension (Table 1.4(b)) of run time is only about 12% and while some experimenting may improve this further it does not appear likely that times sufficient for solutions to later stage growth could be attained.

TABLE 1.4 SMOOTHING TESTS

(a) Smoothing on $\eta(x,t)$

t	$\eta(0,t)$	$\eta(\pi,t)$	area
0.0	4.400	3.600	12.566
0.5	4.435	3.565	12.566
1.0	4.547	3.457	12.566
1.5	4.750	3.263	12.565
2.0	5.053	2.969	12.564
2.5	5.456	2.567	12.559

Monoticity test failure at t = 2.96

Execution time = 216 sec.

TABLE 1.4 (cont'd)

(b) Smoothing on both $\eta(x,t)$ and $\phi(x,1,t)$

t	$\eta(0,t)$	$\eta(\pi,t)$	area
0.0	4.400	3.600	12.566
0.5	4.435	3.565	12.566
1.0	4.547	3.457	12.566
1.5	4.750	3.263	12.565
2.0	5.053	2.969	12.564
2.5	5.456	2.567	12.559
3.0	5.955	2.048	12.542

Monoticity test failure at t = 3.14

Execution time = 251 sec.

Therefore, we have decided not to use smoothing in the calculations. We note however, that the failure of the smoothing to elicit the same significantly longer run times with our co-ordinate transformation method than it does when used with Pullen's vortex method is somewhat curious.

1.7 NUMERICAL AND PERTURBATION RESULTS AND DISCUSSION

In the following calculations we use the grid given by (1.6.1) and a time step of $\Delta t = .02$.

Table 1.5 gives solutions for selected wave numbers $K < 1.0$ ($K-1 \neq O(\varepsilon^2)$) with an initial disturbance amplitude of $\varepsilon = .1$, and an undisturbed liquid depth of $h = 4.0$. Nayfeh's perturbation results (Nayfeh [1969]) are obtained from (1.3.3) which we recall to be invalid for times as large as $O(\varepsilon^{-1})$ in this case as well as being singular at $K = .5$. The columns under $\Delta\eta(0,t)$ and $\Delta\eta(\pi,t)$ denote the difference between the analytic and numerical solutions at the spike and bubble tips respectively. As before, the area of the fluid domain is monitored during the numerical calculations.

Referring to Table 1.5 and recalling (from 1.2) that K can be interpreted as the ratio of surface tension force to gravity force we note that the growth rate of the disturbance decreases with increasing surface tension as one

TABLE 1.5 EFFECT OF K ON GROWTH RATE

(a) K = 0.0

t	$\eta(0,t)$		$\Delta\eta(0,t)$	$\eta(\pi,t)$		$\Delta\eta(\pi,t)$	area
	num.	pert.		num.	pert.		
0.0	4.100	4.100	-	3.900	3.900	-	12.566
0.5	4.113	4.113	.000	3.887	3.887	.000	12.566
1.0	4.154	4.155	.001	3.847	3.847	.000	12.566
1.5	4.233	4.241	.008	3.769	3.772	.003	12.566
2.0	4.369	4.403	.034	3.636	3.653	.017	12.566
2.5	4.588	4.712	.124	3.425	3.490	.065	12.565
3.0	4.914	5.331	.417	3.110	3.327	.217	12.564

TABLE 1.5 (cont'd)

(b) K = 0.3

t	η(0,t)		Δη(0,t)	η(π,t)		Δη(π,t)	area
	num.	pert.		num.	pert.		
0.0	4.100	4.100	-	3.900	3.900	-	12.566
0.5	4.111	4.112	.001	3.889	3.889	.000	12.566
1.0	4.148	4.150	.002	3.852	3.852	.000	12.566
1.5	4.219	4.225	.006	3.782	3.784	.002	12.566
2.0	4.338	4.363	.025	3.665	3.677	.012	12.566
2.5	4.467	4.615	.148	3.481	3.525	.044	12.565
3.0	4.811	5.086	.275	3.207	3.342	.135	12.565

TABLE 1.5 (cont'd)

(c) $K = 0.5$

(singular point in the perturbation expansion)

t	$\eta(0,t)$		$\Delta\eta(0,t)$	$\eta(\pi,t)$		$\Delta\eta(\pi,t)$	area
	num.	pert.		num.	pert.		12.566
0.0	4.100	-	-	3.900	-	-	12.566
0.5	4.109	-	-	3.891	-	-	12.566
1.0	4.139	-	-	3.861	-	-	12.566
1.5	4.195	-	-	3.805	-	-	12.566
2.0	4.288	-	-	3.715	-	-	12.566
2.5	4.430	-	-	3.574	-	-	12.565
3.0	4.643	-	-	3.367	-	-	12.565

TABLE 1.5 (cont'd)

(d) K = 0.7

t	η(0,t)		Δη(0,t)	η(π,t)		Δη(π,t)	area
	num.	pert.		num.	pert.		
0.0	4.100	4.100	-	3.900	3.900	-	12.566
0.5	4.106	4.106	.000	3.894	3.894	.000	12.566
1.0	4.126	4.127	.001	3.874	3.874	.000	12.566
1.5	4.162	4.164	.002	3.838	3.838	.000	12.566
2.0	4.219	4.225	.006	3.782	3.783	.001	12.566
2.5	4.303	4.317	.014	3.699	3.702	.003	12.566
3.0	4.423	4.455	.032	3.579	3.589	.010	12.566

would expect. In particular, by comparing the case K = 0.7 at t = 2.0 with the case K = 0.3 at t = 1.5, it is seen that the increased surface tension has retarded the growth of the former to an amplitude similar to the latter by a time of .5 seconds. It can also be seen that the disagreements between the analytic and numerical solutions for the spike and bubble tip displacements are less than .01 in all cases for times as large as t = 1.5 and that agreement for larger times improves with decreased growth rate. The divergence of the two solutions takes the form of a decreased spike amplitude and an increased bubble amplitude for the numerical solutions when compared to the analytic solutions. We also note that the divergence is consistently smaller at the slower growing bubble tip. A precise determination of which solutions are closer to the "true" solution is of course, not possible. On the one hand, the numerical solution will contain the effects of truncation, convergence and round-off errors, while on the other hand, the perturbation solution ignores higher order effects and ceases to be valid for times of the order of ten seconds. However, since the agreement between the two solutions to t = 3.0 increases with increased K (decreased growth rate) and that the numerical solution then conserves the area better as well, and since the time of validity of the perturbation solution should be invariant with K, it seems

likely that the divergence is principally due to the growth of amplitude-dependent error in the numerical scheme. This is further supported by the observation that the divergence is less at the slower growing bubble tip than at the faster growing spike tip in all of the solutions. Results showing $\Delta a(x,t)$ where

$$\Delta a(x,t) = [\eta(x,t) - h]/\varepsilon^{\dagger}$$

are plotted in Figure 1.4 for the case corresponding to Table 1.5(c).

We shall next investigate the effect of initial amplitude on growth rate. We choose $K = .7$ and compare the cases $\varepsilon = .1$, $\varepsilon = .2$ and $\varepsilon = .4$. In Table 1.6 results to only $t = 2.0$ are given since calculations for $\varepsilon = .4$ failed the monoticity test at $t = 2.34$. Values of $\Delta a(x,t)$ at the end points and at the latest time are also given.

The numerical and perturbation solutions disagree qualitatively as well as quantitatively at the fluid spike. Here the former indicates an inverse relationship between the growth rate and the initial amplitude while the latter indicates the reverse. Also, it is seen from Table 1.6(b), (c) that unlike (a) and the results from Table 1.5 that initially the perturbation solutions for the bubble tip show a slightly increased amplitude relative to the

† η values more accurate than the table values (which are rounded to the third decimal) are used in these calculations.

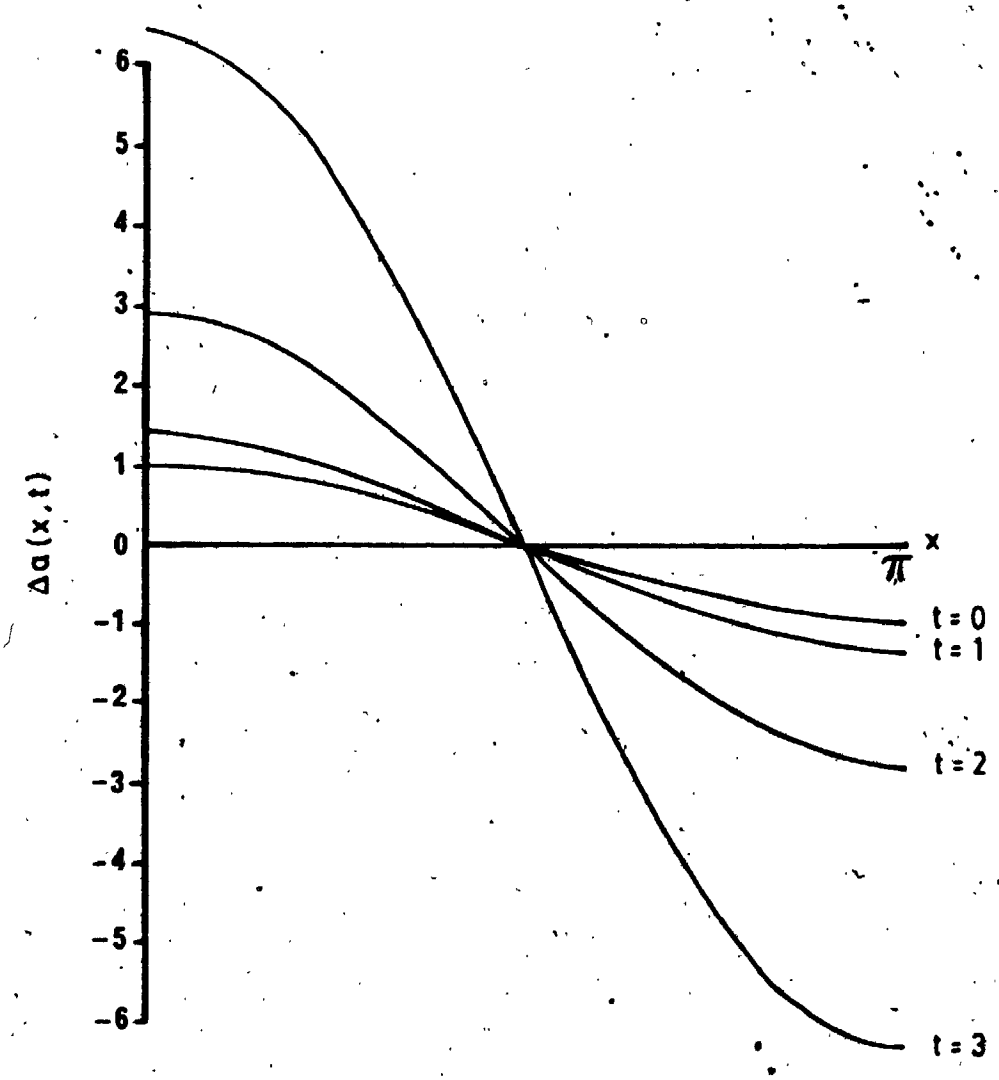

FIGURE 1.4 Monotonic growth; K = .5, ϵ = .1, h = 4.

TABLE 1.6 EFFECT OF INITIAL AMPLITUDE ON GROWTH RATE

(a) $\varepsilon = .1$

t	$\eta(0,t)$ num.	$\eta(0,t)$ pert.	$\Delta\eta(0,t)$	$\eta(\pi,t)$ num.	$\eta(\pi,t)$ pert.	$\Delta\eta(\pi,t)$	area
0.0	4.100	4.100	-	3.900	3.900	-	12.566
0.5	4.106	4.106	.000	3.894	3.894	.000	12.566
1.0	4.126	4.127	.001	3.874	3.874	.000	12.566
1.5	4.162	4.164	.002	3.838	3.838	.000	12.566
2.0	4.219	4.225	.006	3.782	3.783	.001	12.566

$\Delta a(0,2)$		$\Delta a(\pi,2)$	
2.190	2.246	-2.182	-2.172

TABLE 1.6 (cont'd)

(b) $\varepsilon = .2$

t	$\eta(0,t)$		$\Delta\eta(0,t)$	$\eta(\pi,t)$		$\Delta\eta(\pi,t)$	area
	num.	pert.		num.	pert.		
0.0	4.200	4.200	-	3.800	3.800	-	12.566
0.5	4.212	4.213	.001	3.788	3.787	-.001	12.566
1.0	4.252	4.255	.003	3.749	3.747	-.002	12.566
1.5	4.324	4.332	.008	3.678	3.677	-.001	12.566
2.0	4.436	4.459	.023	3.567	3.571	.004	12.566

$\Delta a(0,2)$		$\Delta a(\pi,2)$	
2.178	2.297	-2.166	-2.147

TABLE 1.6 (cont'd)

(c) $\varepsilon = .4$

t	$\eta(0,t)$ num.	$\eta(0,t)$ pert.	$\Delta\eta(0,t)$	$\eta(\pi,t)$ num.	$\eta(\pi,t)$ pert.	$\Delta\eta(\pi,t)$	area
0.0	4.400	4.400	-	3.600	3.600	-	12.566
0.5	4.423	4.427	.004	3.578	3.573	-.005	12.566
1.0	4.500	4.516	.016	3.504	3.492	-.012	12.566
1.5	4.641	4.686	.045	3.367	3.354	-.013	12.566
2.0	4.851	4.975	.124	3.156	3.155	-.001	12.566

$\Delta a(0,2)$		$\Delta a(\pi,2)$	
2.128	2.439	-2.111	-2.113

numerical solutions but that this tends to the reverse for later times so that the numerical solution again tends to give smaller spike amplitudes and larger bubble amplitudes than the perturbation solution. One may also note that, similar to previous results, there is a general increase in disagreement between the two solutions with increased initial amplitude. While it is again probable that this is partly due to numerical amplitude-dependent error it is also possible that the effects of reduced times of validity for the larger initial amplitudes contribute substantially.

In Table 1.7 we compare the effects of differing average initial fluid depths on the growth rate to t = 3.0. We choose K = 0.7, ε = .1 and the cases h = 4.0, h = 3.0, h = 2.0 and h = 1.0.

Table 1.7 shows a definite decrease of growth rate with decreasing h. The relatively small differences for both solutions between the h = 4.0 and h = 3.0 cases indicate that a choice of say, h = 8.0, could be used to approximate the case of infinite fluid depth.

We shall next examine the growth for disturbances with wave-numbers equal to the linear cut-off i.e., K = 1. According to Nayfeh's determination of the non-linear amplitude-dependent cut-off given by (1.3.12) i.e.,

TABLE 1.7 EFFECT OF h ON GROWTH RATE

(a) h = 4.0

t	$\eta(0,t)$		$\Delta\eta(0,t)$	$\eta(\pi,t)$		$\Delta\eta(\pi,t)$	area
	num.	pert.		num.	pert.		
0.0	4.100	4.100	-	3.900	3.900	-	12.566
0.5	4.106	4.106	.000	3.894	3.894	.000	12.566
1.0	4.126	4.127	.001	3.874	3.874	.000	12.566
1.5	4.162	4.164	.002	3.838	3.838	.000	12.566
2.0	4.219	4.225	.006	3.782	3.783	.001	12.566
2.5	4.303	4.315	.014	3.699	3.702	.003	12.566
3.0	4.423	4.455	.032	3.579	3.589	.010	12.566

$\Delta a(0,3)$		$\Delta a(\pi,3)$	
4.229	4.455	-4.205	-4.111

TABLE 1.7 (cont'd)

(b) $h = 3.0$

t	$\eta(0,t)$ num.	$\eta(0,t)$ pert.	$\Delta\eta(0,t)$	$\eta(\pi,t)$ num.	$\eta(\pi,t)$ pert.	$\Delta\eta(\pi,t)$	area
0.0	3.100	3.100	-	2.900	2.900	-	9.425
0.5	3.106	3.106	.000	2.894	2.894	.000	9.425
1.0	3.126	3.127	.001	2.874	2.874	.000	9.425
1.5	3.162	3.164	.002	2.838	2.838	.000	9.425
2.0	3.219	3.224	.005	2.782	2.783	.001	9.425
2.5	3.302	3.316	.014	2.699	2.704	.005	9.424
3.0	3.422	3.453	.031	2.579	2.591	.012	9.424

$\Delta a(0,3)$		$\Delta a(\pi,3)$	
4.225	4.529	-4.210	-4.091

TABLE 1.7 (cont'd)

(c) h = 2.0

t	η(0,t)		Δη(0,t)	η(π,t)		Δη(π,t)	area
	num.	pert.		num.	pert.		
0.0	2.100	2.100	-	1.900	1.900	-	6.283
0.5	2.106	2.106	.000	1.894	1.894	.000	6.283
1.0	2.126	2.126	.000	1.875	1.875	.000	6.283
1.5	2.160	2.162	.002	1.840	1.841	.001	6.283
2.0	2.215	2.220	.005	1.786	1.788	.002	6.283
2.5	2.296	2.308	.012	1.707	1.712	.005	6.283
3.0	2.411	2.439	.028	1.594	1.605	.011	6.282

Δa(0,3)		Δa(π,3)	
4.112	4.393	-4.063	-3.950

TABLE 1.7 (cont'd)

(d) $h = 1.0$

t	$\eta(0,t)$ num.	$\eta(0,t)$ pert.	$\Delta\eta(0,t)$	$\eta(\pi,t)$ num.	$\eta(\pi,t)$ pert.	$\Delta\eta(\pi,t)$	area
0.0	1.100	1.100	-	.900	.900	-	3.142
0.5	1.105	1.105	.000	.895	.895	.000	3.142
1.0	1.121	1.121	.000	.881	.881	.000	3.142
1.5	1.148	1.149	.001	.855	.855	.000	3.142
2.0	1.191	1.194	.003	.816	.817	.001	3.142
2.5	1.252	1.260	.008	.761	.763	.002	3.141
3.0	1.337	1.356	.019	.688	.690	.002	3.141

$\Delta a(0,3)$		$\Delta a(\pi,3)$	
3.375	3.556	-3.124	-3.102

$$k_{cn} = [1 + \frac{3}{8}\varepsilon^2 - \frac{21}{514}\varepsilon^4]^{1/2} + O(\varepsilon^6),$$

disturbances with $k = k_c$ should still grow. We choose $h = 4.0$ and the cases $\varepsilon = .1$, $\varepsilon = .2$, $\varepsilon = .4$ which correspond respectively to $k_{cn} \approx 1.002$, 1.007, 1.029. Because the value $K = 1.0$ is so close to the non-linear cut-off for these cases we would expect to see little if any growth in the numerical results. Since $K-1$ is within $O(\varepsilon^2)$ the perturbation solution in this case is given by (1.3.10) which requires the numerical solution of (1.3.11). However, since the growth is expected to be small, the introduction of numerical error into (1.3.10) would make subsequent comparison with the numerical solution rather meaningless and hence we shall present only the latter. Table 1.8 shows times until $t = 3.0$ for the cases $\varepsilon = .1$ and $\varepsilon = .2$ but only to $t = 1.5$ for $\varepsilon = .4$ since this case is found to fail the monoticity test at $t = 1.58$.

As Nayfeh predicts, the results do show that there is still growth at the linear cut-off wave number. However, comparison with Table 1.6 ($K = .7$) shows that the trend of the numerical solution to yield increased growth rates for decreased initial amplitudes is reversed in Table 1.8. Also different from the other tables is the fact

TABLE 1.8 EFFECT OF INITIAL AMPLITUDE ON GROWTH AT K = 1.0

(a) $\varepsilon = .1$

t	$\eta(0,t)$	$\eta(\pi,t)$	area
0.0	4.100	3.900	12.566
0.5	4.100	3.900	12.566
1.0	4.100	3.900	12.566
1.5	4.100	3.900	12.566
2.0	4.101	3.899	12.566
2.5	4.101	3.899	12.566
3.0	4.102	3.898	12.566

$\Delta a(0,1.5) = 1.004$ $\Delta a(\pi,1.5) = -1.004$

$\Delta a(0,3) = 1.011$ $\Delta a(\pi,3) = -1.016$

TABLE 1.8 (cont'd)

(b) $\varepsilon = .2$

t	$\eta(0,t)$	$\eta(\pi,t)$	area
0.0	4.200	3.800	12.566
0.5	4.200	3.800	12.566
1.0	4.201	3.799	12.566
1.5	4.203	3.797	12.566
2.0	4.205	3.795	12.566
2.5	4.209	3.791	12.566
3.0	4.213	3.787	12.566

$\Delta a(0,1.5) = 1.016$ $\Delta a(\pi,1.5) = -1.016$

$\Delta a(0,3) = 1.065$ $\Delta a(\pi,1.5) = -1.065$

TABLE 1.8 (cont'd)

(c) $\varepsilon = .4$

t	$\eta(0,t)$	$\eta(\pi,t)$	area
0.0	4.400	3.600	12.566
0.5	4.398	3.602	12.566
1.0	4.407	3.594	12.566
1.5	4.423	3.575	12.567

$\Delta a(0,1.5) = 1.059$ $\Delta a(\pi,1.5) = -1.062$

that in this case the growth rate of the bubble tip appears to be equal to or greater than the growth rate of the spike tip. The entries of Table 1.8(c) are of particular interest in that they indicate an initial tendency for the disturbance amplitude to diminish before switching to monotonic growth. Whether this behaviour is physically realistic or merely due to vagaries of the numerical scheme is not known.

For the last investigation we shall examine the effect of initial amplitude on the oscillation frequency for a wave-number greater than the non-linear cut-off. We shall choose h = 4.0 with initial amplitudes of ε = .1, .2, .4 and K = 1.5. These choices of ε and K should again allow us to use (1.3.3) which now becomes a uniformly valid expansion (see 1.3). For these calculations, the monoticity test is removed; the displacements of the spike and bubble tips are printed out at each time step and the displacement of the whole interface is printed out every .5 seconds. The case ε = .1 was run to t = 6.5 at which time the saw-tooth instability was found to appear. Therefore these last values will not be given in Table 1.9. The cases ε = .2, .4 ran to t = 3.84 and t = 2.58 respectively, before failing to meet the convergence criterion (1.5.21) in the required number of iterations. The off-set values in Table 1.9 give the times and corresponding displacements of the spike and bubble tips after one oscillation.

TABLE 1.9 EFFECT OF INITIAL AMPLITUDE ON OSCILLATION FREQUENCY

(a) $\varepsilon = .1$

t	$\eta(0,t)$		$\Delta\eta(0,t)$	$\eta(\pi,t)$		$\Delta\eta(\pi,t)$	area
	num.	pert.		num.	pert.		
0.0	4.100	4.100	-	3.900	3.900	-	12.566
0.5	4.085	4.085	.000	3.915	3.915	.000	12.566
1.0	4.045	4.045	.000	3.955	3.956	.001	12.566
1.5	3.991	3.991	.000	4.009	4.011	.002	12.566
2.0	3.940	3.939	-.001	4.060	4.062	.002	12.566
2.5	3.907	3.906	-.001	4.093	4.093	.000	12.566
3.0	3.902	3.902	.000	4.098	4.098	.000	12.566
3.5	3.926	3.928	.002	4.074	4.073	-.001	12.566
4.0	3.973	3.975	.002	4.027	4.026	-.001	12.566
4.5	4.028	4.030	.002	3.972	3.971	-.001	12.566
5.0	4.074	4.076	.002	3.926	3.925	-.001	12.566
5.5	4.098	4.098	.000	3.902	3.901	-.001	12.566
5.65	4.100	5.64	4.100	5.67	3.900	5.64	3.900
6.0	4.093	4.092	-.001	3.907	3.908	.001	12.566

TABLE 1.9 (cont'd)

(b) $\epsilon = .2$

t	$\eta(0,t)$ num.	$\eta(0,t)$ pert.	$\Delta\eta(0,t)$	$\eta(\pi,t)$ num.	$\eta(\pi,t)$ pert.	$\Delta\eta(\pi,t)$	area
0.0	4.200	4.200	-	3.800	3.800	-	12.566
0.5	4.170	4.171	.001	3.830	3.830	.000	12.566
1.0	4.092	4.093	.001	3.909	3.912	.003	12.567
1.5	3.984	3.988	.004	4.016	4.021	.005	12.567
2.0	3.882	3.884	.002	4.118	4.120	.002	12.566
2.5	3.815	3.814	-.001	4.184	4.185	.001	12.566
3.0	3.802	3.803	.001	4.197	4.197	.000	12.566
3.5	3.848	3.850	.002	4.152	4.152	.000	12.567
4.0		3.943	-		4.063	-	-
4.5		4.053	-		3.955	-	-
5.0		4.145	-		3.859	-	-
5.5		4.194	-		3.804	-	-
	5.72	4.199	-	5.70	3.799	-	-
6.0		4.189	-		3.811	-	-

TABLE 1.9 (cont'd)

(c) $\varepsilon = .4$

t	$\eta(0,t)$ num.	$\eta(0,t)$ pert.	$\Delta\eta(0,t)$	$\eta(\pi,t)$ num.	$\eta(\pi,t)$ pert.	$\Delta\eta(\pi,t)$	area
0.0	4.400	4.400	-	3.600	3.600	-	12.566
0.5	4.342	4.346	.004	3.657	3.655	-.002	12.566
1.0	4.201	4.206	.005	3.801	3.812	.011	12.567
1.5	3.989	4.013	.025	4.011	4.023	.012	12.567
2.0	3.788	4.805	.017	4.215	4.216	.001	12.567
2.5	3.645	3.649	.004	4.353	4.349	-.004	12.567
3.0	-	3.600	-	-	4.400	-	-
3.5	-	3.662	-	-	4.343	-	-
4.0	-	3.820	-	-	4.197	-	-
4.5	-	4.032	-	-	4.003	-	-
5.0	-	4.225	-	-	3.798	-	-
5.5	-	4.353	-	-	3.643	-	-
	5.98	4.398	-	-	5.94 3.598	-	-
6.0	-	4.398	-	-	3.599	-	-

From the table values we can calculate that at $t = 2.5$ the surface has passed through approximately .965 of a half cycle of oscillation for $\epsilon = .1$ while the values for $\epsilon = .2$ and $\epsilon = .4$ are about .961 and .943 respectively. Therefore the numerical results are similar to the perturbation results in that they both predict increased frequencies of oscillation for decreased amplitudes. The agreement on instantaneous displacements between the two solutions is particularly good for the $\epsilon = .1$ case throughout the calculations. The agreement on the period is also good, the difference being approximately .02 seconds. The results for the $\epsilon = .1$ case also show that after one oscillation the amplitude has not sensibly changed. Unfortunately, due to the growth of the saw-tooth instability, we are prevented from determining numerically whether this amplitude time-independence continues. However, for the cases $\epsilon = .2, .4$, the perturbation solution seems to indicate that, while the maximum spike tip to bubble tip displacement may not change, asymmetries in the sine wave are developing that allow for slightly different periods at these points. Numerically obtained values of $\Delta a(x,t)$ for the whole interface corresponding to the $\epsilon = .1$ case are plotted in Figures 1.5(a),(b),(c). The growth is monotonic in each figure and results to $t = 6.5$ have been included. The saw-tooth instability that first becomes evident at

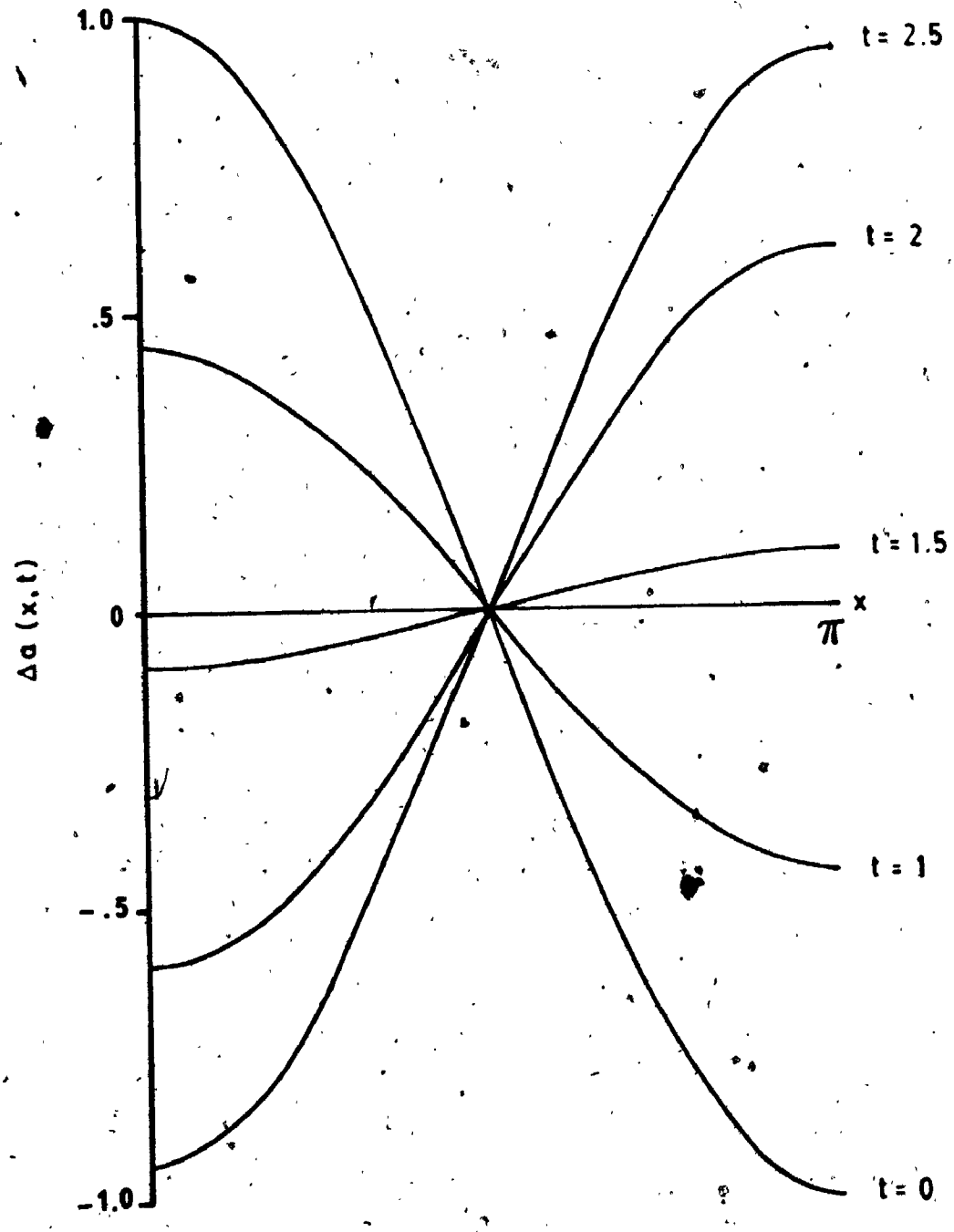

FIGURE 1.5(a) Oscillatory behaviour; K = 1.5, ϵ = .1, h = 4

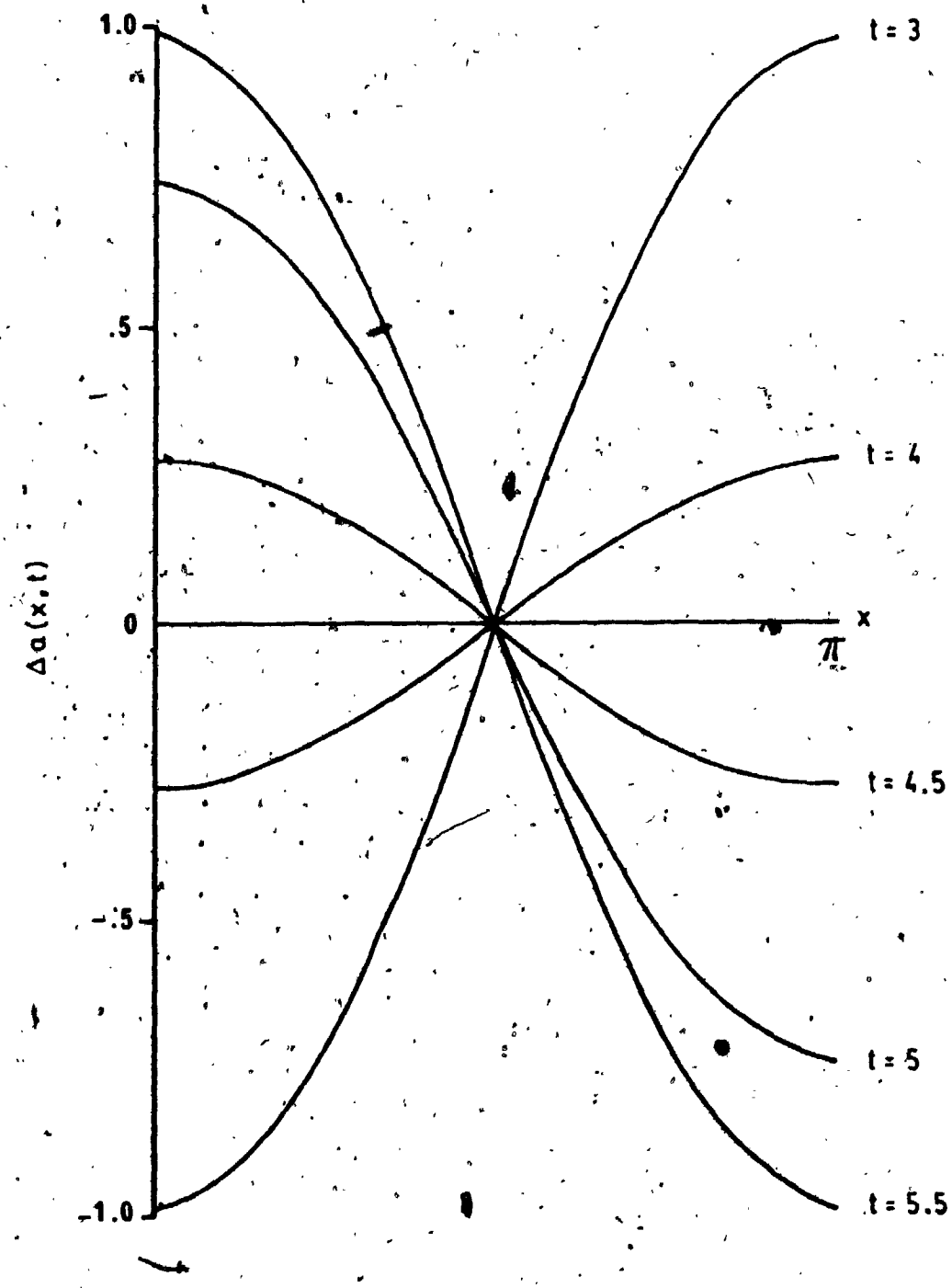

FIGURE 1.5(b) Oscillatory behaviour cont'd.,

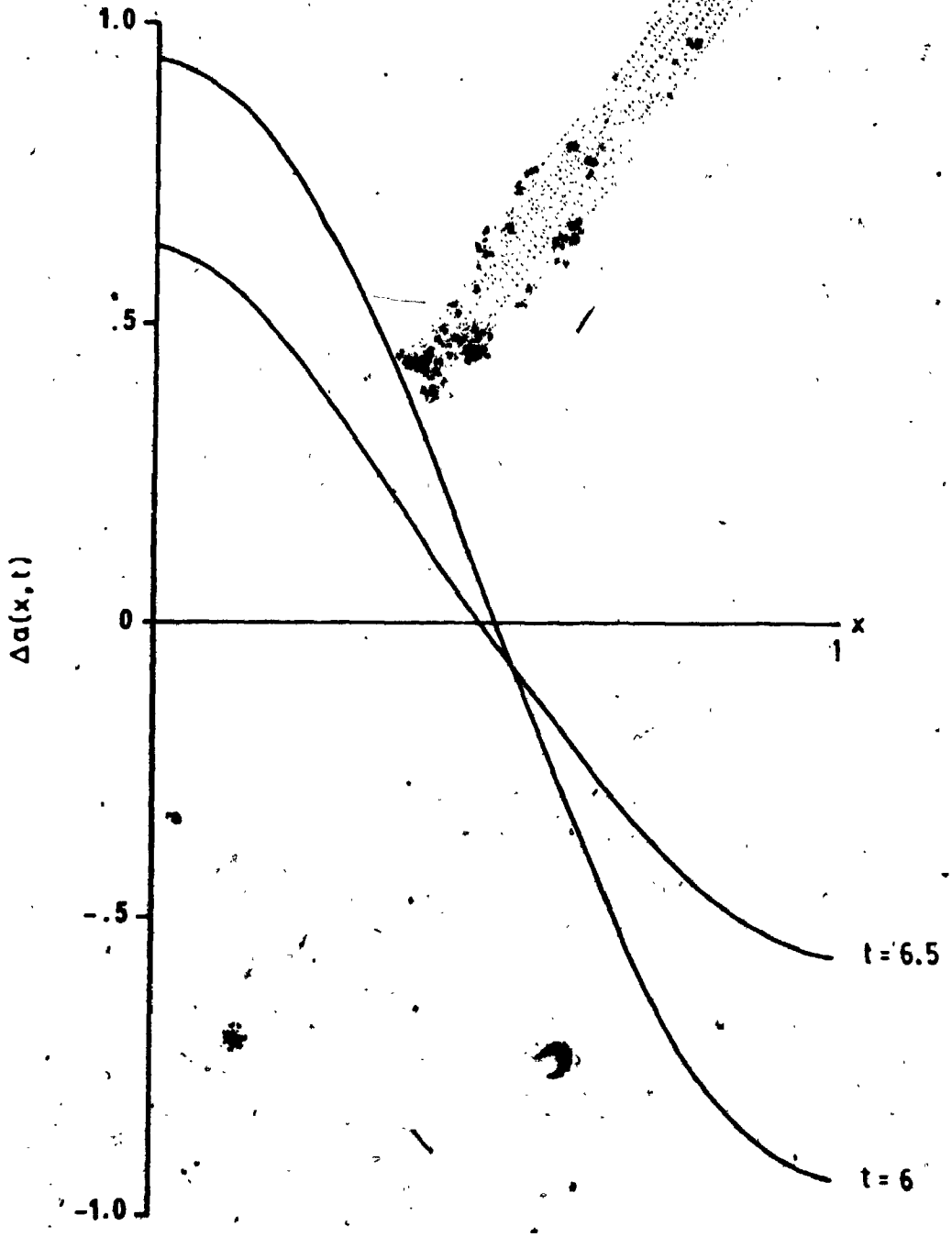

FIGURE 1.5 (c) Oscillatory behaviour cont'd.

t = 6.5 is not discernible from the corresponding plot since the oscillation occurs in the third decimal place.

1.8 CONCLUSIONS

In most cases the numerical results are seen to be in qualitative agreement with the predictions of Nayfeh's perturbation theory (see 1.3).

For K = 1.5 there is good quantitative agreement, especially in the $\varepsilon = .1$ case. For $K < 1.0$, there is good quantitative agreement only for small amplitudes and short times. For larger amplitudes and longer times the agreement degrades and the numerical solution gives smaller spike amplitudes and larger bubble amplitudes than the perturbation solution. This divergence is thought to be due mainly to the growth of amplitude-dependent error in the numerical scheme resulting, principally, from inaccuracies in the determination of increasing η_x and η_{xx} values. Evidence for this (besides that already mentioned in 1.5 concerning the use of higher order finite difference formulae) would seem to be given by the observation that the run times of the $\varepsilon = .4$ case are found to decrease in the order $K = .5$, $K = .7$, $K = 1.0$. Reference to (1.5.18) reveals that this exactly anti-parallels the emphasis of the non-linear curvature term which involves these derivatives. However, a subsequent trial calculation for this case using

$K = 0.0$ (i.e., the curvature is neglected) was not found to run longer or to larger amplitudes than for $K = 0.5$. This seems to indicate that the growth of the numerical error is dependent not only on the magnitude of the amplitude but also on its rate of growth. On this basis, one would expect that the $\varepsilon = .4$, $K = 1.0$ case would run much longer considering the small growth. Perhaps the failure to do so is related to the small initial contraction of the amplitude.

In any event, whatever the precise mechanics of the error growth may be, it is evident that our co-ordinate transformation technique is not suitable for the investigation of growth to large distortions in Rayleigh-Taylor instability. Hence we have not tested predictions on later stage growth.

ADDENDUM - VALUES OF RELAXATION PARAMETERS

SOV: $\omega = 1.65$, $\omega^* = 1.2$, $\omega' = 1.0$

SONV: $\omega = 1.7$, $\omega^* = 1.0$, $\omega' = 1.0$

FONV: $\omega = 1.0$, $\omega^* = 1.0$, $\omega' = 1.0$

CHAPTER II

SOLUTION OF A MELTING/SOLIDIFICATION FRONT INSTABILITY PROBLEM

2.1 INTRODUCTION

In this chapter we shall numerically solve another problem associated with interfacial stability. Here, the interface will represent the line of demarcation between the solid and liquid phases of a system that may be undergoing a process of melting or solidification. Chadam and Ortoleva [1981] have developed a simple model of the above processes that may be thought of as pertaining to a pure substance in a melt and have presented a perturbation analysis based on this model. Their results indicate that planar melting is linearly stable with respect to a small shape perturbation with or without surface tension, while planar solidification is linearly unstable without surface tension and linearly stable with its inclusion. Our purpose is to determine if these qualitative predictions can be confirmed numerically.

Change of phase may involve any or all of the following types of transformation (Fine [1964]): (1) change in structure, (2) change in composition, and (3) change in degree of order. In general, problems involving phase changes in a system are extremely complicated and defy

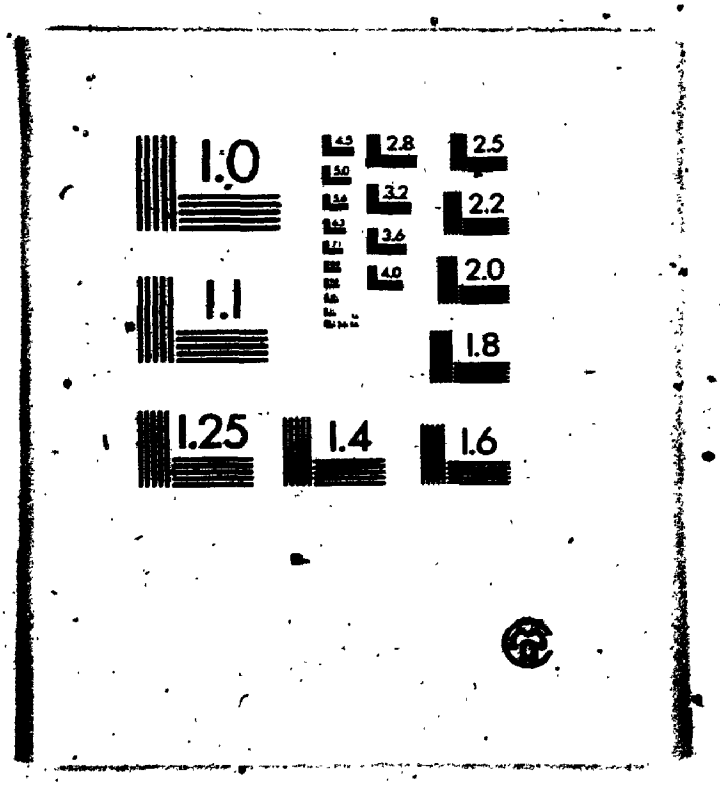

mathematical treatment without the use of severely simplifying assumptions. Usually, the possibility of convection in the fluid is omitted as well as a number of potentially crucial effects caused by impurities or other defects in the system. As well, it is usually assumed that all interfaces are molecularly rough (i.e., not faceted) and that all effects of crystalline anisotropy can be neglected. These anisotropies may be manifest as orientational dependencies in the surface tension, the molecular attachment kinetics at the interface or the heat flow in the solid to name but a few possibilities (Langer [1980]). It is also common practice to approximate conditions near the interface as being consistent with a state of local thermodynamic equilibrium despite the fact that this can only be rigorously true if the interface is stationary and to assume that the density of the system remains constant.

Other approximations are often introduced by the necessity of specifying "response" functions for the interface (Baker and Cahn [1971]). These functions reflect the thermodynamics and/or the molecular attachment kinetics mentioned above in that they describe the response of the interface to these factors. For example, in the case of a binary system, the solid and liquid compositions near the interface may be given as functions of the interfacial temperature and velocity. In simpler systems, these

functions are usually determined experimentally while in the case of more complex systems more approximate determinations are necessary.

For some of the mathematical details of processes involving phase changes in general see Fine [1964] and for those involving solidification (or melting) in particular see Baker and Cahn [1971], Tiller [1971] and Cole [1971].

In the next section (2.2), we shall present the model developed by Chadam and Ortoleva. Then in section 2.3 we shall give a review of some of the more important experimental and analytic work pertaining to the morphological stability of an interface in a developing (solidifying or melting) system. Section 2.4 will review numerical work and section 2.5 will outline our methods of solution. Section 2.6 will present general results as well as details of numerical testing and an attendant discussion. Lastly, section 2.7 will present a brief conclusion.

2.2 THE MODEL OF CHADAM AND ORTOLEVA

The model to be presented may be thought of as a simplified version of a solid composed of a pure substance developing (solidifying or melting) in a melt. The melt may be considered to be made up of a solute consisting of the pure substance dissolved in a solvent. The system is assumed to be isotropic and isothermal and the solid

density ρ, is assumed to remain constant. Also, mass transport in the melt is limited to diffusion.

We take the solid/melt interface to be $y = \eta(x,t)$ with the solid occupying $y > \eta(x,t)$ [†] and the liquid occupying $y < \eta(x,t)$ where $-\infty < x < \infty$, $-\infty < y < \infty$. The solute concentration in the melt $c(x,y,t)$ (expressed as mass per unit volume), satisfies the well known diffusion equation i.e.,

$$\frac{\partial c}{\partial t} = D\,(c_{xx}+c_{yy}) \quad \text{for } y < \eta(x,t),\ t > 0 \qquad (2.2.1)$$

where D is the diffusivity of the solute.

The kinematic condition at the interface is $d[\eta(x,t)-y] = 0$ which gives

$$\frac{\partial \eta}{\partial t} = \frac{dy}{dt} - \frac{\partial \eta}{\partial x}\frac{dx}{dt}\,. \qquad (2.2.2)$$

This can be written as

$$\frac{\partial \eta}{\partial t} = \vec{q}\,.\,(-\vec{n}) \qquad (2.2.3)$$

where $\vec{q}$ $(= \hat{i}\,dx/dt + \hat{j}\,dy/dt)$ represents the velocity at the interface and $\vec{n}$ $(= \hat{i}\,\partial\eta/\partial x - \hat{j})$ represents a vector normal to the interface and pointing into the liquid.

The equation representing the conservation of mass condition at the interface is (Sekerka [1973]§ 15.2)

---

† We note that the original formulation of Chadam and Ortoleva expresses the interface in terms of the surface $S(x,y,t) = \eta(x,t)-y = 0$.

$$D\vec{\nabla}c.\vec{n} = (\rho-c)\vec{q} \cdot \vec{n} \ . \qquad (2.2.4)$$

Substituting for $\vec{q} \cdot \vec{n}$ from (2.2.3) gives

$$D\vec{\nabla}c.\vec{n} = -(\rho-c)\ \frac{\partial \eta}{\partial t} \ . \qquad (2.2.5)$$

A typical response function for the normal growth (or melting) velocity $\vec{q} \cdot \frac{\vec{n}}{|\vec{n}|}$ is given by

$$\vec{q} \cdot \frac{\vec{n}}{|\vec{n}|} = q^*[c-c_{eq}(1 + r^*\beta)] \qquad (2.2.6)$$

where the surface reaction rate q^*, the planar concentration c_{eq}, and r^* are non-negative constants and the mean curvature β is given by

$$\beta = \eta_{xx}/2(1 + \eta_x^2)^{3/2} \ . \qquad (2.2.7)$$

If the rate q^* is taken to be very large, say $q^* >> 1$, then the interface is maintained at approximately the equilibrium concentration

$$c = c_{eq}(1 + r^*\beta) \ .$$

If we make this assumption the problem becomes (taking $D = 1$ with no loss of generality):

$$\frac{\partial c}{\partial t} = \frac{\partial^2 c}{\partial x^2} + \frac{\partial^2 c}{\partial y^2} \quad y < \eta(x,t), \ -\infty<x<\infty, \ t>0 \qquad (2.2.8a)$$

$$c = c_{eq}(1 + r^*\beta) \qquad (2.2.8b)$$

$$\text{on } y=\eta(x,t), t>0$$

$$\vec{\nabla}c \cdot \vec{n} = -(\rho-c)\ \frac{\partial \eta}{\partial t} \qquad (2.2.8c)$$

with

$$c(x,y,0) = c_o(x,y) \quad y < \eta(x,t) \tag{2.2.8d}$$

where

$$c_o(x,y) \to c_{-\infty} \geq 0 \text{ as } y \to -\infty. \tag{2.2.8e}$$

One more simplification is obtained by assuming $\rho >> c$. Letting $u = c - c_{eq}$ then also $\rho - c_{eq} >> u$ and the problem becomes:

$$\frac{\partial u}{\partial t} = \frac{\partial^2 u}{\partial x^2} + \frac{\partial^2 u}{\partial y^2} \quad y<\eta(x,t),\ -\infty<x<\infty,\ t>0 \tag{2.2.9a}$$

$$u = \gamma^*\beta \tag{2.2.9b}$$

$$\text{on } y=\eta(x,t),\ t>0$$

$$\vec{\nabla}u \cdot \vec{n} = -k^* \frac{\partial \eta}{\partial t} \tag{2.2.9c}$$

with

$$u(x,y,0) = u_o(x,y) \quad y < \eta(x,0) \tag{2.2.9d}$$

$$u_o(x,y) \to u_{-\infty} \text{ as } y \to -\infty \tag{2.2.9e}$$

where $\gamma^* = c_{eq}r^*$, $k^* = \rho - c_{eq}$, $u_o(x,y) = c_o(x,y) - c_{eq}$, $u_{-\infty} = c_{-\infty} - c_{eq}$, and we recall that $\vec{n} = \hat{i}\,\partial\eta/\partial x - \hat{j}$.

We note that for the case $\gamma^* = 0$ the problem reduces to the classic Stefan type (Rubinstein [1971]). When $\gamma^* \neq 0$ a higher interfacial concentration is required on the

surface of a protuberance into the liquid. Thus in the case of a growing solid, for example, the surface tension's flattening action mollifies the body's tendency to shoot dendrites straight out to regions of higher concentration. The stability of the interface in this model is determined by the interplay of these two mechanisms.

Chadam and Ortoleva have performed a linear perturbation analysis on the interfacial stability of this model by adapting a technique used by Rubinstein [1981] in his study that shows the standard two-phase Stefan problem to be morphologically stable under melting conditions. As we have mentioned previously, the results of Chadam and Ortoleva predict that planar melting is stable with respect to shape perturbations independent of surface tension but that planar solidification is an unstable process without surface tension effects and is completely stabilized with their inclusion.

2.3 REVIEW OF EXPERIMENTAL AND ANALYTIC WORK

Interface instability in solidification was first discussed in connection with experiments reported by Rutter and Chalmers [1953] on the unidirectional crystallization of dilute tin alloys in horizontal troughs. The resulting tin crystals exhibited corrugations on the upper surface of the solid and hexagonal cells on the growing

solid/liquid interface. It was found that these substructures could be suppressed by low speeds of growth and steep temperature gradients. Rutter and Chalmers postulated that impurities rejected† by the freezing solid concentrate ahead of the advancing interface in such a manner as to increase the equilibrium freezing temperature of the liquid adjacent to the interface above its actual temperature. They referred to this phenomenon as "constitutional supercooling" and argued that if this situation exists an irregularity on the interface would have the opportunity to grow spontaneously i.e., the interface could become unstable.

Tiller et al. [1953] showed analytically that the actual temperature of the liquid immediately adjacent to the interface agrees with the equilibrium freezing temperature at the crystallization front and that therefore constitutional supercooling exists if the actual temperature gradient in the liquid just ahead of the interface is less than the gradient of the equilibrium temperature there.

Sekerka [1968] details the results of a number of experiments designed to test the constitutional supercooling hypothesis as a predictor of interfacial stability.

---

† A solute is either preferentially incorporated or rejected at a solidification front. This leads to different solute concentrations in the solid and liquid and this difference is known as the "miscibility gap".

They appear to indicate that the hypothesis has some predictive merit. We note that this stability theory is based on thermodynamic considerations involving only the liquid and not the whole system. Also, dynamic factors such as diffusion and convection are completely ignored.

Mullins and Sekerka [1963] were the first to publish an interface stability theory for a solidifying system based on a first-order perturbation analysis. In particular, they studied the shape stability of a sphere of pure substance that is growing into a melt that is initially uniformly supersaturated. They determined a critical radius below which the sphere is stable with respect to an infinitesimal deformation and above which it is not. Mullins and Sekerka [1964] and Voronkov [1965] independently analysed the stability of a planar crystallization front to sinusoidal perturbations and have developed stability criteria. In the former this involved the determination of a critical disturbance wavelength while in the latter a critical value of the thermal gradient in the melt was found.

In the above analyses the principal physical assumptions are those of isotropy of bulk and surface parameters and of local equilibrium at the interface. Mass and thermal transport are assumed to be diffusive only and the rate of

evolution of the system is assumed to be limited only by these processes and not by molecular interfacial kinetics. The critical mathematical simplification is the use of steady state values (independent of time in the reference frame attached to the interface) for the chemical and thermal diffusion fields. In the case of the chemical diffusion field this is a good approximation only if the change in the interface is small in the time it takes concentration deviations to relax. If this is the case then the steady state assumption concerning the thermal field should also be justified since thermal diffusion is always a much faster process than chemical diffusion (Langer [1980]). Due to these steady state assumptions, the theories do not consider explicit time dependence of the growth of an unstable perturbation and so they do not admit direct comparison with experiment.

Coriell and Parker [1965] adapted the theory to the case of an infinitely long right circular cylinder and determined a critical radius for instability. Then in Coriell and Parker [1966] they studied the effect of surface diffusion along the interface on the stability of spherical and cylindrical shapes in an isothermal field and found that the inclusion of surface diffusion in the theory increases the critical radius of instability in each case. Coriell and Parker [1967] examined the effects of

molecular interfacial kinetics on the morphological stability of a sphere and found that slower kinetics could lead to a significant increase in the radius of instability.

Sekerka [1967] developed a fully time-dependent treatment (i.e. no steady-state approximations) of planar interfacial stability. Of most importance was his conclusion that the grosser details of the evolved (unstable) interface are independent of the shape of the initial perturbation. In a joint analytic and experimental study, Coriell and Hardy [1969] extended this theory to the case of a growing ice cylinder and they found good agreement between the experimental and theoretical results. Coriell, Hardy, and Sekerka [1971] developed a non-linear time-dependent theory and were able to obtain improved agreement with the previous experimental results.

A study of the effects of convective mixing on the morphological stability of a planar solidification front was performed by Hurle [1969] by employing a boundary layer model with the stability analysis. He found that the dependence of the critical disturbance wavelength on the temperature gradient in the liquid and the growth velocity is strongly influenced by the degree of convective mixing. Coriell et al. [1980] used a combined perturbation-numerical technique to study the onset of convective and interfacial

instabilities during the unidirectional solidification of a system without the assumption of constant density. They found that if the average velocity at the solidification front is greater than a critical value the predictions agree with the results of previous stability theory in which density changes and convection are neglected.

So far, all of the work that we have cited has dealt with solidifying systems and this is due primarily to the great interest in the practical problems of alloy solidification. However, Chen and Jackson [1971] have conducted experiments on the morphological stability at melting interfaces and have found good agreement with their results of a perturbation analysis. Of particular interest is the fact that while the predictions of the constitutional supercooling hypothesis and perturbation stability theory often more or less agree there is a greater difference between an analogous "constitutional superheating" hypothesis and the perturbation theory (Sekerka [1973]).

2.4 REVIEW OF NUMERICAL WORK

While there is an abundance of literature concerning the numerical solution of Stefan type problems (see for example reviews by Meyer [1978] and Shamsundar [1978]) this does not appear to be the case for the so-called "generalized" Stefan problem† of which the model of Chadam and

† A Stefan problem is referred to as "generalized when the problem variable is not constant at the interface.

Ortoleva is an example. In fact, we are aware of only one case in which a numerical solution has been presented.

Smith [1981] has solved a problem based on the model of a pure melt solidifying in a diffusive temperature field by employing a weak variational formulation method (also called an enthalpy or single-domain method). His results agree well with an approximate analytic solution. However, he was forced to use various ad hoc procedures such as "freezing" values of the local curvature after a number of iterations in order to obtain convergence in the solution of the temperature field.

We note that Fix [1978] and Ockendon [1978] have developed weak formulations for the alloy solidification problem but subsequent numerical results do not seem to have appeared. In the next section we shall present the details of our numerical method of solution for the problem given in section 2.2.

2.5 NUMERICAL METHOD OF SOLUTION

To solve the problem given by equation (2.2.9) numerically, we must first remove the infinities in x and y. To remove the former we shall assume the original planar interface is perturbed by a sinusoidal disturbance and that the concentration field becomes similarly periodic so that we need to deal only with a domain bounded in the x

direction by two successive extremal points (i.e., a half-wavelength). We remove the infinity in y by replacing (2.2.9e) by

$$u_o(x,y) \to u_{-\infty} \quad \text{as } y \to 0$$

and moving the interface up a distance h where h is finite. It is noted that we are implicitly assuming that if we choose a large enough value of h that the problem we solve will suitably approximate the original model.

We must also specify the function $u_o(x,y)$ as well as the parameters γ^*, k^* and $u_{-\infty}$. We choose $u_o(x,y)$ to satisfy Laplace's equation so that at $t = 0$ the melt concentration can be visualized as having achieved equilibrium throughout a domain that is constrained to having static boundaries. Then for times $t > 0$ we can consider the constraint on the interface to be removed so that it is free to adapt to the influences of $u_{-\infty}$ and the surface tension.

Thus, we first solve the equilibrium concentration problem

$$u_{o_{xx}} + u_{o_{yy}} = 0 \quad 0 < y < \eta(x,0),\ 0 \le x \le 1 \qquad (2.5.1a)$$

$$u_o = \gamma^* \eta_{xx}/2(1+\eta_x^2)^{3/2} \quad y = \eta(x,0) \qquad (2.5.1b)$$

$$u_o = u_{-\infty} \quad y = 0 \qquad (2.5.1c)$$

$$u_{o_x}(0,y) = \eta_x(0,0) = u_{o_x}(1,y) = \eta_x(1,0) = 0 \qquad (2.5.1d)$$

$$\eta(x,0) = a \cos \pi x + h \qquad (2.5.1e)$$

where a is the disturbance amplitude and we have written the mean curvature β explicitly. Then we solve the moving boundary problem

$$u_t = u_{xx} + u_{yy} \quad 0 < y < \eta(x,t), \; 0 \leq x \leq 1, \; t>0 \qquad (2.5.2a)$$

$$u = \gamma^* \eta_{xx} / 2(1+\eta_x^2)^{3/2} \qquad (2.5.2b)$$

$$y = \eta(x,t), \; t>0$$

$$\eta_t = (u_y - u_x \eta_x)/k^* \qquad (2.5.2c)$$

$$u = u_{-\infty} \qquad y = 0 \qquad (2.5.2d)$$

$$u_x(0,y,t) = \eta_x(0,t) = u_x(1,y,t) = \eta_x(1,t) = 0 \qquad (2.5.2e)$$

with the initial conditions

$$u(x,y,0) = u_o(x,y) \qquad (2.5.2f)$$

and

$$\eta(x,0) = a \cos \pi x + h \qquad (2.5.2g)$$

where (2.5.2c) has been obtained by writing $\vec{n}$ of (2.2.9c) explicitly.

As in the case of the Rayleigh-Taylor instability

problem that was solved earlier our method of solution will again involve the use of the co-ordinate transformation

$$x = x$$

$$z = y/\eta(x,t) \quad . \tag{2.5.3}$$

However, in this case, since our numerical solutions will only be intended for qualitative comparisons with the perturbative results the possibility that large amplitude solutions may not be obtained is unimportant.

After transformation (2.5.1) becomes:

$$u_{o_{xx}} + P(x,z)u_{o_{zz}} + Q^*(x,z)u_{o_{xz}} + U(x,z)u_{o_z} = 0$$

$$0<z<1,\ 0\leq x\leq 1 \tag{2.5.3a}$$

$$u_o = \gamma^*\eta_{xx}/2(1+\eta_x^2)^{3/2} \qquad z = 1 \tag{2.5.3b}$$

$$u_o = u_{-\infty} \qquad z = 0 \tag{2.5.3c}$$

$$u_{o_x}(0,z) = \eta_x(0,0) = u_{o_x}(1,z) = \eta_x(1,0) = 0 \tag{2.5.3d}$$

$$\eta(x,0) = a\cos\pi x + h \tag{2.5.3e}$$

where $P(x,z)$, $Q^*(x,z)$ and $U(x,z)$ are given by (1.5.11).

Similarly, (2.5.2) becomes:

$$u_t = u_{xx} + P(x,z)u_{zz} + Q^*(x,z)u_{xz} + U^*(x,z)u_z$$

$$0<z<1,\ 0\leq x\leq 1,\ t>0 \qquad (2.5.4a)$$

$$u = \gamma^*\eta_{xx}/2(1+\eta_x^2)^{3/2} \qquad (2.5.4b)$$

$$z=1, t>0$$

$$\eta_t = [(1+\eta_x^2)u_z/\eta - \eta_x u_x]/k^* \qquad (2.5.4c)$$

$$u = u_{-\infty} \qquad z = 0 \qquad (2.5.4d)$$

$$u_x(0,z,t) = \eta_x(0,t) = u_x(1,z,t)$$

$$= \eta_x(1,t) = 0 \qquad (2.5.4e)$$

$$u(x,y,0) = u_o(x,y) \qquad (2.5.4f)$$

$$\eta(x,0) = a\cos\pi x + h \qquad (2.5.4g)$$

where $U^*(x,z) = U(x,z) + z\eta_t/\eta$.

To solve (2.5.3) and (2.5.4) we have written two programs which we shall call SONV2 and FONV2. These are analogous to the programs SONV and FONV developed for the Rayleigh-Taylor instability problem in that SONV2 uses finite difference formulae that are accurate to second order for the discretization of the field equations while FONV2 uses fourth order formulae.† Fourth order formulae are again used for the discretization of interfacial terms

† All required finite difference formulae can be found in the Appendix.

and the solution for the field concentrations is carried out in a manner similar to that of the potential problem in Chapter I i.e., SOR by rows. In fact, for the initial equilibrium concentration problem (2.5.3) the algorithms (1.5.9) and (1.5.13) can be used for SONV2 and FONV2 respectively if one takes into account the new non-symmetry boundary condition $u = u_{-\infty}$ at $z = 0$. With this change the required formulae for (1.5.9) are still given by (1.5.12) if we replace ϕ by u (but otherwise use the same notation as in section 1.5) except that k now ranges from 2 to KMAX-1 instead of 1 to KMAX-1.

For the algorithm (1.5.13) the required formulae remain the same for the rows $k = 3,\ldots,KMAX-1$. For $k = 2$ they become:

$$
\begin{aligned}
M_{\ell-2,k} &= 1 + 10Q^*_{\ell,k}\gamma/12\Delta \\
M_{\ell-1,k} &= -16 - 80Q^*_{\ell,k}\gamma/12\Delta \\
M_{\ell,k} &= 30 + 15P_{\ell,k}\gamma^2/\Delta^2 + 10U_{\ell,k}\gamma^2/\Delta \\
M_{\ell+1,k} &= -16 + 80Q^*_{\ell,k}\gamma/12\Delta \\
M_{\ell+2,k} &= 1 - 10Q^*_{\ell,k}\gamma/12\Delta \\
W_{\ell,k} &= 12\gamma^2[P_{\ell,k}u^N_{zz_{\ell,k}} + Q^*_{\ell,k}u^N_{xz_{\ell,k}} + U_{\ell,k}u^N_{z_{\ell,k}}] \\
&\quad + 15P_{\ell,k}u^N_{\ell,k}\gamma^2/\Delta^2 + 10U_{\ell,k}u^N_{\ell,k}\gamma^2/\Delta.
\end{aligned}
\tag{2.5.5}
$$

In the case of the moving boundary problem (2.5.4) the field equation becomes explicitly time-dependent and we solve for the field concentrations by using the Crank-Nicholson method:

$$u^{N+1}_{\ell,k,p+1} = u_{\ell,k,p} + \frac{\Delta t}{2}[u_{t_{\ell,k,p}} + u^{N}_{t_{\ell,k,p+1}}]. \quad (2.5.6)$$

The formulae required for the iteration algorithms (1.5.9) and (1.5.13) now include this method implicitly. For (1.5.9) we have for the rows k = 2,...,KMAX-1:

$$S_{\ell-1,k} = -1$$

$$Q_{\ell,k} = 2[1+\gamma^2/\Delta t + \gamma^2 P_{\ell,k,p+1}/\Delta^2]$$

$$S_{\ell,k} = -1$$

$$W_{\ell,k} = 2\gamma^2 u_{\ell,k,p}/\Delta t$$

$$+ \gamma^2 [u_{xx_{\ell,k,p}} + Q^*_{\ell,k,p} u_{xz_{\ell,k,p}} \quad (2.5.7)$$

$$+ P_{\ell,k,p} u_{zz_{\ell,k,p}} + U^*_{\ell,k,p} u_{z_{\ell,k,p}}$$

$$+ Q^*_{\ell,k,p+1} u^N_{xz_{\ell,k,p+1}} + P_{\ell,k,p+1} u^N_{zz_{\ell,k,p+1}}$$

$$+ U^*_{\ell,k,p+1} u^N_{z_{\ell,k,p+1}}] + 2\gamma^2 P_{\ell,k,p+1} u^N_{\ell,k,p+1}/\Delta^2.$$

The formulae required for the algorithm (1.5.13) are given below.

For k = KMAX-1:

$$M_{\ell-2,k} = 1 - 10Q^*_{\ell,k,p+1}\gamma/12\Delta$$

$$M_{\ell-1,k} = -16 + 80Q^*_{\ell,k,p+1}\gamma/12\Delta$$

$$M_{\ell,k} = 30 + 15P_{\ell,k,p+1}\gamma^2/\Delta^2 - 10U^*_{\ell,k,p+1}\gamma^2/\Delta + 12\gamma^2/\Delta t$$

$$M_{\ell+1,k} = -16 - 80Q^*_{\ell,k,p+1}\gamma/12\Delta$$

$$M_{\ell+2,k} = 1 + 10Q^*_{\ell,k,p+1}\gamma/12\Delta$$

$$W_{\ell,k} = 12u_{\ell,k,p}\gamma^2/\Delta t + 6\gamma^2[u_{xx_{\ell,k,p}} + Q^*_{\ell,k,p}u_{xz_{\ell,k,p}} + P_{\ell,k,p}u_{zz_{\ell,k,p}} + U^*_{\ell,k,p}u_{z_{\ell,k,p}}] + 12\gamma^2[Q^*_{\ell,k,p+1}u^N_{xz_{\ell,k,p+1}} + P_{\ell,k,p+1}u^N_{zz_{\ell,k,p+1}} + U^*_{\ell,k,p+1}u^N_{z_{\ell,k,p+1}}] + 15P_{\ell,k,p+1}u^N_{\ell,k,p+1}\gamma^2/\Delta^2 - 10U^*_{\ell,k,p+1}u^N_{\ell,k,p+1}\gamma^2/\Delta - Q^*_{\ell,k,p+1}[10u^N_{\ell-2,k,p+1} - 80u^N_{\ell-1,k,p+1} + 80u^N_{\ell+1,k,p+1} - 10u^N_{\ell+2,k,p+1}]\gamma/12\Delta. \quad (2.5.8)$$

For k = 2:

$$M_{\ell-2,k} = 1 + 10Q^*_{\ell,k,p+1}\gamma/12\Delta$$

$$M_{\ell-1,k} = -16 - 80Q^*_{\ell,k,p+1}\gamma/12\Delta$$

$$M_{\ell,k} = 30 + 15P_{\ell,k,p+1}\gamma^2/\Delta^2 + 10U^*_{\ell,k,p+1}\gamma^2/\Delta + 12\gamma^2/\Delta t$$

$$M_{\ell+1,k} = -16 + 80Q^*_{\ell,k,p+1}\gamma/12\Delta$$

$$M_{\ell+2,k} = 1 - 10Q^*_{\ell,k,p+1}\gamma/12\Delta$$

$$W_{\ell,k} = 12u_{\ell,k,p}\gamma^2/\Delta t + 6\gamma^2[u_{xx_{\ell,k,p}} + Q^*_{\ell,k,p}u_{xz_{\ell,k,p}} + P_{\ell,k,p}u_{zz_{\ell,k,p}} + U^*_{\ell,k,p}u_{z_{\ell,k,p}}] + 12\gamma^2[Q^*_{\ell,k,p+1}u^N_{xz_{\ell,k,p+1}} + P_{\ell,k,p+1}u^N_{zz_{\ell,k,p+1}} + U^*_{\ell,k,p+1}u^N_{z_{\ell,k,p+1}}] + 15P_{\ell,k,p+1}u^N_{\ell,k,p+1}\gamma^2/\Delta^2 + 10U^*_{\ell,k,p+1}u^N_{\ell,k,p+1}\gamma^2/\Delta + Q^*_{\ell,k,p+1}[10u^N_{\ell-2,k,p+1} - 80u^N_{\ell-1,k,p+1} + 80u^N_{\ell+1,k,p+1} - 10u^N_{\ell+2,k,p+1}]\gamma/12\Delta. \quad (2.5.9)$$

Finally, for all the other rows i.e., k = 3,...,KMAX-2:

$$M_{\ell-2,k} = 1$$

$$M_{\ell-1,k} = -16$$

$$M_{\ell,k} = 30 + 30P_{\ell,k,p+1}\gamma^2/\Delta^2$$

$$M_{\ell+1,k} = -16$$

$$M_{\ell+2,k} = 1$$

(2.5.10)

$$W_{\ell,k} = 12u_{\ell,k,p}\gamma^2/\Delta t$$

$$+ 6\gamma^2[u_{xx_{\ell,k,p}} + Q^*_{\ell,k,p}u_{xz_{\ell,k,p}} + P_{\ell,k,p}u_{zz_{\ell,k,p}}$$

$$+ U^*_{\ell,k,p}u_{z_{\ell,k,p}}] + 12\gamma^2[Q^*_{\ell,k,p+1}u^N_{xz_{\ell,k,p+1}}$$

$$+ P_{\ell,k,p+1}u^N_{zz_{\ell,k,p+1}} + U^*_{\ell,k,p+1}u^N_{z_{\ell,k,p+1}}]$$

$$+ 30P_{\ell,k,p+1}u^N_{\ell,k,p+1}\gamma^2/\Delta^2.$$

Again, in a manner analogous to the case in the potential problem of Chapter I, the previous formulae and algorithms are easily modified at the beginning and end of each row by making use of the symmetry in the concentration about the vertical boundaries at $x = 0$ and $x = 1$. Also, we still employ the same LINPACK band matrix solver with both of the iteration algorithms. Iteration on the field concentration problem is stopped when the criterion

$$\max\left|u^{N+1}_{\ell,k,p+1} - u^{N}_{\ell,k,p+1}\right| < 10^{-6} \qquad (2.5.11)$$

is met.

We solve for the interface displacements $\eta_{\ell,p+1}$ by a predictor-corrector algorithm consisting of the following steps:

1) we predict

$$\eta_{\ell,p+1} = \eta^{o}_{\ell,p+1} = \eta_{\ell,p} + \Delta t \eta_{t_{\ell,p}} \qquad (2.5.12a)$$

$$u_{\ell,k,p+1} = u^{o}_{\ell,k,p+1} = u_{\ell,k,p} + \Delta t\, u_{t_{\ell,k,p}}$$

$$\text{for } 2 \leq k \leq \text{KMAX}-1 \qquad (2.5.12b)$$

where $\eta_{t_{\ell,p}}$ and $u_{t_{\ell,k,p}}$ are determined from the right-hand sides of (2.5.4c) and (2.5.4a) respectively,

2) we use $\eta^{o}_{\ell,p+1}$ to calculate $\eta^{o}_{x_{\ell,p+1}}$, $\eta^{o}_{xx_{\ell,p+1}}$, and $u^{o}_{\ell,\text{KMAX},p+1}$ (from the right-hand side of (2.5.4b)); from $u^{o}_{\ell,\text{KMAX},p+1}$ we calculate $u^{o}_{x_{\ell,\text{KMAX},p+1}}$ and we use $\eta^{o}_{\ell,p+1}$ and $u^{o}_{\ell,k,p+1}$ together to calculate $u^{o}_{z_{\ell,\text{KMAX},p+1}}$ and $u^{o}_{t_{\ell,k,p+1}}$,

3) we solve the field concentration problem to obtain the first corrected values

$$u_{\ell,k,p+1} = u^{1}_{\ell,k,p+1} = (1-\omega')u^{o}_{\ell,k,p+1} + \omega'\{u_{\ell,k,p} + \frac{\Delta t}{2}[u_{t_{\ell,k,p}} + u^{o}_{t_{\ell,k,p+1}}]\} \text{ for } 2 \leq k \leq \text{KMAX}-1, \qquad (2.5.13)$$

4) we calculate $u^1_{z_{\ell,KMAX,p+1}}$ from $\eta^0_{\ell,k,p+1}$ and $u^1_{\ell,k,p+1}$ and hence determine $\eta_{t_{\ell,p+1}}$

5) we obtain the first corrected values for the interface displacement from

$$\eta_{\ell,p+1} = \eta^1_{\ell,p+1} = (1-\omega^*)\,\eta^0_{\ell,p+1} + \omega^*\{\eta_{\ell,p} + \frac{\Delta t}{2}[\eta_{t_{\ell,p}} + \eta^0_{t_{\ell,p+1}}]\}, \qquad (2.5.14)$$

6) we continue correction by repeating steps 2) through 5), increasing the superscripts by one unit each cycle until the convergence criterion

$$\max\left|\eta^{M+1}_{\ell,p+1} - \eta^M_{\ell,p+1}\right| < 10^{-6} \qquad (2.5.15)$$

is satisfied.

If we use a grid such that $\Delta = \gamma$ then the Crank-Nicholson method employed in this algorithm yields a truncation error of $O(\Delta t^2 + \gamma^4)$ at the interface and either $O(\Delta t^2 + \gamma^2)$ or $O(\Delta t^2 + \gamma^4)$ in the field depending upon whether SONV2 or FONV2 is used. In the next section we shall give and discuss both the results of a calculation comparing these two methods as well as general results.

2.6 RESULTS AND DISCUSSION

In all of the following computations we use a finite

difference grid similar to that of Figure 1.3 with:

$$\gamma_\ell = \gamma = .05 \qquad 1 \le \ell < \text{LMAX} = 21$$

$$\Delta_k = \Delta = .05 \qquad 1 \le k < \text{KMAX} = 21 \tag{2.6.1}$$

Also, we shall always use the value 1.0 for the parameter k*.

The first results that we present are associated with planar melting. As such, we must choose $u_{-\infty} < 0$ (i.e., $c_{-\infty} < c_{eq}$) since sustained melting will only take place if the boundary at z = 0 acts like a solute sink. For the investigation of melting without surface tension, we choose the parameters of problems (2.5.3) and (2.5.4) as

$$\begin{aligned} \gamma^* &= 0.0 \\ u_{-\infty} &= -1.0 \\ a &= .1 \\ h &= 5.0 . \end{aligned} \tag{2.6.2}$$

To investigate the effect of surface tension we use (2.6.2) with the change $\gamma^* = .1$. The calculations are performed with FONV2 to a time of t = 1.0 using a time step of $\Delta t = .001$ for the case without surface tension and $\Delta t = .002$ for the other (time step size will be discussed later). The results are given below in Tables 2.1 and 2.2. Note that the entries labelled $\Delta e(t)$ represent the difference

between the displacements of the two end points.†

The results in Tables 2.1 and 2.2 support the prediction of Chadam and Ortoleva's linear theory that planar melting is stable with respect to small shape perturbations with or without surface tension. Examination of $\Delta e(t)$ indicates that the inclusion of surface tension results in an increase of the flattening rate. In particular, the calculations with surface tension included (with "weight" of .1) indicate that $\Delta e(1.0)$ is approximately three and a half times smaller than for the case with no surface tension effects included. One may also note that the flattening rate decreases with the disturbance amplitude.

We now present results for planar solidification. In this case we choose $u_{-\infty} > 0$ since the boundary at $z = 0$ must act like a solute source if solidification is to be sustained. Table 2.3 gives results for solidification without surface tension. The physical parameters are given by

$$\begin{aligned} \gamma^* &= 0.0 \\ u_{-\infty} &= 1.0 \\ a &= .1 \\ h &= 5.0 \end{aligned} \qquad (2.6.3)$$

---

† These are calculated from η values that are rounded to five decimal places.

TABLE 2.1 MELTING WITHOUT SURFACE TENSION

t	$\eta(0,t)$	$\eta(1,t)$	$\Delta e(t)$
0.0	5.100	4.900	.200
0.1	5.113	4.924	.189
0.2	5.127	4.948	.179
0.3	5.140	4.970	.170
0.4	5.153	4.992	.161
0.5	5.166	5.013	.153
0.6	5.179	5.034	.145
0.7	5.193	5.055	.138
0.8	5.206	5.075	.131
0.9	5.219	5.094	.125
1.0	5.233	5.114	.119

TABLE 2.2 MELTING WITH SURFACE TENSION

t	$\eta(0,t)$	$\eta(1,t)$	$\Delta e(t)$
0.0	5.100	4.900	.200
0.1	5.101	4.936	.165
0.2	5.105	4.967	.138
0.3	5.111	4.996	.115
0.4	5.119	5.023	.096
0.5	5.128	5.048	.080
0.6	5.138	5.071	.067
0.7	5.149	5.093	.056
0.8	5.161	5.114	.047
0.9	5.173	5.134	.039
1.0	5.186	5.154	.033

and FONV2 was used with a time step of $\Delta t = .001$.

The results in Table 2.3 show that after one second the interfacial disturbance has almost doubled its initial amplitude. Thus the numerical results clearly show that planar solidification without surface tension is unstable as predicted by Chadam and Ortoleva.

To investigate solidification with surface tension we use (2.6.3) with the change $\gamma^* = .1$. In this case we give results obtained by both SONV2 and FONV2 with $\Delta t = .001$. To save computing time, the initial concentration problem (2.5.3) was solved using FONV2. These results were recorded and then used as initial guesses for the consecutive solutions of (2.5.3) and (2.5.4) by both SONV2 and FONV2. In this case FONV2 requires only one iteration to solve (2.5.3) while SONV2 requires a few more since the fourth order and second order solutions differ somewhat. Table 2.4 gives the results and includes the execution times (on the CDC 170-835).

It is clear from either calculation in Table 2.4 that the inclusion of surface tension has a stabilizing effect on planar solidification as predicted by the theory of Chadam and Ortoleva. However, the SONV2 calculation shows a markedly quicker flattening rate than the FONV2 calculation. This discrepancy is of course entirely due to the

TABLE 2.3 SOLIDIFICATION WITHOUT SURFACE TENSION

t	$\eta(0,t)$	$\eta(1,t)$	$\Delta e(t)$
0.0	5.100	4.900	.200
0.1	5.086	4.873	.213
0.2	5.071	4.844	.227
0.3	5.056	4.813	.243
0.4	5.042	4.782	.260
0.5	5.028	4.749	.279
0.6	5.014	4.715	.299
0.7	5.000	4.679	.321
0.8	4.988	4.643	.345
0.9	4.975	4.605	.371
1.0	4.964	4.565	.399

TABLE 2.4 SOLIDIFICATION WITH SURFACE TENSION

a) Using SONV2

t	$\eta(0,t)$	$\eta(1,t)$	$\Delta e(t)$
0.0	5.100	4.900	.200
0.1	5.056	4.879	.177
0.2	5.012	4.855	.158
0.3	4.969	4.828	.141
0.4	4.925	4.799	.126
0.5	4.881	4.769	.113
0.6	4.838	4.737	.101
0.7	4.794	4.704	.090
0.8	4.750	4.669	.081
0.9	4.728	4.651	.077
1.0	4.662	4.596	.066

Execution time = 492 sec.

TABLE 2.4 (cont'd)

b) Using FONV2

t	η(0,t)	η(1,t)	Δe(t)
0.0	5.100	4.900	.200
0.1	5.071	4.887	.184
0.2	5.041	4.872	.169
0.3	5.012	4.856	.156
0.4	4.982	4.838	.144
0.5	4.953	4.820	.133
0.6	4.924	4.801	.123
0.7	4.894	4.780	.114
0.8	4.864	4.759	.105
0.9	4.835	4.737	.098
1.0	4.805	4.714	.090

Execution time = 357 sec.

use of less accurate second order formulae in SONV2. An indication of the effect of this is given by the fact that SONV2 required twenty-nine interations to solve the initial concentration problem after the fourth-order solution had been input as an initial estimate. Subsequent examination of the two solutions showed that the second order solution yields larger concentration gradients at the interface (i.e., $u_{o_{z_{\ell,KMAX}}}$) in regions of negative curvature and smaller values for regions of positive curvature than the fourth-order solution. If we assume that this trend continues during the solution of the time-dependent concentration problem then an examination of (2.5.4c) shows that the effect should in fact be to increase the flattening rate. This in turn influences the interfacial terms P, Q* and U* in the concentration problem and the interaction of these two effects appears to also increase the solid volume over that in the fourth-order case since the mean interfacial height (taken as $\simeq [\eta(0,t) + \eta(1,t)]/2$) is decreased. We attribute the greater cost of the SONV2 calculation to this greater interfacial movement (as well as the extra twenty-eight iterations on the initial concentration problem) since more iterations are then required to meet the convergence criterion (2.5.15). In any event, there seems to be no reason for preferring the use of SONV2 instead of the more accurate FONV2 and that is why

we have used the latter in all of the other calculations.

It is noted that in the calculations performed above we probably could have increased the sizes of the time steps somewhat. We have performed a number of calculations to shorter times using different combinations of physical parameters and time steps that lead to some interesting observations. For example, a calculation to t = .4 using $\Delta t = .004$ and the same physical parameters that were used in Table 2.4 (i.e., $\gamma^* = .1$, $u_{-\infty} = 1.0$, a = .1, h = 5.0) produced results identical to those of Table 2.4 (in which $\Delta t = .001$ was used) to at least five decimal places but, a calculation using $\Delta t = .005$ failed to converge at t = .06. It was also found that the largest usable time step decreased as the effect of curvature was increased through larger values of γ^* and/or a (as expected, these larger values increase the flattening rate). For example, a calculation using $\gamma^* = .2$, $u_{-\infty} = 1.0$, a = .1, h = 5.0 and $\Delta t = .004$ failed to converge after completing only one time step.

The necessity of using such relatively small time steps (compared, for example, to the case in the Rayleigh-Taylor instability problem) and the dependence of the maximum usable time step size on γ^* and a is probably attributable to the dependence of $u^{\circ}_{z_{\ell,KMAX,p+1}}$ on the linear

prediction mechanisms of (2.5.12a) and (2.5.12b). If the predicted interfacial concentrations (obtained via (2.5.12a) and (2.5.4b)) and the predicted field concentrations are not suitably compatible then the values of $u^{o}_{z_{\ell,KMAX,p+1}}$ that are calculated from these predictions may cause numerical instability. Also, if the influence of curvature is increased through larger values of γ^* and/or a, the effects of the non-linearities in the problem become more pronounced and thus the linear approximations of (2.5.12a) and (2.5.12b) only produce compatible results for smaller time steps. From equations (2.5.12a) and (2.5.4c) we can also deduce that the maximum usable time step will also vary inversely with k^*.

We also carried out some short-time calculations with $\gamma^* = .1$, $u_{-\infty} = 1.0$ and $a = .1$ to determine the effect of varying h. It was found that for cases in which $h \geq 2.0$ larger values of h resulted in decreased flattening rates while smaller values produced increased flattening rates. This is of course due to the resulting change in concentration gradients in the field solution i.e., solutions with smaller values of h have larger gradients below regions of negative interfacial curvature and smaller gradients below regions of positive curvature than solutions with larger values of h. However, a calculation with $h = 2.0$ shows a slight initial flattening and then a reversal as

the interface becomes unstable. We attribute this behaviour to the fact that the extent of the melt has become small enough to affect interfacial stability to the point where it now overrides surface tension effects so that we are no longer solving a problem that is suitably approximate to the original model in which the extent of the melt is infinite.

2.7 CONCLUSION

For the parameter values that we have used, the numerical results confirm the predictions of Chadam and Ortoleva concerning the qualitative effects of surface tension on the morphological stability of a planar interface undergoing melting or solidification. These are illustrated in Figures 2.1, 2.2, 2.3 and 2.4 wherein $\Delta a(x,t)$ is defined as in (1.7.1) if ϵ is replaced by a.

ADDENDUM - VALUES OF RELAXATION PARAMETERS

SONV2: $\omega = 1.7$, $\omega^* = 1.0$, $\omega' = 1.0$

FONV2: $\omega = 1.0$, $\omega^* = 1.0$, $\omega' = 1.0$

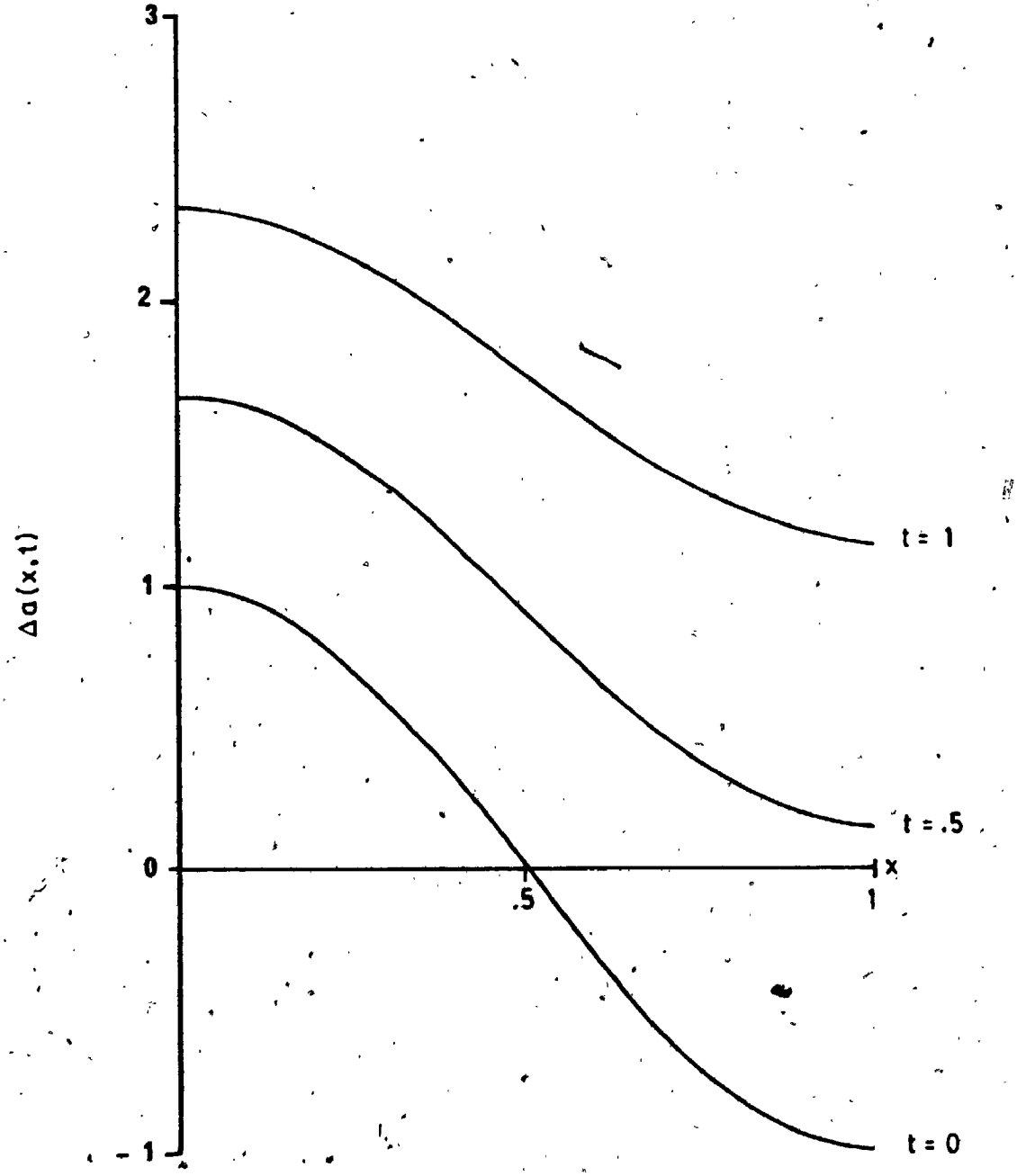

FIGURE 2.1 Melting without surface tension; $\gamma^* = 0$, $k^* = 1$, $u_{-\infty} = -1$, $a = .1$, $h = 5$.

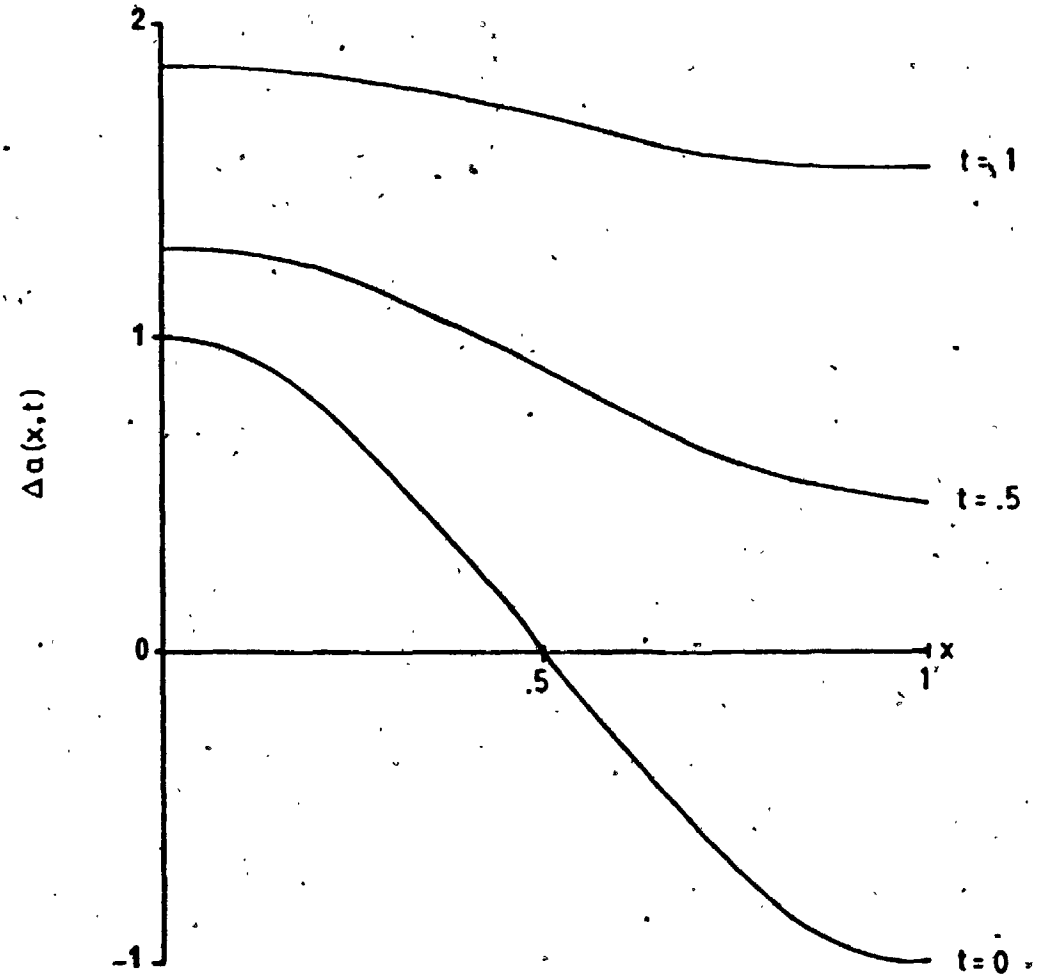

FIGURE 2.2 Melting with surface tension; $\gamma^* = .1$, $k^* = 1$, $u_{-\infty} = -1$, $a = .1$, $h = 5$.

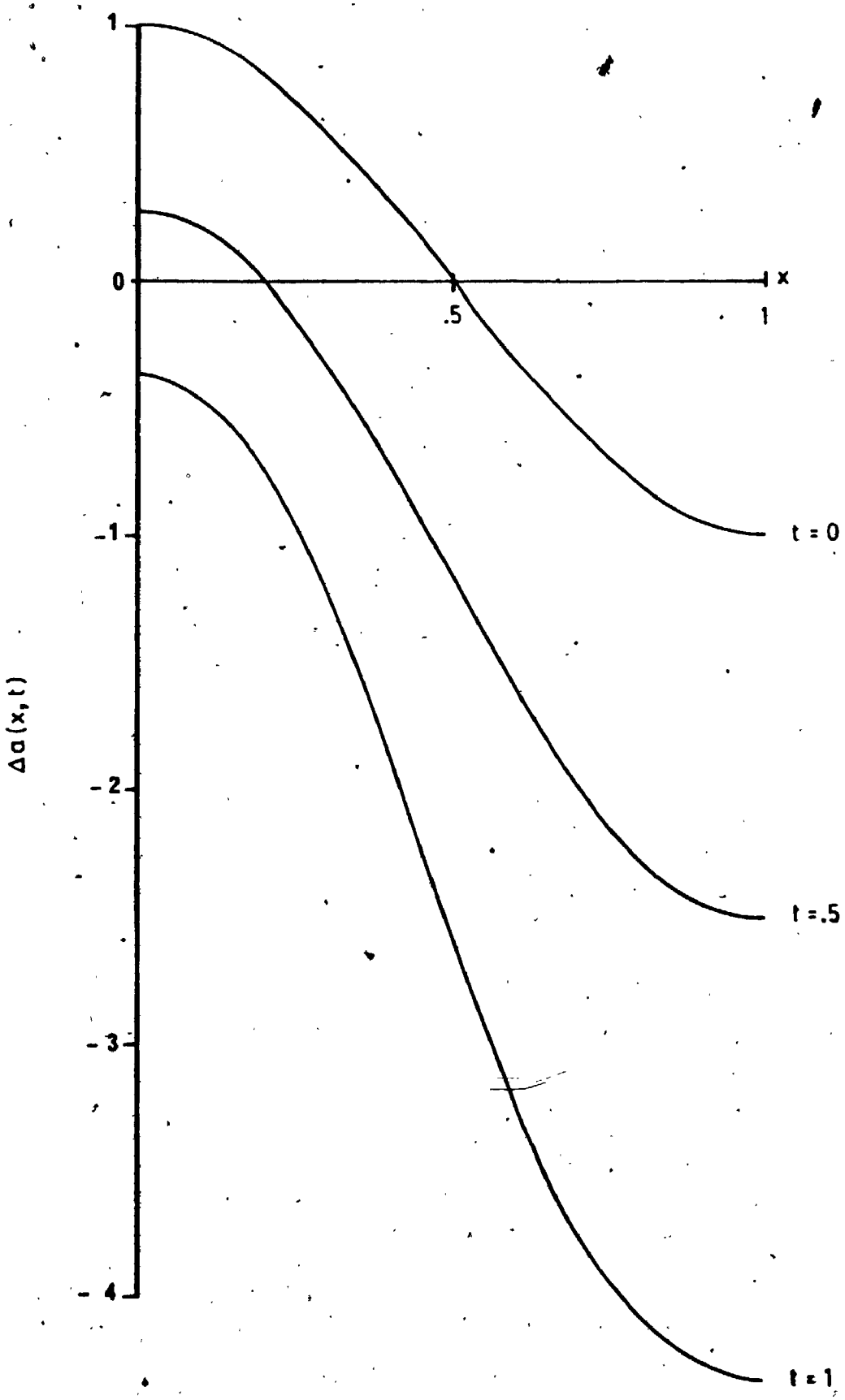

FIGURE 2.3 Solidification without surface tension; $\overset{*}{\tau}=0, \overset{*}{k}=1, u_{-\infty}=1, a=.1, h=5$.

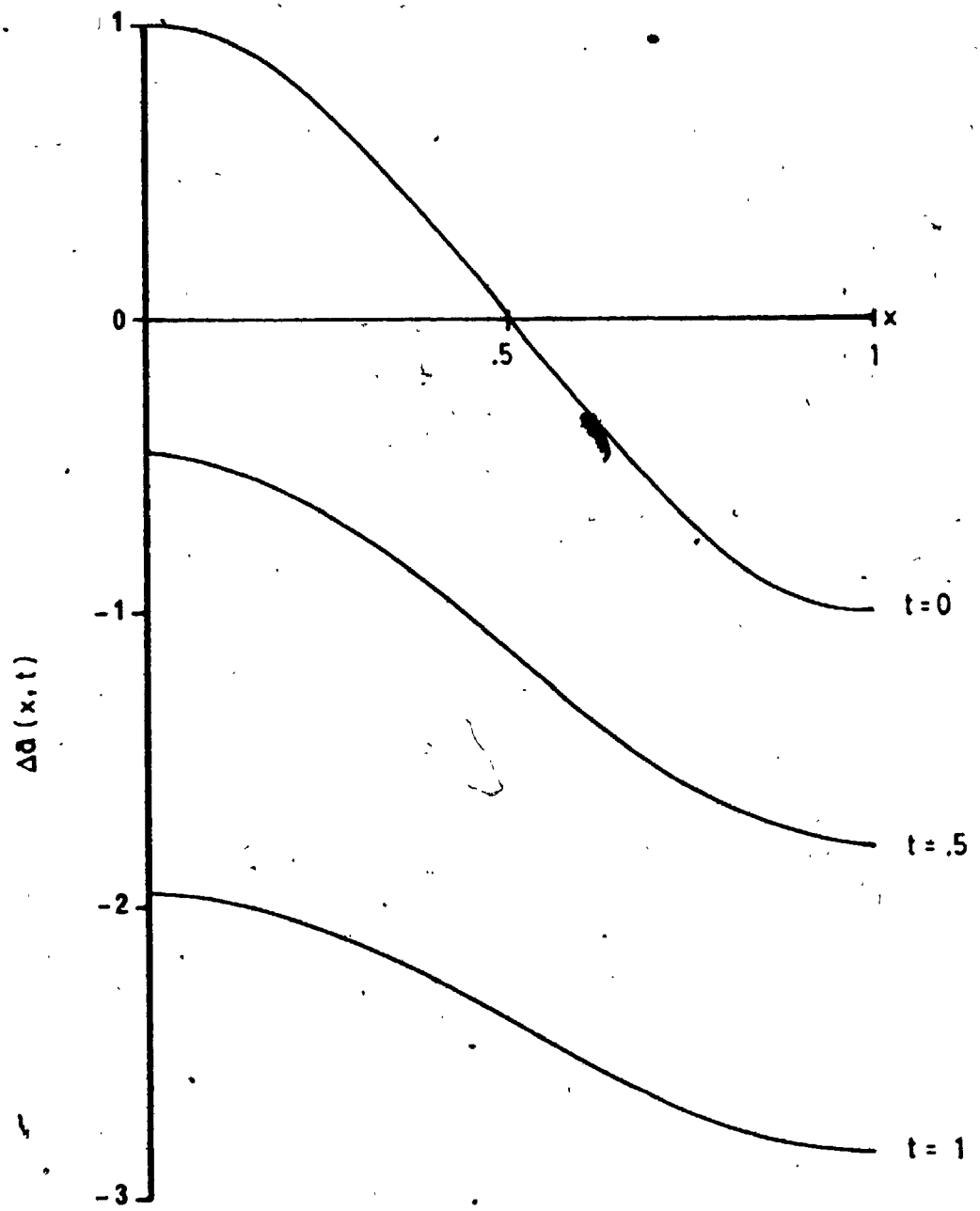

FIGURE 2.4 Solidification with surface tension; $\gamma^*=.1$, $k^*=1$, $u_{-\infty}=.1$, $a=-1$, $h=5$.

CHAPTER III

SOLUTION OF A CONVECTIVE INSTABILITY PROBLEM

3.1 INTRODUCTION

We shall now examine a problem which differs fundamentally from the previous two in that a free surface is not involved. The problem is tangentially related to a physical system that is currently of considerable interest. That system consists of an extremely viscous oil embedded in a porous matrix such as can be found in the Cold Lake, Peace River or Athabasca tar sand deposits in Alberta.

The viscosity of these oils is so high under normal conditions that they will not flow even through the very porous matrix of unconsolidated sand within the reservoir. Some of these deposits are close enough to the surface to be economically retrieved by strip mining, but most are too deep and in-situ methods must be used. These consist of reducing the viscosity of the oil while it is still in the reservoir by either chemical or thermal means such as solvent dilution or steam injection. With regard to the latter, Butler, McNab and Lo [1979] have suggested that the dependence of the oil's kinematic viscosity ν (= viscosity/density), on the temperature can be suitably approximated viz.

$$\frac{1}{\nu} = \frac{1}{\nu_s}\left[\frac{T-T_r}{T_s-T_r}\right]^m \qquad (3.1.1)$$

where ν_s represents the kinematic viscosity of the steam, T_s and T_r refer to the steam and ambient reservoir temperatures respectively, and m ranges from 3 to 4 under typical conditions.

The effect of temperature-dependent fluid properties on porous flow is often examined within the context of a paradigm problem: flow in an infinite porous slab, heated from below. To our knowledge the effects of a viscosity temperature-dependence of the specific form of (3.1.1) has not yet been examined for this problem and it is our intention to now do so. The examination will involve both a linear stability analysis to determine the conditions under which initially quiescent fluid will begin to convect and the numerical solution of a set of equations that describe the system in order to determine the flow patterns and temperature distributions near these conditions.

In section 3.2 we shall formulate the problem to be solved. Then in section 3.3 we shall review some of the analytic, experimental and numerical work that has been done on flow through porous material heated from below. It will be best to deal with these three approaches together in this case since much of the published work combines two or more of them. In section 3.4 we shall discuss in a general way the numerical methods that have been used

and in section 3.5 the details of the particular method that we use will be given. Section 3.6 outlines the linear stability analysis and its results and section 3.7 presents numerical results and discussion. Lastly, section 3.8 presents conclusions.

3.2 FORMULATION

We consider a viscous, heat conducting fluid permeating a porous layer of infinite horizontal extent and confined between two boundaries a distance h apart and in a gravitational field of magnitude g. The upper and lower boundaries are maintained at temperatures of T_h and T_o respectively, where $T_h < T_o$; the flow is assumed to be two-dimensional and the porous medium is assumed to be homogeneous and isotropic. We shall also assume the fluid to have a linear density variation caused by temperature changes alone and the kinematic viscosity to be of the form of (3.1.1). These equations of state are augmented by the equations of mass, momentum, and energy to give the following set (see Combarnous and Bories [1975]):

$$\rho = \rho_h[1 - \beta(T-T_h)] \qquad (3.2.1)$$

$$\frac{1}{\nu} = \frac{1}{\nu_o}.\left[\frac{T-T_h}{T_o-T_h}\right]^m \qquad (3.2.2)$$

$$\phi_p \frac{\partial \rho}{\partial t} + \vec{\nabla}.(\rho\vec{q}) = 0 \qquad (3.2.3)$$

$$\frac{\rho}{\phi_p}\frac{\partial \vec{q}}{\partial t} + \frac{\rho}{\phi_p^2}(\vec{q}\cdot\vec{\nabla})\vec{q} = -\vec{\nabla}p + \rho\vec{g} - \frac{\mu}{K}\vec{q} \qquad (3.2.4)$$

$$\vec{\nabla}\cdot(\lambda\vec{\nabla}T) - \vec{\nabla}\cdot[(\rho c)_f \vec{q}T] = \frac{\partial}{\partial t}[(\rho c)^* T] \qquad (3.2.5)$$

where ρ = density of the fluid

(ρ_h = reference density)

β = volumetric thermal expansion coefficient of the fluid

ν = kinematic viscosity

(ν_o = reference kinematic viscosity)

μ = viscosity

p = fluid pressure

$\vec{q}$ = fluid velocity = $q_x\hat{i} + q_y\hat{j} = u\hat{i} + v\hat{j}$

$\vec{g} = -g\hat{j}$

$m \geq 0$

K = permeability of the medium

ϕ_p = porosity of the medium

λ = thermal conductivity coefficient of the system

$(\rho c)^*$ = heat capacity of the system

$= (\rho c)_s(1-\phi_p) + (\rho c)_f\phi_p$

$(\rho c)_s$ = heat capacity of the solid matrix

$(\rho c)_f$ = heat capacity of the fluid.

We shall now introduce some simplifying approximations. These are:

1) Since the thermal expansion coefficient β is typically very small (between 10^{-3} and 10^{-4}), we shall ignore the variation in density except in the buoyancy term $\rho\vec{g}$ (the Boussinesq approximation).

2) The quantities λ, $(\rho c)_f$ and $(\rho c)^*$ will be assumed to be constant with the notation $\alpha_1 = (\rho c)_f$ and $\alpha_2 = (\rho c)^*$.

3) We shall assume that both the filtration velocities and the filtration velocity gradients are small enough to allow the exclusion of the inertial term $\frac{\rho}{\phi_p^2}(\vec{q}\cdot\vec{\nabla})\vec{q}$ in (3.2.4).

With these approximations, the equations become

$$\rho = \rho_h[1-\beta(T-T_h)] \tag{3.2.6}$$

$$\frac{1}{\mu} = \frac{1}{\mu_o}\left[\frac{T-T_h}{T_o-T_h}\right]^m \tag{3.2.7}$$

$$\vec{\nabla}\cdot\vec{q} = 0 \tag{3.2.8}$$

$$\vec{q} = -\frac{K}{\mu}[\vec{\nabla}p + \rho g\hat{j}] \tag{3.2.9}$$

$$\lambda\nabla^2 T - \alpha_1\vec{q}\cdot\vec{\nabla}T = \alpha_2 \partial T/\partial t\ . \tag{3.2.10}$$

Let us now define dimensionless quantities by

$$x^* = x/h,\ y^* = y/h,\ \theta = (T-T_h)/\Delta T,\ \phi^* = (p/\rho_h g + y)/h\beta\Delta T$$

$$t^* = \lambda t/\alpha_2 h^2, \text{ and } \vec{q}^* = \mu_o\vec{q}/K\ \rho_h g\beta\Delta T$$

where $\Delta T = T_o - T_h$. Through the use of these quantities and

the substitution of (3.2.9) into (3.2.8) one obtains

$$\vec{q}^* = -\theta^m \vec{\nabla}^* \phi^* + \theta^{m+1} \hat{j} \qquad (3.2.11)$$

where $\vec{\nabla}^* = h\vec{\nabla}$. Let us also define a stream function ψ such that

$$u^* = -\theta^m \frac{\partial \phi^*}{\partial x^*} = \frac{\partial \psi}{\partial y^*}$$

and (3.2.12)

$$v^* = -\theta^m \frac{\partial \phi^*}{\partial y^*} + \theta^{m+1} = -\frac{\partial \psi}{\partial x^*}$$

where $u^*\hat{i} + v^*\hat{j} = \vec{q}^*$. Then, through algebraic manipulation, the original set of equations (3.2.6) to (3.2.10) can be reduced to the following dimensionless pair involving ψ and θ:

$$\nabla^2\psi - \frac{m}{\theta}[\theta_x\psi_x + \theta_y\psi_y] + \theta^m\theta_x = 0 \qquad (3.2.13a)$$

$$\nabla^2\theta - R[\psi_y\theta_x - \psi_x\theta_y] = \theta_t \qquad (3.2.13b)$$

where the Rayleigh number R is given by

$$R = \alpha_1 hK\rho_h \beta\Delta T/\lambda\mu_o,$$

and $m \geq 0$. We have dropped the star superscripts for convenience.

For the purpose of restricting the problem to a finite

region we shall assume that the flow is periodic with a dimensional wavelength of 2w and furthermore that each region of width 2w consists of two mirror image flows of width w. Thus, in terms of non-dimensional distances, we shall obtain solutions in the region $0 \leq y \leq 1$, $0 \leq x \leq w/h$ for $t \geq 0$ and with the following symmetry conditions on the vertical boundaries:

$$\psi = \theta_x = 0 \qquad \text{at } x = 0, w/h \,. \tag{3.2.13c}$$

On the horizontal boundaries we have

$$\psi = 0, \ \theta = 1 \qquad \text{at } y = 0 \tag{3.2.13d}$$

and

$$\psi = \theta = 0 \qquad \text{at } y = 1. \tag{3.2.13e}$$

We shall use both the value $w/h = 1$ and other values to be determined by the linear stability analysis of section 3.6. For the sake of clarity, we note that because of the boundary condition (3.2.13c), the flow in the infinite horizontal slab is identical to the flow in an infinite series of adjacent boxes with insulated boundaries between them.

3.3 REVIEW OF PREVIOUS WORK

Horton and Rogers [1945] were the first to study convection in a fluid-saturated porous layer that is heated

from below. They performed a linearized stability analysis that followed the method of Rayleigh [1916] in his study of convection currents in a homogeneous fluid layer heated from below (Bénard-Rayleigh flow) and they predicted a critical value of the mean temperature gradient above which convection could occur. A subsequent attempt by Morrison, Rogers and Horton [1949] to verify this result experimentally showed that the predicted critical value was too large and this discrepancy was attributed to the fact that fluid properties were assumed to be constant in the stability analysis. Rogers and Morrison [1950] then extended the theory by assuming the viscosity to be exponentially dependent on the temperature and they showed good agreement between the modified theory and experiment for the particular case of certain silicon fluids in unconsolidated sand.

Lapwood [1948] performed a first order stability analysis of his own in which he considered the effects of various temperature and velocity boundary conditions on the critical temperature gradient. In his study, Lapwood did not use non-dimensionalized equations as has since become the fashion, however his best known result is usually given as if he had. This result gives the critical value of the Rayleigh number $R = R_c$ (which is defined in a manner analogous to that in 3.2), above which convection can

occur in an infinite, horizontal and homogeneous porous slab with impervious and isothermal boundaries and in which the saturating fluid is assumed to have constant properties. This value, determined to be $R_c = 4\pi^2$, has been verified experimentally by Katto and Masuoka [1967]. The corresponding flow regime is found to consist of contra-rotating rolls each of which occupies a square region with sides equal to the thickness of the slab. Kassoy and Zebib [1975] performed a similar analysis except that the viscosity was allowed to vary with temperature according to an empirical law applicable to water. They found R_c to be considerably reduced from the constant property case.

Wooding [1957] used empirical laws relating the density and viscosity of water to the temperature to develop approximate solutions for the temperature and stream-function based on a model of the geothermal layer at Wairakei, New Zealand. In brief, he approached the problem by expanding the temperature and stream-function as power-series in terms of a convection parameter that is proportional to the Rayleigh number, then introducing these into the equations of flow and solving for the perturbation coefficients by a numerical scheme. His results were found to be in fair agreement with temperature measurements made in the field. Horne and O'Sullivan [1978a] have solved a very similar problem by a direct numerical attack on the

governing equations.

Elder [1967] conducted an experimental and numerical study of steady free convection in a finite, horizontal porous slab with impervious and isothermal boundaries and saturated by a constant property fluid. Of particular interest was his experimental observation that as the Rayleigh number was continually increased from the critical value, the flow changes from one of steady state convection to one that can be characterized as being more or less oscillatory. This phenomenon was investigated experimentally and numerically by both Horne and O'Sullivan [1974] and Caltagirone [1975] for a constant property fluid. Their results indicate that the value of the so-called second critical Rayleigh number $R = R_{c2}$ required for the onset of fluctuating convection increases with the number of convective cells within the flow, however, they do not agree on the value of R_{c2}. In the case of the unicellular mode for example, Horne and O'Sullivan and Caltagirone give the values $R_{c2} \sim 280$ and $R_{c2} \sim 384$ respectively. A subsequent report by Schubert and Straus [1979b] using the Galerkin method (see Straus [1972]) gives the range $300 \leq R_{c2} \leq 320$. Horne and O'Sullivan [1978b] have investigated numerically the origin of fluctuating convection in porous media heated from below. They conclude that this quasi-regular effect is due to the triggering

of instabilities in the thermal boundary layer that forms over the bottom by small perturbations in the upstream velocity field.

Ribando and Torrance [1976] have presented numerical results for steady-state natural convection in a porous medium wherein the effects of varying viscosity and permeability with different boundary conditions are examined. Gary, Tadjeran and Zebib [1982] have given both perturbation and numerical results on the effects of viscosity variation on convective heat transport in water-saturated porous media. They show that while the temperature difference between the top and bottom boundaries has little effect on steady state convection, it does have a more significant effect on the onset of the oscillatory state.

In all of the analytic and numerical work that has been mentioned so far the Boussinesq approximation has been invoked and the flow has been assumed to be two-dimensional. To this date, Straus and Schubert [1977] appear to have presented the most general perturbative results for two-dimensional flow. They investigated the onset of thermal convection in a water saturated porous layer by including the pressure and temperature dependencies of the fluid properties and the Boussinesq approximation was not used. Their results show that a water-saturated porous layer is much more unstable to thermal convection

than it would be if the water were treated as a Boussinesq fluid having the constant properties of surface water and that the major effects are due to the temperature dependencies of the thermal expansivity and the viscosity.

Straus [1974] and Straus and Schubert [1978] have performed three-dimensional stability analyses for constant property fluid flow in porous media heated from below. Their results indicate that one must exercise considerable care in attempting to apply the results of two-dimensional convective studies to three-dimensional geometries because the results simply may not carry over due to the possibility that instabilities may arise in the orthogonal direction. For example, Straus [1974] has shown that steady single-cell, two-dimensional convection cannot occur in infinitely long cylinders for R larger than 200, although the strictly two-dimensional calculations yield steady flows for R as large as about 300. Possibly related to this is a result found in the experimental work of Combarnous and Le Fur [1969] who measured the heat flux across a layer of porous material in which convection is occurring. They found that the Nusselt number (defined as the ratio of total heat transport across an area to the heat transport due to conduction alone) increases continuously as a function of the Rayleigh number until approximately $R = 7R_c$ and that at this point a change in

the slope of the heat-transport curve occurs. This behaviour is similar to that found by Malkus [1954] for Bénard-Rayleigh flow in which case this phenomenon is thought to be due to the instability of the boundary layers which form at super-critical Rayleigh numbers (Busse [1967]) and an attendant transition to a flow regime in which no stable two-dimensional flow is possible (Busse and Whitehead [1971]). Since viscous and porous flows are often roughly analogous (especially when inertial effects are small; see Elder [1967]), Straus [1974] suggests that the transition noted by Combarnous and Le Fur may correspond to a regime in which only three-dimensional flow is possible.

Three-dimensional numerical calculations have been carried out by Holst and Aziz [1972], Zebib and Kassoy [1978], Horne [1979] and Straus and Schubert [1979a,b]. The latter ([1979a]) give some interesting results for a cubic geometry. They indicate that there is a range of Rayleigh numbers where two or three-dimensional flows are both possible in the system and that the mode that will be adopted within this range is determined solely from the initial conditions. Also, it is found that heat transport is not necessarily maximized and that three-dimensional convection also becomes unsteady at high Rayleigh number.

3.4 DISCUSSION OF NUMERICAL METHODS

Apart from the perturbation expansion method of Wooding [1957] and the Galerkin method used by Straus [1974] and Straus and Schubert [1978, 1979a,b] in which numerical schemes are used to determine the coefficients of series expansions that have been introduced into the governing equations, the other numerical results referred to in section 3.3 have been obtained directly by the solution of finite-difference forms of the governing equations. These equations are often formulated in such a way as to be amenable to a particular numerical approach. For example, Elder's formulation ([1967]) involves four simultaneous equations involving the unknown variables of temperature, stream-function, vorticity, and a source term representing the rate of generation of temperature. He solves for these by the use of a cyclic scheme which takes advantage of the fact that two of these equations are of Poisson type and can hence be readily solved by the use of successive over-relaxation. Also, Horne and O'Sullivan [1978] formulated their problem in such a way as to allow the use of the Arakawa scheme (see Arakawa [1966]) which improves computational stability but requires non-linear terms to be in Jacobian form.

In general, it is found that numerical solutions for this type of problem are often obtained through the use of

alternating direction implicit methods (ADI, see Ames [1977] § 3.12). Gary and Kassoy [1981] have compared an ADI method which is second order accurate in time and uses a fixed time step with a Runge-Kutta-Fehlberg method (RKF, see Combarnous and Bories [1975]) which is fourth order accurate in time and automatically adjusts the time step in accordance with a preassigned error tolerance. Both methods were used for the solution of the problem of constant property fluid flow in an infinite slab with isothermal boundaries for various values of the Rayleigh number. They concluded from the considerations of cost and accuracy that the ADI method was superior for the calculation of steady state solutions and that the RKF method was probably superior for solutions involving fluctuating convection. They also applied a co-ordinate transformation that allowed for the increased representation of boundary layer effects (by increasing the number of data points near the boundaries) while still maintaining the use of an equally spaced computational grid. They compared solutions obtained with and without the use of the co-ordinate transformation to the Galerkin results of Schubert and Straus [1979b] and concluded that the use of the transformation did not significantly improve accuracy. However, they used a relatively coarse 20 x 20 grid and a Rayleigh number of $R = 200$ for their tests and they note that improved results may have been obtained with the use of a finer grid and a

larger Rayleigh number (for more developed boundary layers). They also compared results obtained by the use of second order and fourth order difference formulae and conclude that a given level of accuracy is better attained, from a cost-effectiveness point of view, with the latter.

We note that while we have been referring to predominantly two-dimensional methods in the preceding, they are generally extended in a straightforward manner for use in the three-dimensional case. We shall now give our method of numerical solution of problem (3.2.13) in detail.

3.5 NUMERICAL METHOD OF SOLUTION

Recall that problem (3.1.13) for the stream function ψ, and the non-dimensionalized temperature θ, is given by

$$\nabla^2\psi - \frac{m}{\theta}\left[\theta_x\psi_x + \theta_y\psi_y\right] + \theta^m\theta_x = 0 \qquad (3.2.13a)$$

$$\nabla^2\theta - R[\psi_y\theta_x - \psi_x\theta_y] = \theta_t \qquad (3.2.13b)$$

with

$$\psi = \theta_x = 0 \qquad \text{at } x = 0, w/h, \qquad (3.2.13c)$$

$$\psi = 0,\ \theta = 1 \qquad \text{at } y = 0, \qquad (3.2.13d)$$

and

$$\psi = \theta = 0 \qquad \text{at } y = 1 \qquad (3.2.13e)$$

where m and R are non-negative constants.

The method that we have chosen to solve this problem is particularly straightforward. We start by discretizing (3.2.13a) and (3.2.13b) with the use of fourth-order formulae for the spatial terms. Central differences are used throughout the domain for derivatives in x by making use of the symmetry in θ and skew-symmetry in ψ about the vertical boundaries (recall that we have assumed these boundaries to be lines of reflection). Central differences are also used for derivatives in y except near the horizontal boundaries where the appropriate fourth order backward, forward or combination backward-forward difference formulae are applied. The time derivative in (3.2.13b) is approximated by a first order forward difference. All required formulae can be found in the Appendix.

Given values of ψ and θ at time t we solve for values at time $t+\Delta t$ by sequentially solving (3.2.13a) and (3.2.13b) in an iterative process until convergence criteria are met. Within this process (3.2.13a) is solved using SOR by rows and (3.2.13b) is solved using an ADI method and SOR by rows or columns.

The details are as follows. At the beginning of an "outer" iteration equation (3.2.13a) is solved by a series of "inner" iterations which make use of either initial or latest (iterated) values of θ and which result from the application of the following algorithm:

$$M_{ii-2,j}\lambda_{ii-2} + M_{ii-1,j}\lambda_{ii-1} + M_{ii,j}\lambda_{ii}$$

$$+ M_{ii+1,j+1}\lambda_{ii+1} + M_{ii+2,j}\lambda_{ii+2} = W_{ii,j} \qquad (3.5.1a)$$

$$\psi^{N+1}_{i,j} = (1-\omega)\psi^{N}_{i,j} + \omega\lambda_{ii} \quad (j \text{ fixed}) \qquad (3.5.1b)$$

where ii = i-1. This algorithm differs from (1.5.13) only to the extent that it takes into account the fact that the end point values of ψ are known and hence do not need to be calculated. For a step size of magnitude γ in the x direction and Δ in the y direction and a scan direction from top to bottom, we have for j = JMAX-1:

$$M_{ii-2,j} = -1$$

$$M_{ii-1,j} = 16$$

$$M_{ii,j} = -30 - 15\gamma^2/\Delta^2$$

$$M_{ii+1,j} = 16$$

$$M_{ii+2,j} = -1 \qquad (3.5.2)$$

$$W_{ii,j} = [-10\psi_{i,j+1} + 4\psi^{N}_{i,j-1,p+1} - 14\psi^{N}_{i,j-2,p+1}$$

$$+ 6\psi^{N}_{i,j-3,p+1} - \psi^{N}_{i,j-4,p+1}]\gamma^2/\Delta^2$$

$$+ m[\theta_{x_{i,j,p+1}}\psi^{N}_{x_{i,j,p+1}} + \theta_{y_{i,j,p+1}}\psi^{N}_{y_{i,j,p+1}}$$

$$\gamma^2/\Delta^2]/12\theta_{i,j,p+1} - \gamma\theta^{m}_{i,j,p+1}\theta_{x_{i,j,p+1}}$$

For $2 < j < JMAX$:

$$M_{ii-2,j} = -1$$

$$M_{ii-1,j} = 16$$

$$M_{ii,j} = -30 - 30\gamma^2/\Delta^2$$

$$M_{ii+1,j} = 16$$

$$M_{ii+2,j} = -1 \qquad (3.5.3)$$

$$W_{ii,j} = [\psi^N_{i,j-2,p+1} - 16\psi^N_{i,j-1,p+1} - 16\psi^{N+1}_{i,j+1,p+1} + \psi^{N+1}_{i,j+2,p+1}]\gamma^2/\Delta^2 + m[\theta_{x_{i,j,p+1}}\psi^N_{x_{i,j,p+1}} + \theta_{y_{i,j,p+1}}\psi^N_{y_{i,j,p+1}} \gamma^2/\Delta^2]/12\theta_{i,j,p+1} - \gamma\theta^m_{i,j,p+1}\theta_{x_{i,j,p+1}}$$

For $j = 2$:

$$M_{ii-2,j} = -1$$

$$M_{ii-1,j} = 16$$

$$M_{ii,j} = -30 - 15\gamma^2/\Delta^2$$

$$M_{ii+1,j} = 16$$

$$M_{ii+2,j} = -1 \qquad (3.5.4)$$

$$W_{ii,j} = [-10\psi_{i,j-1} + 4\psi^{N+1}_{i,j+1,p+1} - 14\psi^{N+1}_{i,j+2,p+1}$$

$$+ 6\psi^{N+1}_{i,j+3,p+1} - \psi^{N+1}_{i,j+4,p+1}]\gamma^2/\Delta^2$$

$$+ m[\theta_{x_{i,j,p+1}}\psi^{N}_{x_{i,j,p+1}} + \theta_{y_{i,j,p+1}}\psi^{N}_{y_{i,j,p+1}}\gamma^2/\Delta^2]$$

$$/12\theta_{i,j,p+1} - \gamma\theta^{m}_{i,j,p+1}\theta_{x_{i,j,p+1}}.$$

The last part of an outer iteration consists of the solution of (3.2.13b) by a series of inner iterations that use the latest values of ψ and embody an ADI method. With this method we alternate the direction of scan at every time step from the vertical direction to the horizontal direction or vice versa and the time discretization is implicit in the scan direction and explicit in the orthogonal direction. For the row iterations we use the algorithm (3.5.1) with ψ replaced by θ. Scanning from the bottom to the top we now have the following.

For $2 \leq j \leq$ JMAX-1:

$$M_{ii-2,j} = -1$$

$$M_{ii-1,j} = 16$$

$$M_{ii,j} = -30 - 12\gamma^2/\Delta t$$

$$M_{ii+1,j} = 16$$

$$M_{ii+2,j} = -1 \qquad (3.5.5)$$

$$W_{ii,j} = R[\psi_{y_{i,j,p+1}} \theta^{N}_{x_{i;j,p+1}} - \psi_{x_{i,j,p+1}} \theta_{y_{i,j,p}} \gamma/\Delta]/12$$

$$- \theta_{yy_{i,j,p}} \gamma^2/\Delta^2 - 12\gamma^2 \theta_{i,j,p}/\Delta t.$$

These formulae are easily modified at the beginning and end of each row by use of the symmetry conditions.

For the column iterations we sweep from right to left using the following modified form of (3.5.1)

$$M_{i,jj-2}\lambda_{jj-2} + M_{i,jj-1}\lambda_{jj-1} + M_{i,jj}\lambda_{jj}$$

$$+ M_{i,jj+1}\lambda_{jj+1} + M_{i,jj+2}\lambda_{jj+2} = W_{i,jj} \qquad (3.5.6a)$$

$$\theta^{N+1}_{i,jj} = (1-\omega)\theta^{N}_{i,jj} + \omega\lambda_{jj} \qquad (i \text{ fixed}) \qquad (3.5.6b)$$

Because we do not have symmetry conditions about the horizontal boundaries (3.5.6a) must be modified near the end points. For j=2 (jj=1) we have

$$M_{i,1}\lambda_1 + M_{i,2}\lambda_2 + M_{i,3}\lambda_3 + M_{i,4}\lambda_4$$

$$+ M_{i,5}\lambda_5 = W_{i,1} \qquad (3.5.7)$$

while for j=3 we have

$$M_{i,1}\lambda_1 + M_{i,2}\lambda_2 + M_{i,3}\lambda_3 + M_{i,4}\lambda_4 = W_{i,2}. \qquad (3.5.8)$$

Forms that are completely analogous to (3.5.7) and (3.5.8)

obtain at j = JMAX-1 and j = JMAX-2.

The required formulae for (3.5.7) (j=2) are:

$$M_{i,1} = -15 - 12\Delta^2/\Delta t$$

$$M_{i,2} = -4$$

$$M_{i,3} = 14$$

$$M_{i,4} = -6 \qquad (3.5.9)$$

$$M_{i,5} = 1$$

$$W_{i,1} = R\Delta[\psi_{y_{i,j,p+1}}\theta_{x_{i,j,p}} - \psi_{x_{i,j,p+1}}\theta^{N}_{y_{i,j,p+1}}]/12\gamma$$

$$- \theta_{xx_{i,j,p}}\Delta^2/\gamma^2 - 12\Delta^2\theta_{i,j,p}/\Delta t - 10\theta_{i,j-1}.$$

For (3.5.8) (j=3) we have

$$M_{i,1} = 16$$

$$M_{i,2} = -30 - 12\Delta^2/\Delta t$$

$$M_{i,3} = 16 \qquad (3.5.10)$$

$$M_{i,4} = -1$$

$$W_{i,2} = R\Delta[\psi_{y_{i,j,p+1}}\theta_{x_{i,j,p}} - \psi_{x_{i,j,p+1}}\theta^{N}_{y_{i,j,p+1}}]/12\gamma$$

$$- \theta_{xx_{i,j,p}}\Delta^2/\gamma^2 - 12\Delta^2\theta_{i,j,p}/\Delta t + \theta_{i,j-2}.$$

For (3.5.5a) ($3 \leq j \leq JMAX-1$) we have

$$M_{i,jj-2} = -1$$

$$M_{i,jj-1} = 16$$

$$M_{i,jj} = -30 - 12\Delta^2/\Delta t \qquad (3.5.11)$$

$$M_{i,jj+1} = 16$$

$$M_{i,jj+2} = -1$$

$$W_{i,jj} = R\Delta[\psi_{y_{i,j,p+1}} \theta_{x_{i,j,p}} - \psi_{x_{i,j,p+1}} \theta^{N}_{y_{i,j,p+1}}]/12\gamma$$

$$- \theta_{xx_{i,j,p}} \Delta^2/\gamma^2 - 12\Delta^2\theta_{i,j,p}/\Delta t.$$

These formulae and those that apply for the analogs of (3.5.7) and (3.5.8) at the top boundary are easily modified for the first two and last two columns to take into account the symmetry conditions.

One outer iteration is completed when the solution for θ has been obtained and a series of outer iterations is continued until convergence criteria on both ψ and θ are met. The latest values are then taken as the solution for these variables at time $t+\Delta t$.

The systems of equations that are generated by (3.5.1) or (3.5.6) are solved by using the same LINPACK

band matrix solver as in the previous two chapters. The inner iterations are stopped when

$$\max \left| V^{N+1}_{i,j,p+1} - V^{N}_{i,j,p+1} \right| < 10^{-5} \qquad (3.5.12)$$

and the outer iterations are stopped when

$$\max \left| V^{M+1}_{i,j,p+1} - V^{M}_{i,j,p+1} \right| < 5 \times 10^{-4} \qquad (3.5.13)$$

where $V = \psi, \theta$.

We note that the ADI method gives results that are accurate to $O([2\Delta t]^2)$ in time (Ames [1977] § 5.4) so that the numerical method has a truncation error of $O([2\Delta t]^2 + \max[\gamma^4, \Delta^4])$.

3.6 LINEAR STABILITY ANALYSIS

We shall now perform a linear stability analysis in order to determine approximate values of the critical Rayleigh number for each of the cases m=3 and m=4. Recall from section 3.1 that these cases are purported to correspond to the limits of the range of m that make the viscosity relationship (3.1.1) suitable for use with heavy oil.

The method we shall use follows Kassoy and Zebib [1975].

A steady-state solution of (3.2.13) corresponding to the purely conductive state is given by $\psi = \psi_o = 0$ and $\theta = \theta_o = 1-y$. We assume that for small disturbances from the conductive state we can write

$$\psi = \psi_o + \varepsilon\, \psi_1 + \varepsilon^2\, \psi_2 \ldots \tag{3.6.1}$$

$$\theta = \theta_o + \varepsilon\, \theta_1 + \varepsilon^2\, \theta_2 \ldots \tag{3.6.2}$$

where $\psi_1, \psi_2, \ldots$ and $\theta_1, \theta_2 \ldots$ vanish on the boundaries and are $O(1)$ and $\varepsilon << 1$. If we substitute (3.6.1) and (3.6.2) into (3.2.13a) and (3.2.13b), retain terms that are first order in ε, and take $1-y + \varepsilon\theta_1 \simeq 1-y$ we obtain

$$\nabla^2\psi_1 + \frac{m}{1-y}\, \psi_{1_y} + (1-y)^m \theta_{1_x} = 0 \tag{3.6.3}$$

and

$$\nabla^2\theta_1 - R\, \psi_{1_x} = \theta_{1_t}. \tag{3.6.4}$$

Now let us assume the forms

$$\psi_1 = \sin kx\, f(y) \tag{3.6.5}$$

and

$$\theta_1 = \cos kx\, g(y) \tag{3.6.6}$$

where $f(0) = g(0) = f(1) = g(1) = 0$. Substitution of these into (3.6.3) and (3.6.4) respectively yields

$$f_{yy} + \frac{m}{(1-y)} f_y - k^2 f - k(1-y)^m g = 0 \qquad (3.6.7)$$

and

$$g_{yy} - k^2 g - Rkf = 0. \qquad (3.6.8)$$

Through the use of (3.6.8) and its derivatives we can eliminate f, f_y and f_{yy} from (3.6.7) to obtain

$$(1-y)g_{yyyy} + mg_{yyy} - 2(1-y)k^2 g_{yy} - mk^2 g_y + [(1-y)k^4 - R(1-y)^{m+1}k^2]g = 0 \qquad (3.6.9a)$$

and the boundary conditions

$$g(0) = g_{yy}(0) = g(1) = g_{yy}(1) = 0. \qquad (3.6.9b)$$

Equation (3.6.9) represents an eigenvalue problem for R = R(k) that can be solved numerically. To do this we first discretize (3.6.9a) by using second order formulae and the boundary conditions to obtain a matrix equation of the form

$$\underline{A}g = R\underline{B}g \ . \qquad (3.6.10)$$

Then for a given value of the wave number k an EISPACK matrix eigenvalue solver is used to generate the eigenvalues R. The smallest of these corresponds to the critical Rayleigh number R_c for flow in a porous box of width $w/h = \frac{1}{2}\left(\frac{2\pi}{k}\right) = \pi/k$. By varying k one can determine a critical value $k = k_c$ which gives the smallest possible

value of R_c and this value is taken to be the wave number of the infinitesimal periodic disturbance that can initiate convection first in an infinite porous slab (or equivalently, in a porous box of width $w/h = \pi/k_c$) as the Rayleigh number is increased from zero.

The critical wave and Rayleigh numbers for m=3 are found to be $k_c = 4.68$ and $R_c = 280.26$ while for m=4 we find $k_c = 5.37$ and $R_c = 417.46$. To get some indication of the accuracy of the calculations we tested the case m=0 which corresponds to a constant property fluid. With the use of our grid spacing of $\Delta = .05$ and the value $k = \pi$ we obtained $R_c = 39.40$ which compares well with Lapwood's classic result of $R_c = 4\pi^2 \approx 39.48$.

3.7 RESULTS AND DISCUSSION

We first performed some tests on the numerical scheme by examining solutions obtained for the case m=3, w/h=1 and R = 100 with different combinations of spatial and time step sizes. We initially chose this sub-critical value of the Rayleigh number† because it was known that an initial perturbation in the temperature field should diminish until only steady state conduction occurs ($\theta = 1-y$, $\psi = 0$) and thus we would be able to determine

† We note that for this case $R_c \approx 318$.

roughly how well our numerical steady-state solution approximates the real one.

We first compared solutions with time step sizes of $\Delta t = .01$ and $\Delta t = .005$ using a 20 x 20 spatial grid (i.e., $\gamma = \Delta = .05$). An initial temperature distribution given by

$$\theta = 1-y-.1 \sin\pi y \cos\pi x \tag{3.7.1}$$

was assumed and steady-state was deemed to have been achieved when the condition

$$\max \left|\theta_{i,j,p+1} - \theta_{i,j,p}\right| < \Delta t \times 10^{-1} \tag{3.7.2}$$

was met. Both computations ceased at $t = .19$ and both solutions for ψ gave high values of 3.7×10^{-4} at the same point and there was agreement to three decimals in the θ solutions for most of the grid points. The maximum departure in θ from the solution 1-y was $\simeq .009$.

We next used a 30 x 30 grid (i.e., $\gamma = \Delta \simeq .033$) with $\Delta t = .005$. Again, the computation ceased at $t = .19$ and the ψ solution had a maximum in the same region as in the previous cases but the value was somewhat higher: $\psi = 5.9 \times 10^{-4}$. Also, the maximum departure in θ from 1-y was now $\simeq .011$.

From these results we concluded that a time step of $\Delta t = .005$ is likely small enough to assure convergence in time but that we had not demonstrated adequate convergence with respect to the spatial variables. As well, it appeared that our steady-state criterion (3.7.2) could be made more stringent in light of the accuracy of the numerical method. Nonetheless, we decided to first obtain solutions with the larger grid size and satisfying (3.7.2) for values of R in the convective region. We chose values of R that exceeded the critical by about thirty, initial temperature distributions of the form

$$\theta = 1-y-.1(\pi \sin \pi y \cos k_c x)/k_c , \qquad (3.7.3)$$

and performed computations for the following three cases:

a) m=0 (constant viscosity)

R = 70

w/h = 1.0

grid: 20 x 20,

b) m=3

R = 310

w/h = $\pi/4.68 \approx .671$

grid: 20 x 15,

c) m=4

R = 450

$w/h = \pi/1.71 \simeq .585$

grid: 20 x 15.

The computations ceased at t=.175, t=.61 and t=.67 for the cases a, b and c respectively. We next decreased the grid size by using a 30 x 30 grid for case a and a 30 x 20 grid for both cases b and c and found that we were not able to obtain steady-state solutions. The tolerances $\max\left|\theta_{i,j,p+1} - \theta_{i,j,p}\right|$ at t=.75 were printed out for cases b and c and were found to be $\simeq 1.2 \times 10^{-3}$ and $\simeq 1.7 \times 10^{-3}$ respectively. We then increased the steady-state criterion in (3.7.2) to 10^{-3} from $.5 \times 10^{-3}$ and ran cases b and c again. This time, the computations stopped at t=.09 and t=.055 respectively and therefore it appears that the numerical solutions start to diverge away from the steady-state at some later times.

The reasons for this divergence are not apparent. It is possible that the use of more stringent convergence criteria than (3.5.12) and/or (3.5.13) and a smaller time step may remedy the situation but a few experimental runs indicated to us that the computing costs then soon became prohibitive. This is especially true in light of the fact that we feel a stricter steady-state criterion than (3.7.2) should be used and also, that still smaller grid sizes should be employed to demonstrate convergence in the spatial variables.

In consequence, we present only the results obtained for the larger grid size and these may be found in Figures 3.1, 3.2, and 3.3 for the cases a, b, and c respectively. We believe these results to be qualitatively correct to the extent that they show the effect of variable viscosity in the enhancement of the spatial asymmetry of the flow and temperature fields when compared with the constant viscosity case. Physically, this corresponds to increased localization of the flow toward the lower right corner where heated and less viscous plumes of fluid begin their ascent and less flow near the upper left corner where cooled and more viscous fluid is descending.

3.8 CONCLUSIONS

We have determined approximate critical wave and Rayleigh numbers for the onset of convection in an infinite porous slab with isothermal boundaries, heated from below and saturated with a fluid that has a temperature-dependent viscosity similar to heavy oil for two values of the parameter m in equation (3.1.1). We have also obtained numerical solutions that show the qualitative effects of this temperature dependence on convection near the critical Rayleigh numbers. However, from considerations of stability and/or cost, the numerical method does not appear to be suitable for the computation of more quantitative results.

ADDENDUM - VALUE OF RELAXATION PARAMETER: $\omega = 1.0$.

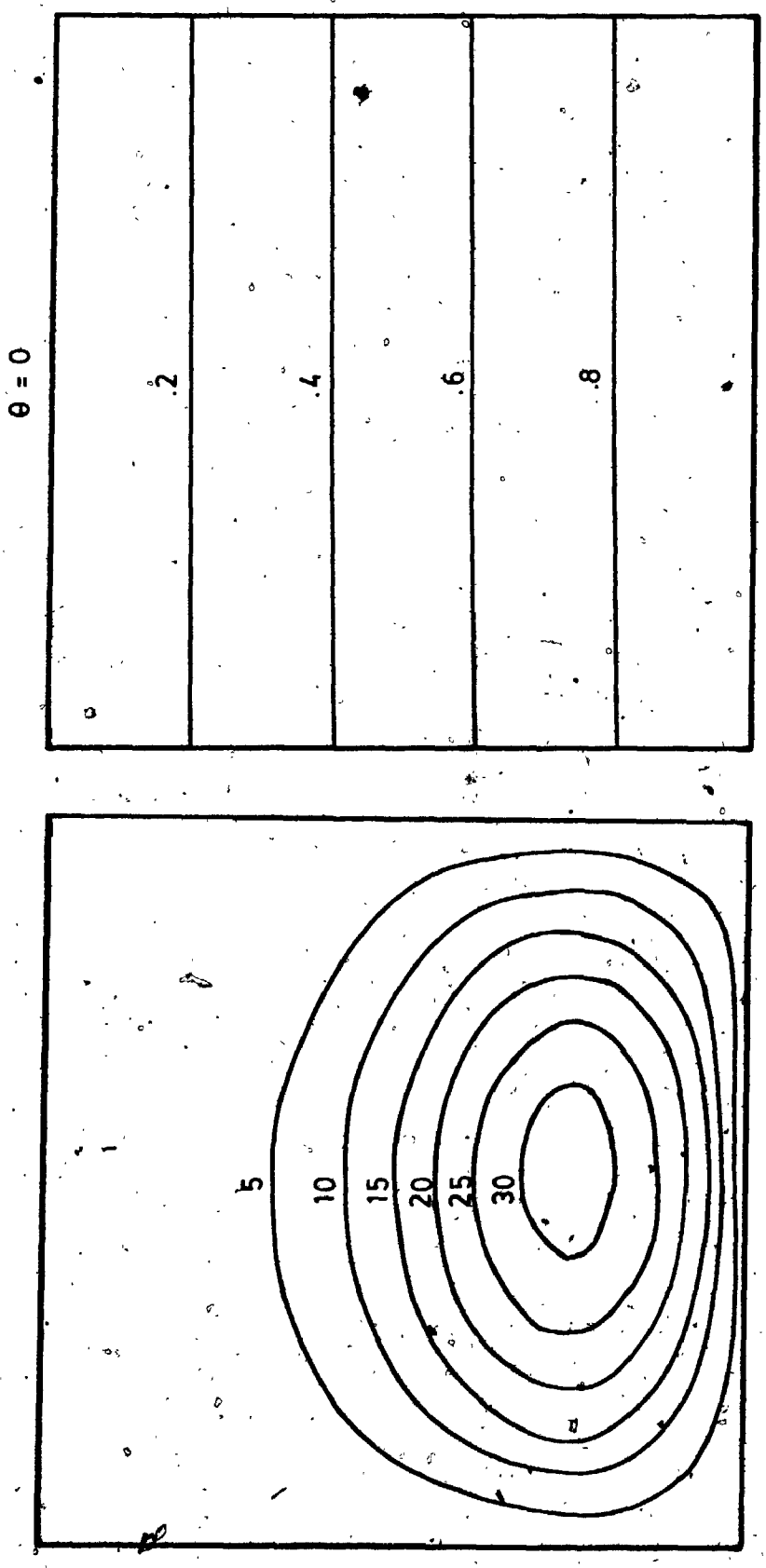

FIGURE 3.1 Streamlines and isotherms for m = 0.

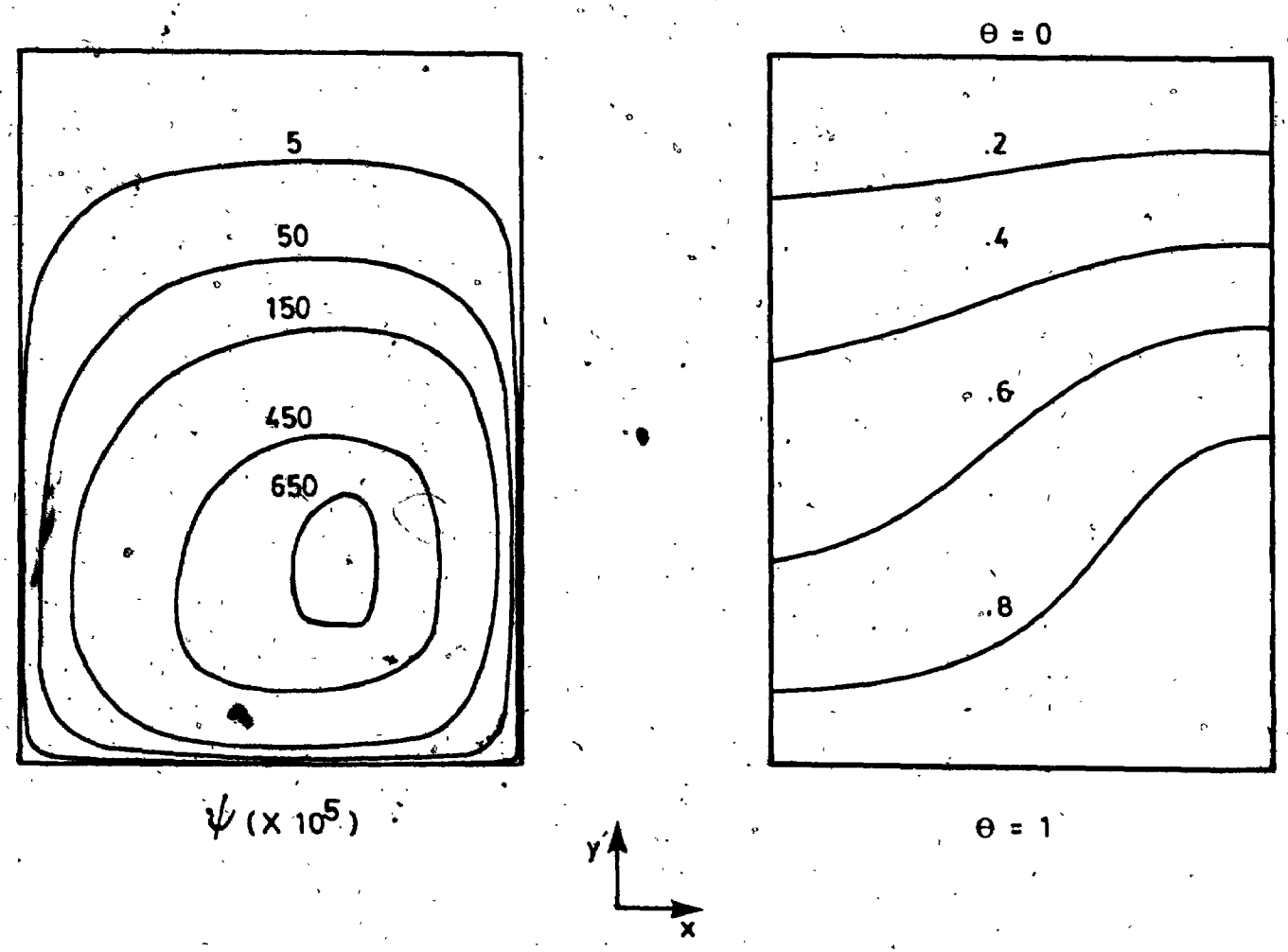

FIGURE 3.2 Streamlines and isotherms for m = 3.

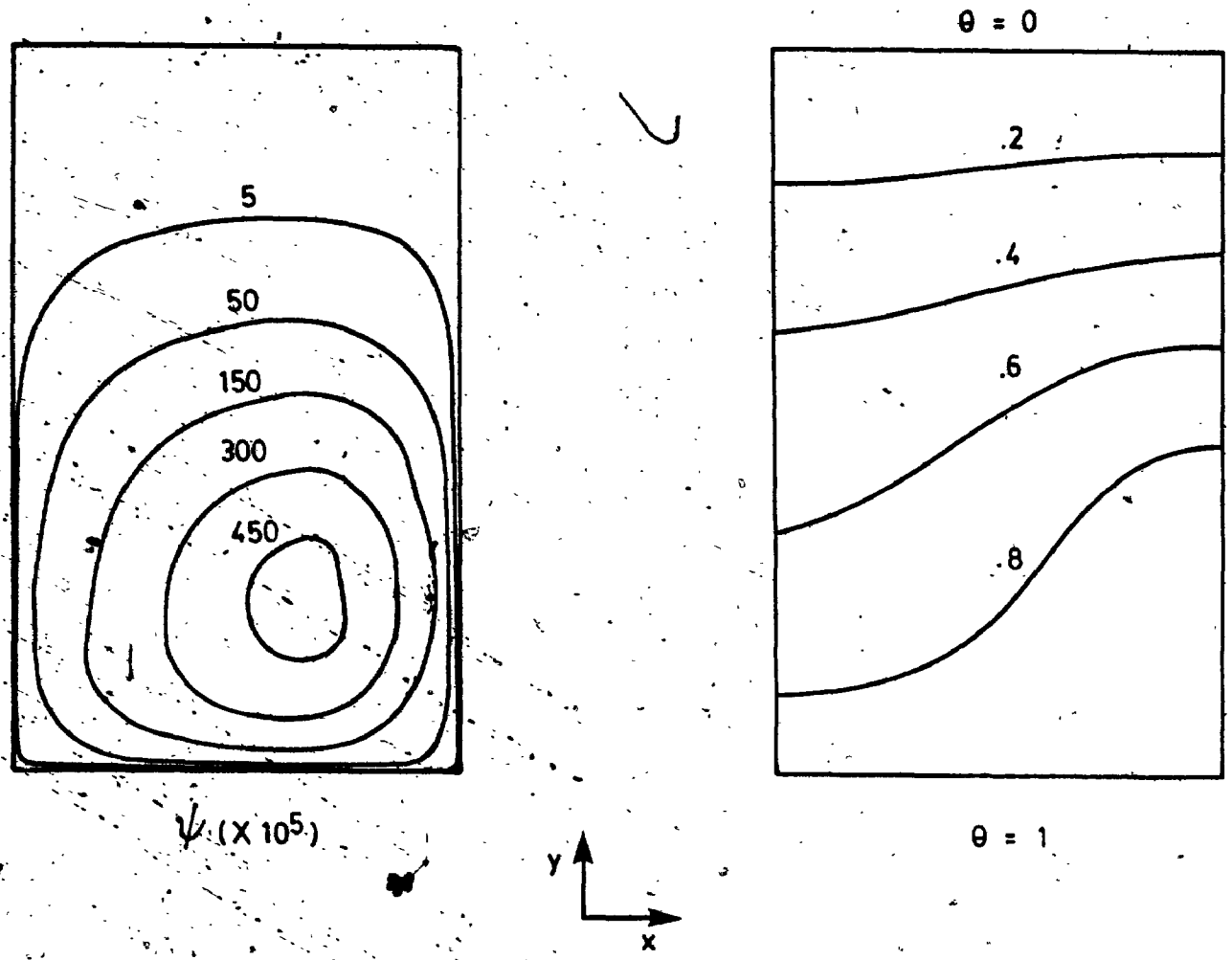

FIGURE 3.3 Streamlines and isotherms for m = 4.

APPENDIX

FINITE DIFFERENCE FORMULAE

This appendix gives all of the finite difference formulae that are necessary to construct the discretized forms of the equations that are used in this thesis. The order of the associated truncation error in each case is also included.

We shall consider the finite difference grid as a rectangle of width $x = x_{IMAX}$ and height $y = y_{JMAX}$ with subdivisions in the x and y directions of size $\gamma_i = x_{i+1} - x_i$ and $\Delta_j = y_{j+1} - y_j$ respectively where $i = 1,2,\ldots,IMAX$ and $j = 1,2,\ldots,JMAX$.† Time is discretized as $t = p\Delta t$ where $p = 0,1,2,\ldots$. Since the difference formulae are similar in all directions we shall give them only for the x direction and the replacement of γ_i with γ will indicate that a formula applies only for a constant grid spacing.

We give central difference formulae first; their modification for use at end points when symmetry conditions apply are self-evident and will not be given.

Letting $f_{x_i} = (df/dx)_{x=i}$ etc. we require the following:

---

† Note that $x_1 = y_1 = 0$ and that γ_{IMAX}, Δ_{JMAX} fall outside of the domain.

$$f_{x_i} = [\gamma_i f_{i+1} + (\gamma_i - \gamma_{i-1}) f_i - \gamma_{i-1} f_{i-1}]/2\gamma_i\gamma_{i-1}$$

$$+ O \begin{cases} \gamma_i^2 \text{ if } \gamma_i = \gamma_{i-1} \\ \max[\gamma_i, \gamma_{i-1}] \text{ if } \gamma_i \neq \gamma_{i-1} \end{cases} \quad (A.1)$$

$$f_{x_i} = [f_{i+1} - f_{i-1}]/2\gamma + O(\gamma^2) \quad (A.2)$$

$$f_{x_i} = [f_{i-2} - 8f_{i-1} + 8f_{i+1} - f_{i+2}]/12\gamma + O(\gamma^4) \quad (A.3)$$

$$f_{x_i} = [-f_{i-3} + 9f_{i-2} - 45f_{i-1} + 45f_{i+1} - 9f_{i+2} + f_{i+3}]/60\gamma$$

$$+ O(\gamma^6) \quad (A.4)$$

$$f_{xx_i} = [f_{i-2} - 2f_i + f_{i+2}]/\gamma^2 + O(\gamma^2) \quad (A.5)$$

$$f_{xx_i} = [-f_{i-2} + 16f_{i-1} - 30f_i + 16f_{i+1} - f_{i+2}]/12\gamma^2$$

$$+ O(\gamma^4) . \quad (A.6)$$

At the point $x = x_1$ we require only the following forward difference formula:

$$f_{x_1} = [f_2 - f_1]/\gamma + O(\gamma) . \quad (A.7)$$

At $x = x_{IMAX}$ we need the following backward difference formulae:

$$f_{x_{IMAX}} = [3f_{IMAX} - 4f_{IMAX-1} + f_{IMAX-2}]/2\gamma + O(\gamma^2) \quad (A.8)$$

$$f_{x_{IMAX}} = [25f_{IMAX} - 48f_{IMAX-1} + 36f_{IMAX-2} - 16f_{IMAX-3} + 3f_{IMAX-4}]/12\gamma + O(\gamma^4). \quad (A.9)$$

At $x = x_2$ we require the following formulae which use a combination of forward and backward points:

$$f_{x_2} = [-3f_1 - 10f_2 + 18f_3 - 6f_4 + f_5]/12\gamma + O(\gamma^4) \quad (A.10)$$

$$f_{xx_2} = [10f_1 - 15f_2 - 4f_3 + 14f_4 - 6f_5 + f_6]/12\gamma^2 + O(\gamma^4). \quad (A.11)$$

Similarly, at $x = x_{IMAX-1}$ we require:

$$f_{x_{IMAX-1}} = [3f_{IMAX} + 10f_{IMAX-1} - 18f_{IMAX-2} + 6f_{IMAX-3} - f_{IMAX-4}]/12\gamma + O(\gamma^4) \quad (A.12)$$

$$f_{xx_{IMAX-1}} = [10f_{IMAX} - 15f_{IMAX-1} - 4f_{IMAX-2} + 14f_{IMAX-3} - 6f_{IMAX-4} + f_{IMAX-5}]/12\gamma^2 + O(\gamma^4). \quad (A.13)$$

Mixed derivative formulae are obtained by replacing f_i by f_{y_i} in the above.

REFERENCES

Ames, W.F. 1977. "Numerical Methods for Partial Differential Equations." Academic Press, New York.

Arakawa, A. 1966. Computational design for long-term numerical integration of the equations of fluid motion - Two-dimensional incompressible flow. Part I. J. Comp. Phys. 1, 119-143.

Baker, G.R., Meiron, D.I. and Orszag, S.A. 1980. Vortex simulations of the Rayleigh-Taylor instability. Phys. Fluids 23, 1485-1490.

Baker, J.C. and Cahn, J.W. 1971. Thermodynamics of solidification. "Solidification," 23-58. 1969 Amer. Soc. Metals Seminar. ASM, Metals Park, Ohio.

Bellman, R. and Pennington, R.M. 1954. Effects of surface tension and viscosity on Taylor instability. Quart. J. Appl. Math. 12, 151-162.

Birkhoff, G. 1962. Helmholtz and Taylor instability. Proc. of XIII Symp. in Applied Math. of the Amer. Math. Soc., 55-76. AMS, Providence, Rhode Island.

Busse, F.H. 1967. On the stability of two-dimensional convection in a layer heated from below. J. Math. Phys. 46, 140-149.

Busse, F.H. and Whitehead, J.A. 1971. Instabilities of convection rolls in a high Prandtl number fluid. J. Fluid Mech. 47, 305-320.

Caltagirone, J.P. 1975. Thermoconvective instabilities in a horizontal porous layer. J. Fluid Mech. 72, 269-287.

Chadam, J. and Ortoleva, P. 1981. The stabilizing effect of surface tension on the development of the free boundary in a planar, one-dimensional, Cauchy-Stefan problem. Indiana Univ. preprint.

Chandrasekhar, S. 1961. "Hydrodynamic and Hydromagnetic Stability." Oxford Press.

Chen, H.S. and Jackson, K.A. 1971. Stability of a melting interface. J. Cryst. Growth 8, 184-190.

Cole, G.S. 1971. Transport processes and fluid flow in solidification. "Solidification", 201-274. 1969 Amer. Soc. Metals Seminar. ASM, Metals Park, Ohio.

Combarnous, M. and Le Fur, B. 1969. Transfert de chaleur par convection naturelle dans une couche poreuse horizontale. Comptes Rendus (B), 269, 1009-1012.

Coriell, S.R. and Parker, R.L. 1965. Stability of the shape of a solid cylinder growing in a diffusion field. J. Appl. Phys. 36, 632-637.

Coriell, S.R. and Parker, R.L. 1966. Role of surface diffusion in stabilizing the surface of a solid growing from solution or vapor. J. Appl. Phys. 37, 1548-1550.

Coriell, S.R. and Parker, R.L. 1967. Interface kinetics and the stability of the shape of a solid sphere growing from the melt. "Crystal Growth", 703-708. Ed. Pelser, H.S. Pergamon Press, Oxford.

Coriell, S.R. and Hardy, S.C. 1969. Morphology of unstable ice cylinders. J. Appl. Phys. 40, 1652-1655.

Coriell, S.R., Hardy, S.C. and Sekerka, R.F. 1971. A non-linear analysis of experiments on the morphological stability of ice cylinders freezing from aqueous solutions. J. Cryst. Growth 11, 53-67.

Coriell, S.R., Cordes, M.R., Boettinger, W.J. and Sekerka, R.F. 1980. Convective and interfacial instabilities during unidirectional solidification of a binary alloy. J. Cryst. Growth 49, 13-28.

Daly, B.J. 1967. Numerical study of two fluid Rayleigh-Taylor instability. Phys. Fluids 10, 297-307.

Daly, B.J. and Pracht, W.E. 1968. Numerical study of density surges. Phys. Fluids 11, 15-30.

Daly, B.J. 1969. Numerical study of the effect of surface tension on interface instability. Phys. Fluids 12, 1340-1354.

Elder, J.W. 1966. Numerical experiments with free convection in a vertical slot. J. Fluid Mech. 24, 823-843.

Elder, J.W. 1967. Steady free convection in a porous medium heated from below. J. Fluid Mech. 27, 29-49.

Emmons, H.W., Chang, C.T. and Watson, B.C. 1960. Taylor instability of finite surface waves. J. Fluid Mech, 7, 177-193.

Fine, M.E. 1964. "Introduction to Phase Transformations in Condensed Systems." The MacMillan Co., New York.

Fix, G.J. 1978. Numerical methods for alloy solidification problems. "Moving Boundary Problems", 109-128. Eds. Wilson, D.G., Solomon, A.D. and Boggs, P.T. Academic Press, New York.

Forsyth Jr., P.A. 1979. "Solution of Electrochemical Machining Problems." Ph.D. thesis, University of Western Ontario.

Forsyth Jr., P.A. and Rasmussen, H. 1979. Solution of time dependent electrochemical machining problems by a co-ordinate transformation. J. Inst. Maths Applics. 24, 411-424.

Gary, J. and Kassoy, D.R. 1981. Computation of steady and oscillatory convection in saturated porous media. J. Comp. Phys. 40, 120-142.

Gary, J., Kassoy, D.R., Tadjeran, H. and Zebib, A. 1982. The effects of significant viscosity variation on convective heat transport in water-saturated porous media. J. Fluid Mech. 117, 233-249.

Greydanus, J. and Rasmussen, H., in press. Numerical solution of a Rayleigh-Taylor instability problem. J. Comp. Phys. and Appl. Math.

Harlow, F.H. and Welch, J.E. 1965. Numerical calculation of time-dependent viscous incompressible flow of fluid with free surface. Phys. Fluids 8, 2182-2189.

Harlow, F.H. and Welch, J.E. 1966. Numerical study of large-amplitude free-surface motions. Phys. Fluids 9, 842-851.

Hirt, C.W., Cook, J.L. and Butler, T.D. 1970. A Lagrangian method for calculating the dynamics of an incompressible fluid with a free surface. J. Comp. Phys. 5, 103-124.

Holst, P.H. and Azziz, K. 1972. Transient three-dimensional natural convection in confined porous media. Int. J. Heat Mass Transfer 15, 73-90.

Horne, R.N. and O'Sullivan, M.J. 1978a. Convection in a porous medium heated from below: the effect of temperature dependent viscosity and thermal expansion coefficient. J. Heat Trans. 100, 448-452.

Horne, R.N. and O'Sullivan, M.J. 1978b. Origin of oscillatory convection in a porous medium heated from below. Phys. Fluids 21, 1260-1264.

Horne, R.N. 1979. Three dimensional natural convection in a confined porous medium heated from below. J. Fluid Mech. 92, 751-766.

Horton, C.W. and Rogers, F.T. 1945. Convection currents in a porous medium. J. Appl. Phys. 16, 367-370.

Hurle, D.T. 1969. Interface stability during the solidification of a stirred binary-alloy melt. J. Cryst. Growth 5, 162-166.

Kassoy, D.R. and Zebib, A. 1975. Variable viscosity effects on the onset of convection in porous media. Phys. Fluids 18, 1649-1651.

Katto, Y. and Masuoka, T. 1967. Criterion for the onset of convective flow in a fluid in a porous medium. Int. J. Heat Mass Transfer 10, 297-309.

Lamb, Sir Horace. 1945. "Hydrodynamics." Dover Publications, New York.

Langer, J.S. 1980. Instabilities and pattern formation in crystal growth. Rev. Mod. Phys. 52, 1-28.

Lapwood, E.R. 1948. Convection of a fluid in a porous medium. Proc. Camb. Phil. Soc. 44, 508-521.

Lewis, D.J. 1950. The instability of liquid surfaces when accelerated in a direction perpendicular to their planes. II. Proc. Roy. Soc. (A) 202, 81-96.

Longuet-Higgins, M.S. and Cokelet, E.D. 1976. The deformation of steep surface waves. I. Proc. Roy. Soc. (A) 350, 1-26.

Malkus, W.V.R. 1954. The heat transport and spectrum of thermal turbulence. Proc. Roy. Soc. (A), 196-212.

Meiron, D.I., Orszag, S.A. and Israeli, M. Applications of numerical conformal mapping. J. Comp. Phys. 40, 345-360.

Meyer, G.H. 1978. The numerical solution of multi-dimensional Stefan problems - a survey. "Moving Boundary Problems", 73-89. Eds. Wilson, D.G., Solomon, A.D. and Boggs, P.T. Academic Press, New York.

Milne-Thompson, L.M. 1949. "Theoretical Hydrodynamics." London Press.

Mullins, W.W. and Sekerka, R.F. 1963. Morphological stability of a particle growing by diffusion or heat flow. J. Appl. Phys. 34, 323-329.

Mullins, W.W. and Sekerka, R.F. 1964. Stability of a planar interface during solidification of a dilute binary alloy. J. Appl. Phys. 35, 444-451.

Nayfeh, A.H. 1969. On the non-linear Lamb-Taylor instability. J. Fluid Mech. 38, 619-631.

Nayfeh, A.H. 1973. "Perturbation Methods." John Wiley & Sons, New York.

Ockendon, J.R. 1978. Numerical and analytic solution solutions of moving boundary problems. "Moving Boundary Problems", 129-145. Eds. Wilson, D.G., Solomon, A.D. and Boggs, P.T. Academic Press, New York.

Ohring, S. 1981. Nonlinear water wave generation using the method of lines. J. Comp. Phys. 39, 137-163.

Pullin, D.I. 1982. Numerical studies of surface-tension effects in nonlinear Kelvin-Helmholtz and Rayleigh-Taylor instability. J. Fluid Mech. 119, 507-532.

Rayleigh, Lord. 1916. On convection currents in a horizontal layer of fluid, when the higher temperature is on the under side. Phil. Mag. 32, 529-546.

Rayleigh, Lord. 1945. "Theory of Sound." Vols. I and II. Dover Publications, New York.

Rasmussen, H. and Salhani, D.S. 1981. Unsteady porous flow with a free surface. IMA J. Appl. Math. 27, 307-318.

Ribando, R.J. and Torrance, K.E. 1976. Natural convection in a porous medium: Effects of confinement, variable permeability, and thermal boundary conditions. J. Heat Trans. 98, 42-48.

Rogers, F.T. and Morrison, H.L. 1950. Convection currents in porous media. III. Extended theory of the critical gradient. J. Appl. Phys. 21, 1177-1180.

Rubinstein, L. 1971. "The Stefan Problem." Translations of Mathematical Monographs, Vol. 27. Amer. Math. Soc. AMS, Providence, Rhode Island.

Rubinstein, L. 1981. Remark on the stability of the free boundary in a one-dimensional, two-phase, Cauchy-Stefan problem. Hebrew Univ. of Jerusalem preprint.

Rutter, J.W. and Chalmers, B. 1953. A prismatic substructure formed during solidification of metals. Can. J. Phys. 31, 15-39.

Saffman, P.G. and Baker, G.R. 1979. Vortex interactions. Ann. Rev. of Fluid Mech. 2, 95-122.

Sekerka, R.F. 1967. Application of the time-dependent theory of interface stability to an isothermal phase transformation. J. Phys. Chem. Solids 28, 983-994.

Sekerka, R.F. 1968. Morphological stability. J. Cryst. Growth 4, 71-81.

Sekerka, R.F. 1973. Morphological stability. "Crystal Growth: An Introduction", 403-443. Ed. Hartman, P. North-Holland Publishing Co., Amsterdam.

Shamsundar, N. 1978. Comparison of numerical methods for diffusion problems with moving boundaries. "Moving Boundary Problems", 165-185. Eds. Wilson, D.G., Solomon, A.D. and Boggs, P.T. Academic Press, New York.

Smith, J.B. 1981. Shape instabilities and pattern formation in solidification: a new method for numerical solution of the moving boundary problem. J. Comp. Phys. 39, 112-127.

Straus, J.M. 1972. Finite amplitude doubly diffusive convection. J. Fluid Mech. 56, 353-374.

Straus, J.M. 1974. Large amplitude convection in porous media. J. Fluid Mech. 64, 51-63.

Straus, J.M. and Schubert, G. 1977. Thermal convection of water in a porous medium: Effects of temperature- and pressure-dependent thermodynamic and transport properties. J. Geophys. Res. 82, 325-333.

Straus, J.M. and Schubert, G. 1978. On the existence of three-dimensional convection in a rectangular box of fluid-saturated porous material. J. Fluid Mech. 87, 385-394.

Straus, J.M. and Schubert, G. 1979a. Three-dimensional convection in a cubic box of fluid-saturated porous material. J. Fluid Mech. 91, 155-165.

Schubert, G. and Straus, J.M. 1979b. Three-dimensional and multicellular steady and unsteady convection in fluid-saturated porous media at high Rayleigh numbers. J. Fluid Mech. 94, 25-38.

Taylor, G.I. 1950. The instability of liquid surfaces when accelerated in a direction perpendicular to their planes. I. Proc. Roy. Soc. (A) 201, 192-196.

Thompson, J.F., Warsi, Z.V. and Mastin, C.W. 1982. Boundary fitted co-ordinate systems for numerical solutions of PDE's - a review. J. Comp. Phys. 47, 1-108.

Tiller, W.A., Jackson, K.A., Rutter, J.W. and Chalmers, B. 1953. The redistribution of solute atoms during the solidification of metals. Acta Met. 1, 428-437.

Tiller, W.A. 1971. On the energetics, kinetics and topography of interfaces. "Solidification", 59-98. 1969 Amer. Soc. Metals Seminar. ASM, Metals Park, Ohio.

Voronkov, V.V. 1965. Conditions for formation of mosaic structure on a crystallization front. Sov. Phys.-Solid State 6, 2378-2381.

Wooding, R.A. 1957. Steady state free thermal convection of liquid in a saturated permeable medium. J. Fluid Mech. 2, 273-285.

Yeung, R.W. 1982. Numerical methods in free surface flows. Ann. Rev. of Fluid Mech. 14, 395-442.

Zebib, A. and Kassoy, D.R. 1978. Three-dimensional natural convection motion in a confined porous media. Phys. Fluids 21, 1-3.

END

19H03184

FIN